Advancing probabilistic design of submerged floating tunnels

't Hart, C.M.P.

DOI
10.4233/uuid:bc042ade-4e5c-41e2-8f72-1259a4da01f7

Publication date
2025

Document Version
Final published version

Citation (APA)
't Hart, C. M. P. (2025). *Advancing probabilistic design of submerged floating tunnels*. [Dissertation (TU Delft), Delft University of Technology]. https://doi.org/10.4233/uuid:bc042ade-4e5c-41e2-8f72-1259a4da01f7

Advancing probabilistic design of submerged floating tunnels

C.M.P. 't Hart

Advancing probabilistic design of submerged floating tunnels

Dissertation

for the purpose of obtaining the degree of doctor
at Delft University of Technology,
by the authority of Rector Magnificus Prof.dr.ir. T.H.J.J. van der Hagen,
chair of the Board of Doctorates,
to be defended publicly on
Thursday 12 June 2025 at 15:00 o'clock

by

Cornelis Marcel Pieter 'T HART

Civiel Ingenieur, Technische Universiteit Delft, Nederland

geboren te Maassluis, Nederland.

This thesis has been approved by the promotors:

Promotor:	Prof.dr.ir. S.N. Jonkman
Promotor:	Dr.ir. O. Morales-Nápoles
Copromotor:	Dr.ir. D.J. Peters

Composition of the doctoral committee:

Rector Magnificus	chairman
Prof.dr.ir. S.N. Jonkman	Delft University of Technology
Dr.ir. O. Morales-Nápoles	Delft University of Technology
Dr.ir. D.J. Peters	Delft University of Technology
Independent members:	
Dr.ir. W. Broere	Delft University of Technology
Prof.dr. T. Bedford	University of Strathclyde Glasgow
Dr. E. Ragno	Delft University of Technology
Prof.dr.ir. M.A.N. Hendriks	Delft University of Technology
Prof.dr.ir. P.H.A.J.M. van Gelder	Delft University of Technology (reserve)

This research was funded by:

Delft University of Technology

Tunnel Engineering Consultants

Royal HaskoningDHV Enhancing Society Together

CCCC China Communications Construction Company

COB Nederlands kenniscentrum voor ondergronds bouwen en ondergronds ruimtegebruik

Keywords:	Submerged Floating Tunnels; Probabilistic analysis; High Performance Computing; Tunnels; Gaussian Random Fields; Bayesian Networks; Vine Copulas
Printed by:	ProefschriftMaken
Cover:	C.M.P. ’t Hart

ISBN 978-94-6510-640-3

An electronic version of this dissertation is available at
`http://repository.tudelft.nl`

In loving memory of

Joke 't Hart-van der Gaag

Contents

Summary

Tunnels can be constructed using different techniques, such as immersion of elements or as a boretunnel. In some circumstances, these techniques are not suitable for connecting two shores. In case the water to cross is deep and wide, such as fjords or deep sea straits, the traditional tunnels would lead to too deep tunnels as slopes for traffic are limited to reach the surface and would result in very long tunnels. Spans can be too long for fixed bridges to accommodate traffic. In such cases, a Submerged Floating Tunnel (SFT) can be considered. An SFT is a tube structure that floats below the water surface and relies on the balance between (self-)weight and dead load and the buoyancy force (Archimedes' law). SFTs are novel structures that have not been built on an operational scale.

The primary objective of this study is to develop comprehensive approaches for designing SFTs that can accurately assess uncertainties in loads, actions, and resistance while minimizing the risk of structural failure. The study aims to bridge the gap in existing design practices by developing advancing probabilistic analysis methods based on design challenges for SFTs but which can also be used in other fields of applications. Specifically, this research seeks to explore and validate alternative design approaches using Vine Copulas, Bayesian Networks, and bivariate copulas. By achieving this objective, the study contribute significantly to the advancement of probabilistic design methods, specifically in the field of SFT design.

In contrast to other civil structures, dedicated codes and standards for designing SFTs are not available. Normally, codes and standards for civil structures are developed and validated by the fact that these structures are actually being built and operated. So, the design of SFT is beyond the current scope of design practices. In order to design safe SFTs, similar to other structures, a target reliability or a target reliability framework is needed which is calibrated and usable. Unlike other types of civil structures, the conditional probability of death is different given the structural failure. As a consequence, the requirement on the probability of structural failure will be more stringent. For civil structures, in many codes such as Eurocode [1], the Load Resistance Factor Method (LRFM) is used for the design. In this approach, partial factors related to the probability of exceedance are used. As the requirement for structural failure of an SFT will differ, standard values of partial factors may not be applied . The LRFM can still be used, though, if the partial factors would specifically be derived for an SFT. The Eurocode specifies methods for deriving these partial factors using reliability based methods. The consequence of these reliability methods is that each individual failure mode and limit state need to be evaluated, which makes the process computationally intensive. It is proposed to select the most important failures modes and limit states with highest risks and derive the partial factors for these and use them for design with a validation afterwards of the partial factors on different limit states.

Alternatively, the economical risk approach could be used. This approach relates

investments to the total coast of safety for a decision parameter, such as material, sectional property, load, etc. The optimal value of a decision parameter that influences safety is found when the additional costs of the decision parameter are equal to the reduction of the total consequence costs. This approach needs to be conducted for each limit state, while the target reliability requirement still needs to be met. The estimation of failure costs is complex and consists of many elements and is the most challenging step as it needs to contain all direct and indirect consequences expressed in a monetary value.

Probabilistic design methods can be considered for the structural design of structures, including SFTs. For example, immersed tunnels are civil structures that are immersed using elements in a pre-dredged trench, coupling the elements results in a tunnel. The structural system in longitudinal direction can be identified as a flexible beam on a bedding. The flexibility is found in the segmentation of the tunnel. In order to have a continuous structure, the segments are coupled in the joints using physical interlocking in the vertical tunnel walls, called shear keys. The envelope of the forces in these keys is found by using an alternating bedding approach without a relation to the spatial variability of the dredging depth or subsoil stiffness, as required by [2]. In chapter 4, a relation between spatial variation of dredging depth and subsoil stiffness, using Gaussian random fields, and shear forces is derived. A probabilistic analysis is conducted by using a Non-Parametric Bayesian Network and a Vine Copula approach. The exceedance probabilities, with and without conditioning, are calculated. Using the Gaussian Random Fields, combined with the probabilistic approach, this results in a more realistic, and in most cases less conservative, estimation of forces in the shear keys.

The SFT concept is based on the balance of buoyancy and the permanent load. The response of SFTs supported by pontoons subjected to traffic loads leads to increase of pontoon draught, whilst this load will lead to a reduction of tether force in tether supported SFTs. An SFT is a civil structure that is designed for a service life of 100 years or more. The structural design should accommodate all possible traffic scenarios. The design of the structure relies on the amount of post-tensioning and its location in the cross section. In Chapter 5, a weight-in-motion model depending on combined copula models is used to compile a sequence of vehicles that is loaded to the structure, as the sequence progresses through the SFT it will result in cross-sectional forces and with the results exceedance probabilities can be found, as the failure is defined by the ability of ingress of water due to cracking of concrete. With this information a designer can adjust the amount of post-tensioning but also a change of the buoyancy weight ratio can be considered to optimise the design.

Waves cause hydrodynamic loads on an SFT. In order to calculate the motion response and/or the reaction forces of the structure, a dynamic mooring analysis (DMA) can be performed. DMA analyses are commonly used for moored ships and pontoons. Using these techniques on SFTs is a novelty. DMAs are computationally expensive in time. There are many different scenarios of wave heights, wave lengths and direction of impact which cannot all be evaluated with individual DMAs. In Chapter 6 a DMA is conducted on a hypothetical tunnel model followed by a probabilistic analysis. A Monte Carlo approach was used to limit the computational effort for DMAs.

The approach results in a dataset that can be used in this probabilistic analysis.

Vine copulas are commonly used in probabilistic analyses, but rare in the design of civil structures. A Vine Copula is a multivariate model that relates variables to each other. The base of the vine copulas consists of bivariate copulas and a regular vine (graphical representation of nested connected trees). The number of possible Regular Vines for a given number of variables increases drastically with the number of variables. Typically, the fitting of a vine copula model for a given dataset is performed using an algorithm based on the dependency between variables. The regular vine found by the algorithm is not necessarily the best fit in terms of the Akaike Information Criterium. A brute-force method was used in order to test all possible regular vines with 8 variables. The compilation of Chimera [3], a database of regular vines up to eight nodes, provides the opportunity to use a brute force method to find the best regular vine. However, 8 variable regular vines have 660,602,880 possibilities to consider and urges to use high performance computing to evaluate all. Considerable differences were found in the 14 different datasets from the DMA analyses, which leads to the conclusion that the use of an algorithm based on dependency to determine a regular vine is too simplistic.

In summary, the design of tunnels in general but specifically SFTs will benefit from advanced probabilistic analyses to analyse uncertainties in loads, actions and resistance. The common approach of the LRFM simplifies the correlation and dependency between the parameters, for example, the all partial material factors are considered to be on the lower bound and the partial load factors are for permanent loads always considered as constant and for variable loads these factors can differ based on the distinction between leading and accompanying values of the loads. If the variation of the parameters is considered, more sophisticated exceedance probabilities can be identified and used in the validation of the design structures.

The use of Vine Copulas, but also other probabilistic methods such as Bayesian Networks and bivariate copulas, will improve and support the design process, optimise structures, and avoid significant failure or the loss of structures.

Samenvatting

Tunnels kunnen worden gebouwd met behulp van verschillende technieken, zoals het afzinken van geprefabriceerde elementen of als een boortunnel. In sommige gevallen zijn deze technieken niet geschikt om twee oevers met elkaar te verbinden. In het geval dat het water dat moet worden overgestoken diep en breed is, zoals fjorden of diepe zeestraten, zouden de traditionele tunnels leiden tot te diepe tunnels omdat hellingen voor verkeer beperkt zijn om het oppervlak te bereiken en zouden resulteren in zeer lange tunnels. Overspanningen kunnen te lang zijn voor vaste bruggen om verkeer te accommoderen. In dergelijke gevallen kan een drijvende Tunnel (SFT) worden overwogen. Een SFT is een buisconstructie die onder het wateroppervlak drijft en waarbij gebruik gemaakt wordt van de balans tussen permanente belasting, en de opwaartse kracht (Wet van Archimedes). SFT's zijn een nieuwe type constructies die niet op operationele schaal zijn gebouwd.

Het primaire doel van deze studie is om uitgebreide benaderingen te ontwikkelen voor het ontwerpen van SFT's die nauwkeurig onzekerheden in belastingen, acties en capaciteit kunnen beoordelen en tegelijkertijd het risico op structureel falen minimaliseren. De studie heeft als doel om de kloof in bestaande ontwerppraktijken te dichten door geavanceerde probabilistische analysemethoden te ontwikkelen op basis van ontwerpuitdagingen voor SFT's, maar die ook kunnen worden gebruikt in andere toepassingsgebieden. Dit onderzoek probeert met name alternatieve ontwerpbenaderingen te verkennen en valideren met behulp van Vine Copula's, Bayesiaanse netwerken en bivariate copula's. Door dit doel te bereiken, draagt de studie aanzienlijk bij aan de vooruitgang van probabilistische methodes, met name op het gebied van het ontwerpen van SFT's.

In tegenstelling tot andere civiele constructies zijn er geen specifieke richtlijnen en normen voor het ontwerpen van SFT's beschikbaar. Normaal gesproken worden codes en normen voor civiele constructies ontwikkeld en gevalideerd door het feit dat deze constructies daadwerkelijk worden gebouwd en gebruikt. Het ontwerp van SFT's valt dus buiten het huidige bereik van huidige ontwerppraktijken. Om veilige SFT's te ontwerpen, vergelijkbaar met andere constructies, is een betrouwbaarheidskader nodig dat gekalibreerd en bruikbaar is. In tegenstelling tot andere typen civiele constructies is de voorwaardelijke kans op overlijden door het constructief falen groter. Als gevolg hiervan zal de eis aan de kans op constructief falen strenger zijn. Voor civiele constructies wordt in veel codes, zoals Eurocode [1], de Load Resistance Factor Method (LRFM) gebruikt voor het ontwerp. In deze benadering worden partiële factoren gebruikt die gerelateerd zijn aan de kans op overschrijding. Omdat de eis voor constructief falen zal verschillen, kunnen traditionele partiële factoren niet rechtstreeks worden toegepast. De LRFM kan echter nog steeds worden gebruikt als de partiële factoren specifiek zouden worden afgeleid voor een SFT. De Eurocode specificeert methoden voor het afleiden van deze partiële factoren met behulp van be-

trouwbaarheidsmethodes. Het gevolg van deze betrouwbaarheidsmethodes is dat elke individueel faal mechanisme en grenstoestand moet worden geëvalueerd, wat het proces rekenintensief maakt. Er wordt daarom voorgesteld om de belangrijkste faalmodi en grenstoestanden met de hoogste risico's te selecteren en de partiële factoren hiervan af te leiden en deze te gebruiken voor het ontwerp, met een latere kalibratie van de partiele factoren op andere grenstoestanden.

Daarnaast kan de economische risicobenadering worden gebruikt. Deze benadering relateert investeringen aan de totale veiligheidskosten voor een specifieke beslissingsparameter, zoals een materiaal parameter, een sectie-eigenschap, een belasting, enz. De optimale waarde van een beslissingsparameter die de veiligheid beïnvloedt, wordt gevonden wanneer de extra kosten van deze beslissingsparameter gelijk zijn aan de vermindering van de totale kosten als gevolg van falen. Deze benadering moet worden uitgevoerd voor elke grenstoestand, terwijl nog steeds aan de beoogde betrouwbaarheidseis moet worden voldaan. Echter, de inschatting van de totale kosten als gevolg van falen is complex en bestaat uit veel directe en indirecte elementen die in een monetaire waarde moeten worden uitgedrukt.

Probabilistische ontwerpmethoden kunnen ook worden overwogen voor het constructief ontwerp van constructies, inclusief drijvende tunnels. Bijvoorbeeld, afgezonken tunnels zijn civiele constructies die worden afgezonken met behulp van elementen in een vooraf gebaggerde sleuf, het koppelen van de elementen resulteert in een tunnel. Het constructieve systeem in longitudinale richting kan beschouwd worden als een flexibele balk op een bedding. De flexibiliteit is te vinden in de segmentering van de tunnel. Om een continue constructie te hebben, worden de segmenten gekoppeld in de voegen met behulp van fysieke vergrendeling in de verticale tunnelwanden, zogenaamde tand verbindingen. De omhulling van de krachten in deze sleutels wordt gevonden door een afwisselende beddingbenadering te gebruiken zonder een relatie met de ruimtelijke variabiliteit van de baggerdiepte of de stijfheid van de ondergrond, zoals vereist door [2]. In hoofdstuk 4 wordt een relatie afgeleid tussen ruimtelijke variatie van de baggerdiepte en de stijfheid van de ondergrond, met behulp van Gaussische random fields, en dwarskrachten in de tandverbindingen tussen tunnelsegmenten. Een probabilistische analyse wordt uitgevoerd met behulp van een niet-parametrisch Bayesiaans netwerk en een Vine Copula-benadering. De overschrijdingskansen, met en zonder conditionering, worden berekend. Met behulp van de Gaussische random fields, gecombineerd met de probabilistische benadering, resulteert dit in een realistischere en in de meeste gevallen minder conservatieve schatting van krachten in de tandverbindingen.

Het SFT-concept is gebaseerd op de balans tussen drijfvermogen en de permanente belasting. De respons van SFT's ondersteund door pontons die worden blootgesteld aan verkeersbelastingen leidt tot een toename van de pontonbelasting, terwijl deze belasting zal leiden tot een vermindering van de kabelkracht in kabelondersteunde SFT's. Een SFT is een civiele constructie die is ontworpen voor een levensduur van 100 jaar of meer. Het constructieve ontwerp moet alle mogelijke verkeersscenario's accommoderen. Het ontwerp van de constructie is afhankelijk van de hoeveelheid naspanning en de locatie ervan in de dwarsdoorsnede. In hoofdstuk 5 wordt een weight-in-motion-model dat afhankelijk is van gecombineerde copula-modellen gebruikt om een reeks voertuigen samen te stellen die de constructie belasten, naarmate de reeks door de SFT vordert, zal dit resulteren in doorsnedekrachten en met de resultaten kunnen overschrijdingskansen worden gevonden, aangezien het falen van de constructie wordt gedefinieerd door het vermogen van binnendringend water als gevolg van scheuren in beton. Met deze informatie kan een ontwerper de hoeveelheid voorspanning aanpassen, maar ook een verandering van de verhouding tussen de opdrijvende kracht op de tunnel en de permanente belasting kan worden overwogen om het ontwerp te optimaliseren.

Golven veroorzaken hydrodynamische belastingen op een SFT. Om de bewegingsrespons en/of de reactiekrachten van de constructie te berekenen, kan een dynamische afmeeranalyse (DMA) worden uitgevoerd. DMA-analyses worden vaak gebruikt voor afgemeerde schepen en pontons. Het gebruik van deze technieken op SFT's is een noviteit. DMA's zijn rekenkundig duur in de tijd. Er zijn veel verschillende scenario's van golfhoogten, golflengten en impactrichting die niet allemaal kunnen worden geëvalueerd met individuele DMA's. In hoofdstuk 6 wordt een DMA uitgevoerd op een hypothetisch tunnelmodel gevolgd door een probabilistische analyse. Een Monte Carlo-benadering werd gebruikt om de rekeninspanning voor DMA's te beperken. Deze benadering resulteert in een dataset die kan worden gebruikt in deze probabilistische analyse.

Vine copula's worden vaak gebruikt in probabilistische analyses, maar zelden in het ontwerp van civiele constructies. Een Vine Copula is een multivariabel model dat variabelen aan elkaar relateert. De basis van de vine copula's bestaat uit bivariate copula's en een regular vine (graphische representatie hierarchische structuur van afhankelijkheden tussen variabelen). Het aantal mogelijke regular vines voor een gegeven aantal variabelen neemt drastisch toe met het aantal variabelen. Normaal gesproken wordt de regular vine van een vine copula model voor een gegeven dataset bepaald met behulp van een algoritme gebaseerd op de afhankelijkheid tussen variabelen. De regular vine die door het algoritme wordt gevonden, is niet per se de beste fit op basis van het Akaike Information Criterium. Een brute-force methode werd gebruikt om alle mogelijke regular vines met 8 variabelen te testen. De compilatie van Chimera [3], een database van regular vines tot acht variabelen, biedt de mogelijkheid om een brute-force methode te gebruiken om de beste regular vine te vinden. Echter, regular vines met 8 variabelen hebben 660.602.880 mogelijkheden en is het gebruik van high performance computing methodes nodig om alle mogelijkheden te evalueren. Er werden aanzienlijke verschillen gevonden in de 14 verschillende datasets van de DMA-analyses, wat leidt tot de conclusie dat het gebruik van een algoritme op basis van afhankelijkheid om een regular vine te bepalen te simplistisch is.

Samenvattend, het ontwerp van tunnels in het algemeen, maar specifiek SFT's, zal profiteren van geavanceerdere probabilistische analyses om onzekerheid onzekerheden in belastingen, sceanrios en capaciteit te analyseren. De aanpak van de LRFM versimpeld de correlatie en onafhankelijkheid van de parameters, bijvoorbeeld, alle gedeeltelijke materiële factoren worden beschouwd als op de ondergrens en de partiele belastingfactoren worden voor permanente belastingen altijd als constant beschouwd en voor variabele belastingen kunnen deze verschillen op basis van de momentane factoren van de belastingen. Als de variatie van de parameters wordt beschouwd, kunnen geavanceerdere overschrijdingskansen worden geïdentificeerd en gebruikt bij de validatie van de ontwerpmethodieken en toetsingen.

Het gebruik van Vine Copulas, maar ook andere methoden zoals Bayesiaanse netwerken en bivariate copulas, zal het ontwerpproces verbeteren en ondersteunen, constructies optimaliseren en aanzienlijk falen of het verlies van constructies voorkomen.

1

Introduction

1.1. Historical perspective

Over time, water served humanity not only as one of the basic sources of life but also in many other ways. Over centuries, transportation developed, whilst in the early days, no highways as we know them today were part of the transportation system. In the early days, for ease of transportation, people used water. Not specifically water but the natural elements that kept the water moving. In prehistoric times, people used canoes and started developing better ship designs when their tools advanced as well. Using moving water, due to wind, tidal effects, and natural currents, waterways, and seas, became important parts of human development. Not surprising, early settlements of groups of people were close to the shore or along the rivers. In these early cities, which are still existing, businesses developed, fish was caught on the sea, and crops were gathered around the fertile area around the deltas. The only option to exchange goods with people in other areas was to use water as a transportation system. People started to discover other parts of their close surroundings and further around the world. They travelled and started trading with other cultures. For a bright future, living in a river delta would make your life easier, no wonder these settlements grew over time. However, living in the river deltas also came with challenges. For example, living close to the coast in a river delta also comes with the probability of flooding the area. Polder structures behind dikes and dunes lowered these probabilities. These probabilities by itself are low; however, a day-to-day challenge is travelling within the river delta. Move to the other side of the city and avoid going through the entire delta area of the river. Soon the need for water crossings came together with the development of the river delta, with an important requirement, the transportation and navigation on the water could not be blocked as that was essential for the settlement and the expanding city around the river delta. Starting with bridges of small spans in the early days to replace ferries and other small boats, over time the need for large spans for wider shore connections developed. In the last century, the rate of development increased several large bridges and both bored and immersed tunnels were realised.

1.2. River crossings

Traditionally, moving from one shore to another, a boat or ferry connection was the most obvious solution. But a ferry involves a ship, people that operate and there is a dependency on weather, and the need to deal with other ships navigating along the river. Secondly, a connection with a ferry involves time. A bridge is traditionally the easiest option to replace a ferry connection. But a bridge comes with penalties, as there is a limitation on navigating ships crossing the bridge. A fixed link has a certain height under the bridge and can act as a barrier to the accessibility of the ports behind the bridge. Of course, bridges can be built higher, but transition structures involve a maximum slope for traffic. Increasing the height of the bridge structure will increase the length of the approaches. As the height requirement became critical, another option could be to realise a movable bridge, which serves navigation of high ships, but comes with the penalty to the traffic crossing the bridge. Over time, traffic increases, and especially on highways it is undesirable to have a temporary obstruction in the traffic flow that causes large traffic jams.

In order to avoid the problems caused by the height of ships, tunnels are considered. Several types of tunnel can be made. Two main types are Immersed Tunnels (IMT) and Bored Tunnels. Bored tunnels come in a variety as they are also applied in other areas and do not cross only waterways. Long metro networks are constructed using this technique, which can be applied in both (rather) hard soil types and in soft soil. Depending on the soil layout, hard or soft, the soil cover above the tunnel must be respected to have a stable tunnel construction.

In river deltas, typical soft soil, a cover of 1 to 1.5 times the diameter of the bored tunnel needs to be maintained. A limitation of bore tunnels is the circular cross section, so currently only a maximum diameter up to 17.6 meter (Tuen Mun-Chek Lap Kok Link) is applied, serving directions with multiple lanes will cause at least two tubes separated from each other. Concerning the depth and the cover requirement, the start and arrival shaft of the boring machine will be deep, and consequently accounting for the maximum slope for traffic, the bore tunnel will be equivalently long as the high bridge option.

Immersed tunnels are based on a different construction. Traditionally, these tunnels are constructed using pre-fabricated buoyant elements which are immersed in a dredged trench and then covered. While the bored tunnels have a cover of 1 to 1.5 times the diameter, the top of an IMT can be placed about two meter below the current depth of the waterway. In addition, the cross section is rectangular and split into different tubes separated by walls, and an escape gallery can also be created. The realisation of this type of structures, of course, is only possible if the navigation of elements is possible, in which the required depth and width of the navigation channel needs to be considered. However, compared to the higher bridge and the bored tunnel the length of the total crossing is shorter. Important to mention is that increasing the depth of the navigation channel after realisation is limited in this matter. The length of the tunnel is defined by the vertical alignment. The combination of the depth and the maximum slopes allowed for traffic defined the minimum length of either crossing. It is obvious that the length of a tunnel will increase by larger depths.

Either solution, bridge, IMT or bored tunnel is not feasible for deep and long crossings such as Fjords and deep seas. Fjords can have shore distances of kilometres and depths of several hundreds of metres. For these particular crossings, a Submerged Floating Tunnel (SFT) may be a solution. This type of structure floats at a certain depth and is tethered to the sea bottom or hanging on floaters at the surface. After construction of an SFT navigation is unhindered and the slopes in the tunnel are limited, so the length of the tunnel is slightly larger than the water to be crossed. A schematic overview of different crossings is presented in Figure 1.1

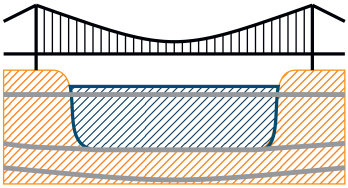

Figure 1.1: Schematic of different types of crossings

Although the construction of an SFT was already conceived at the end of the 19^{th} century, an SFT has not yet been built for several reasons, in the early years mainly due to a lack of technology. In recent years, the development of other fields of application has brought the feasibility of an SFT closer. Closer considerations of an SFT show that it has the underwater environment of a submarine vessel, the fixed positioning of off-shore platforms in marine environments, the dynamic behaviour of floating breakwaters while it will be used, loaded as a civil structure with an expected lifetime of 120 years. While most civil structures such as large bridges and tunnels are unique structures, an SFT is a superlative, as it not only is a unique structure, but it has never been built in any large operation-scaled situation. The design of traditional structures relies on codes and standards, which, in itself, are validated by the fact that these structures are actually built, and codes and standards are adjusted to new situations. SFTs can be considered as special structures to which no dedicated code or standard is applicable. One could state to use the conservative approach and use the upper bound of all standards of the fields of applications above when designing an SFT.

However, all these objects not only have different design methods, but also different target reliabilities and different expected lifetimes, together with different risk profiles. For example, this can be identified by comparing the failure of a bridge with the failure of a submarine vessel. The failure of a bridge, as recently in Baltimore, can lead not only to fatalities but also to significant economic damage. If a submarine by itself fails, considering the nuclear power facility within, the risk profile and consequences on the number of fatalities (the crew) are limited in comparison to the bridge, but the long-term effect on the environment will be large. In addition, these objects also rely on different properties to avoid structural failure. Watertightness is not a particular structural issue for a bridge, but it is an issue for a tunnel and a serious issue for an SFT.

Just adding the different requirements would probably lead to a conservative approach in terms of a feasible design, but whether the structure is economically feasible would be questionable and might result in a "more safe than needed" structure. In order to design SFTs, not only do advanced analysis methods need to be developed, but also probabilistic analyses can be used to estimate probabilities of failure related the consequences of failure. The consequences of failure are for civil structures coupled with the target reliability, which sets the safety and reliability requirements for structural safety.

Consequently, the design can be adjusted to change the risk profile by applying mitigation matters and applying robustness to reduce probabilities, in general. This approach is not limited to SFTs but to all structures that are outside the boundaries set by codes and standards. For example, the design of specific structures, such as high-rise buildings, to which the wind load definitions are not sufficient, large span bridges or wide immersed tunnels could benefit from probabilistic methods.

1.3. Knowledge gaps

SFTs are unique and special structures that are designed for a marine environment and have never been built on an operational scale to date. The development of tension leg platforms in the oil & gas industry in the 1980s of the last century brought the promising application of it back to the discussion tables, and SFT structures have been considered at several crossings such as the Sognefjord in Norway [4], and even a prototype is realised at the Qiandao lake [5, 6]. Until now, confidence in a successful construction has delayed a realisation. In addition, developments on other types of crossings, such as floating or long-span bridges, are also ongoing, the development of these alternatives also competes with a solution of an SFTs. SFTs may become a reality in the coming years. However, SFTs are impacted by both hydrodynamic and structural loads and need to be evaluated for both in design. The combination of the natural environment of an SFT and the usage by traffic identifies the uniqueness of the structure.

The responses are influenced by a variety of circumstances that cannot all be analysed by individual impact scenarios of load combinations. To predict the probability of exceeding the limits, such as forces, displacements, and accelerations, probabilistic methods can be used in combination with numerical simulations.

Probabilistic methods in structural design and specifically tunnels are rare, although Yu (2017) [7] shows a probabilistic risk analysis in simulations of the construction of a diversion tunnel, Liu (2024) [8] shows a probabilistic seismic hazard analysis which is based on an enhanced Bayesian network in which information about frequency is used in inferencing, and Pan (2024) [9] shows a method to reduce costs and excavation-induced risks by proposing a probabilistic deep reinforcement learning framework to optimise monitoring plans.

Traditional tunnels, not limited to IMT, are based on geotechnical and structural analysis. Soil properties vary spatially, and this variability should be considered in the design of tunnels. A way to incorporate this variability are random fields. Random fields for geotechnical loads have been applied in a comparison study by Cheng (2019) [10] of a pressurised tunnel face of a bored tunnel and provide a practical design tool. Gong (2018) [11] presents a probabilistic analysis based on random field generation for a longitudinal analysis of a bored tunnel. For a bored tunnel section, Yu (2019)

[12] presents a 2D plain strain approach that includes random field generation, which confirms the reliability of the tunnel lining.

The application of spatial variability or (Gaussian) random fields is still uncommon in designs of IMT foundations. Random fields are stochastic processes in space, or in other words, random functions over a given domain [13], [14]. Random fields are used in many research areas, such as environmental engineering, social sciences, finance, astronomy, and many others. Liu (2019) [15] shows the development in the research of these random fields. Within research in the field of civil engineering, the application of GRF is frequently observed in geotechnical analysis, for example, for levees and embankments by Hicks et al. (2018) [16] and Li et al. (2017) [17] . The spatial variability of a soil continuum can be described using this method; see, for example, Papaioannou et al. (2015) [18], Soubra et al. (2008) [19] and Kasama et al. (2011) [20]. In addition to geotechnical applications, random fields are also used in structural mechanical cases. Bucher (2006) [21] shows its application in material properties, such as the calculation of the modulus of elasticity or strength, as well as in geometrical properties, such as thickness in shell models. The application of random fields to trusses was researched by Bocchini (2008) [22] and discusses the application in the reliability analysis of cable-stayed bridges. In these examples the concept of random fields in Finite Element analysis is used. A description of this approach is given by van Marcke et al. (1986) [23]. The combination of spatial variability and a probabilistic approach to estimate the shear key forces in immersed tunnels is a topic that is not yet addressed in the literature.

The fact that an SFT has not been realised yet is the lack of experience and research regarding possible SFT's structural responses to the different load actions, and there is no clear insight in its safety or structural reliability. Since an SFT is located in a marine environment, the loads on an SFT can be divided into environmental loads, permanent loads, operational loads, deformation loads, and accidental loads. The effect of the aforementioned loads on the structure can be very complex as described by Shengzhong et al. (2016) [24]. Generally, the reliability assessment of structures is carried out by applying variables as deterministic values. In addition, insight is required into the structural reliability and risk levels associated with a certain design and loading conditions. Using an advanced traffic load simulation as developed by Mendoza et al. (2020, 2019) [25, 26] that impacts the SFT will lead to cross-sectional results, such as bending moments. Excessive bending moments lead to cracking of concrete and ingress of water. If an SFT suffers from the ingress of water and floods, the balance of the structure is lost, and ultimately the structure is lost. The relation of the traffic load simulation resulting in flooding as a scenario is not reported as such in literature as such and can be identified as a knowledge gap.

SFT structures are loaded by hydrodynamic forces. The response of a moored structure as a consequence of hydrodynamic loads can be found by a dynamic mooring analysis (DMA). DMA has been used for other moored floating structures, such as ships and pontoons as presented in different publications [27–31]. More detailed information on both tools can be found in [32].

The application of a DMA on SFT is a novelty, as SFTs are novel and have not yet been built. The impact of waves, defined by wave height, period, and angle of impact, are continuous stochastic variables. In order to find exceedance probabilities of the response, series of DMA are used to find data sets of 8 variables which are used to create multivariate models based on Vine Copulas (VC) to calculate exceeding probabilities.

Regarding VC, the fitting of RV structures to the data is done primarily with a popular algorithm based on maximising a function of the correlation matrix of variables or with *ad hoc* approaches. The fitting of all possible regular vines to the data has not been documented for multivariate probability distributions with 8 or more variables.

Fitting data sets using an algorithm like presented by Dissmann (2012) [33] is a common probabilistic method, but using brute-forcing using high performance computing [34] to fit data sets to Regular Vines with 8 variables is a novelty, as the Chimera [35] database containing RV up to 8 variables has recently been released. Due to the amount of RV possible with eight variables, HPC has been used, which is uncommon in combination with VC and structural assessment of structural designs.

1.4. Research objectives

Present practice with known types of civil engineering structures is that the design and the design analysis are mainly performed using the load-resistance factor design method. Probabilistic methods are used to establish or calibrate the partial factors. It is observed that probabilistic design methods are not often used directly and could be used more widely.

For specific risks, semi-probabilistic methods are too general, and probabilistic methods are recommended to achieve safe and economic designs.

Specific for new types of structure that cannot be verified using calibrated semi-probabilistic methods, probabilistic design methods are the only possible option.

The novelty and the risk profile of submerged floating tunnels is an example for which probabilistic design is indispensable. Probabilistic design methods can be improved to accommodate the evaluation of specific risks and to improve their applicability in structural design of complex civil structures such as SFTs.

The main objective of this research is to advance probabilistic methods for the design of immersed and submerged floating tunnels. The research is divided into the following parts:

1. Civil engineering structures are designed to face known and common threats. The reliability of the structure and the risk to the general public associated with its functions and use are defined in codes and standards. The question is how the reliability could be defined for a fundamentally new type of structure, such as SFTs. The safe use of infrastructure has many aspects, as commonly allowed under the traffic and tunnel safety regulations. This thesis focusses mainly on risks that threaten structural integrity. Given the risk profile, the question at stake is "how structurally safe should an SFT be?" The methodology for answering this question should be improved. The sub-question can hence be reformulated as: ***How can the (target) reliability of an SFT be defined based on existing risk and reliability frameworks?***

2. As SFTs are closely related to other tunnels, the application of probabilistic methods in e.g. IMT structures can be an important step towards the application of probabilistic methods in SFT design. In IMT design, addressing the uncertainty in the foundation is important. Specifically, the sub-question can be raised: ***How can Gaussian Random Fields for the modelling of the foundation properties be used in combination with other probabilistic methods to estimate forces in IMT shear connections?***

3. SFTs are designed using their buoyancy to balance permanent loads. The environmental condition, common service loads, and hazardous scenarios are addressed in the design. The most common load is road traffic. Increasing road traffic on bridges is monitored to support probabilistic evaluation of structures, as published by Mendosa et al. (2019) [25]. For SFTs, extreme traffic loads can potentially affect the exceedance of stress limits and, consequently, watertightness criteria, and ultimately loss of its floating equilibrium. ***How can structural failure of an SFT initiated by leakage caused by time-dependent traffic loads be evaluated using probabilistic methods?***

4. SFTs are planned to be realised in hydrodynamic environments. Waves and currents that impact the SFT will cause responses, such as forces, displacements, and foundation loads. Dynamic response analyses are rare for submerged structures and expensive in terms of elapsed time, so not every single hydraulic circumstance of wave height, wave length, and angle of impact on the structure can be individually evaluated. For design analyses, probabilistic methods can be applied to compute exceedance probabilities. It is of specific interest to find multivariate distributions describing the data to cover the entire set of combinations of hydraulic situations. Currently, an algorithm-based fitting procedure is usually used to find the best regular vine structure. It is of interest to answer the sub-question: ***How can selection of regular vines be advanced with a brute force method and what are the advantages and disadvantages of such a method?***

1.5. Research approach

The research approach to answer the questions raised in the research objectives is presented in Figure 1.2. The approach is divided into three parts; first common overarching topics are addressed, to introduce the subject, but also to introduce common theoretical methods and target reliability concepts for structures and specifically for SFT.

The target reliability research starts with an overview of the different safety considerations of different types of similar structures. Based on this overview, headings to come to a target reliability are specified, as the question for an SFT will be about how safe and structurally reliable the structure needs to be. In the continuation of this part, more focus in this research is given on the relation between structural safety and uncertainty and how to apply probabilistic methods and even how to extend methods to apply them in design.

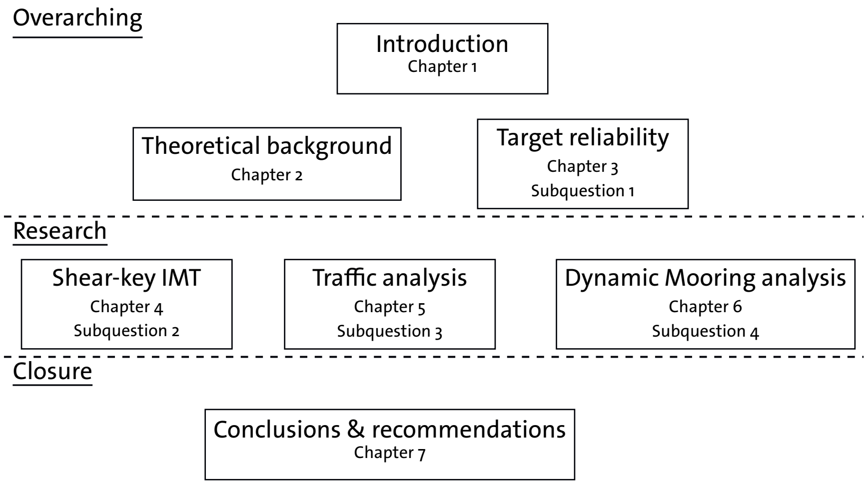

Figure 1.2: Research approach

In the second part of the approach, the focus is shifted to specific research topics. Starting with a study on the spatial variation of soil and dredging and the influence on the shear key forces. As an SFT is a civil structure closely related to other tunnels and specifically to IMT, the focus of the first study is the application of probabilistic design and the use of uncertainty in IMT tunnel foundations, but also to relate bedding uncertainty to shear key forces. In current IMT designs, the design of the shear keys is based on a Dutch design guide by Rijkswaterstaat Centre for Infrastructure [2], in which variations in the support conditions of the bedding are strictly based on the geometry of the tunnel, specific to the length of the tunnel segments. Using an approach with spatial variations for both the bedding and depth of dredging, multiple situations can be considered and combined. Additionally, coupling this method with probabilistic design will give designers the option to relate the uncertainty of the bedding to the shear key requirements.

The second study concerns the effect of traffic load on SFT structures that are supported by pontoons. The traffic load on pontoon supported SFTs is delicate, as the resulting load of buoyancy loads and permanent loads acts in the same vertical downward direction as the traffic loads. SFTs will be particularly vulnerable to vertical unbalance, which could result in loss of the structure, and these loads do not compensate but intensify each other and result in larger stress distributions and sequentially to possible damage such as cracking. Therefore, leakage due to structural cracking is of interest as a potential risk. In a study in which traffic simulations based on copulas are applied to a hypothetical SFT a relation for different buoyancy weight ratios are evaluated. Although more impacts on SFT need to be evaluated in design, specifically, this method relates the probability of failure to traffic for different buoyancy weight ratios.

In the final study, a dynamic mooring analysis (DMA) is used on a hypothetical SFT. Although DMA are already conducted on mooring ships and barges, it has not been applied to submerged structures. That is a knowledge gap, but not the main focus of the last study. In the DMA only one specific combination of wave height, wave length, and angle impact could be analysed and related responses could be found. Using a selection of situations found in monitoring data, multiple datasets were found in which input and output were combined together. These data sets are the basis for further probabilistic research. The method of Vine Copulas is used. Using Vine Copulas, Multivariate models are constructed based on data to calculate probabilities. In Vine Copulas the regular vine structure is of interest, and the number of possible regular vine structures increases drastically with the number of variables in the given dataset. Typically, the regular vine structure is found based on the largest dependency between variables without considering all possible Regular Vine structures. Evaluation of all possible Regular Vines for datasets is intensive in terms of computer resources. With the release of *Chimera*, a database with all Regular Vines up to eight nodes, together with the possibilities of a high-performance computer, an alternative is shaped to use a brute-force method.

1.6. Dissertation outline

The dissertation is split into different parts, also presented in 1.2; after this introduction, the theoretical background of the different aspects and tools used is explained. The target reliability of general structures and SFT specific and how SFT relate to other structures are discussed in chapter 3. Three chapters with different demonstrations contain, respectively, the use of spatial variability of immersed tunnel foundations and the application of both non-parametric Bayesian Networks and Vine Copulas, the analysis of traffic loads on an SFT and the quantification of the probability of failure due to bending moments, and the application of regular vines on a dynamic mooring analysis of a hypothetical SFT model. A specific extension regular vines using brute force techniques and assessed to the mostly used algorithm in selecting RV. The thesis closed with conclusions and recommendations.

1.7. Research programme

This dissertation is part of a larger research programme on SFTs. In this programme, the expertise of Delft University of Technology, CCCC and TEC has been combined. The three research groups in the programme are internationally recognised and experienced in applied research with practical relevance. The results of the research programme will be utilised to translate them into procedures to design and assess SFT in the first place, but also to use them in other fields of application within the industry. Based on a market and literature survey, in the research program scientific challenges have been initially identified:

- Reliability and risk assessment of an SFT. It requires new methodologies since the risk to an SFT is not simply the sum of the risk to each SFT component in the life cycle.
- The behaviour of (e.g. concrete and steel) tubular structure in water has not yet been well investigated. We will apply modern numerical modelling tools in combination with experimental work (e.g., laboratory experiments to validate these models) to assess the structural behaviour;
- Construction and installation
- Integration of SFTs into water landscape. The SFT is now often seen as a potential alternative water crossing measure for wide and deep-water environment, and the challenge is to find ways to design and construct it economically and reliably;
- The flexibility and ability to adapt to SFT to accommodate large uncertainty in future safety standards (due to changing hydrological conditions or socio-economic evolution);
- The integration of the challenges above into design and construction of SFT

Within the research programme, three Ph.D. researchers conducted their work at Delft University of Technology. Pengxu Zou researched the dynamic response of an SFT subjected to hydraulic loading [36], Gina Torres researched the risk and reliability of SFTs [37] and had a equal topic as presented in this thesis, resulting in a collaboration article [38] to which both contributed equally.

2

Theoretical background

2.1. Introduction

This thesis focusses on the application of probabilistic methods on SFT and IMT structures. Tunnels are civil structures; however, SFTs are novice structures that have never been built on an operational scale. In the following two sections, they are the backbone of the research presented. Chapter 4 contains research on the foundation of an IMT and Chapters 5 and 6 contain research on a SFT structure.

All the research presented uses different probabilistic and statistical methods. Since both SFT combined with advanced probabilistic methods are novices, an intermediate research step has been conducted, and probabilistic methods have been applied on a known and already constructed type of construction, IMT.

In Chapters 4, 5, and 6, the different probabilistic methods and terminology repeat, but the application to specific research differs. First, the bivariate copulas are discussed in this chapter. In the non-parametric Bayesian networks (used in Chapter 5), the Guassian copulas are applied, while in the Vine Copulas (used in Chapters 4 and 6) different copulas can be applied, which are explained in the following sections.

Finally, Gaussian Random Fields are introduced as these are used in Chapter 4 for the spatial variation of soil stiffness and dredging depths.

2.2. Submerged floating tunnels

If a water crossing needs to be crossed with a fixed connection, traditionally bridges were built. Later, bored and immersed tunnels were constructed. However, these types of structures do not serve as a solution in the case of long and deep crossings. The bridge spans would be too large without an intermediate support and, if such a support was considered, it would require a foundation deep in the water. Bored and immersed tunnels would be unpractical because in case of the maximum slope that would be required for traffic and trains, it would lead to very long approach structures. An SFT is a solution for these specific types of situation. An SFT is a structure that “floats” below the water surface and in which traffic can cross the water at large depths. An SFT construction is also known as 'Archimedes bridge', literally a bridge underwater. The different concepts of crossing are shown in Figure 1.1.

Taking into account SFTs, four different concepts are identified and schematically presented in Figure 2.1. If the distance between the shores and the hydraulic loads on the structure is limited, a fixed connection between the shores can be applied. In this case, the Bouyancy Weight Ratio (BWR), which is the ratio between the self-weight and the dead load of the structure and the Archimedes force, is close to neutral. In the second option (b), the SFT is supported by piers, in this concept, the structure is heavier than the Archimedes force. The concept requires a less deep crossing, as the piers require a fixed and robust foundation. This concept has been used for the Citybanan in the Söderströmtunneln in Stockholm, Sweden, and was considered for the Golden Horn crossing in Istanbul, Turkey. Both concepts rely on the BWR of the structure, but are not suitable for long and deep crossings.

For long and deep crossings, SFT supported by tethers or pontoons can be considered. In the tether supported SFT (c), the SFT structure the self-weight and dead load is lower than the Archimedes force and have an upward resulting force. The SFT structure is stabilised using tension tethers that are anchored at the sea bed. Another option is to stabilise the structure using pontoons (d). In this option, the self-weight and dead load are larger than the Archimedes forces and have a downward resulting force. The buoyancy of the structure is facilitated by the pontoons at the water level. Current feasibility designs such as Bjornafjorden 2016 [39] show both options (see Figure 2.2).

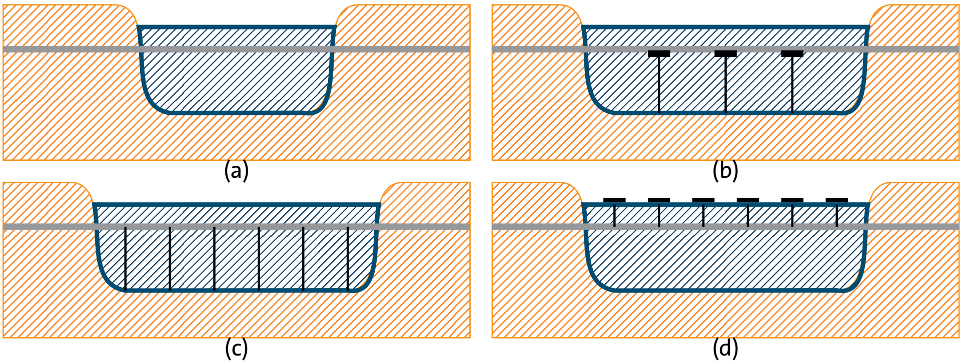

Figure 2.1: Schematic of different types of SFTs; shore (a), pier (b), tether (c) and pontoon (d) supported

In this research, an SFT supported by pontoons has been used in the traffic analysis in Chapter 5 and the SFT supported by tethers has been used in the Dynamic Mooring Analysis (DMA) in Chapter 6.

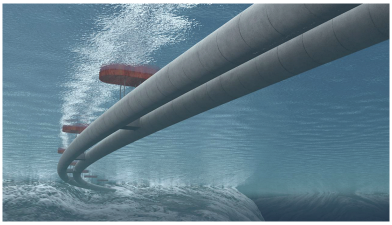

(a) Pontoon supported

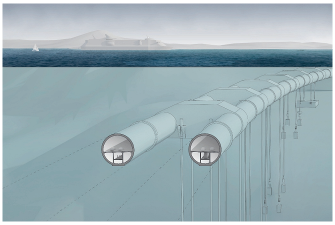

(b) Tether supported

Figure 2.2: Rendering of SFT (source: NPRA)

2.3. Immersed tunnels

Immersed tunnels (IMT) are tunnels supported by soft soil and a foundation layer that acts as a bedding. Most of these types of tunnel are constructed using pre-fabricated elements immersed in a trench in the seabed. After immersion and finalisation, the structure behaves as a segmented lining with segments of a length of about 20 to 25m that are connected with joints. Using this approach, the tunnel is less vulnerable to differential settlements as the segment joints transfer only shear forces through shear key constructions and large bending moments are avoided over the length of the structure. Different types of immersed tunnels (IMT) and their construction methods are discussed by Rasmussen (1997) [40]. A general description of the IMT construction technique and a historical perspective is given by de Wit (2014) in [41] and the design principles are described by Grantz (1997) [42]. Glerum (1992) gives a description of the development over the years [43]. IMTs traditionally have a foundation of a gravel or a sand-flow foundation, both have their advantages and disadvantages, but the differences between both methods were already described in 1978 by van Tongeren [44] and scale model tests on sand-flow were performed and researched by Li et al. (2014) [45]. Sand-jetting or sand-flow is highlighted by Glerum (1995) [46]. This technique was applied, for example, on the Maastunnel in 1942 which is described by Gravesen and Rasmussen (1993) ([47]. The gravel foundation was applied to the Øresund link between Copenhagen and Malmö. Currently, most IMTs are constructed using prefabricated elements of 100 to 150 metres in a dry dock situation. The elements consist of segments of 20 to 25m which are compressed to each other for transportation by a post-tensioning system. After casting and post-tensioning the element, it is towed to the tunnel location and immersed in a dredged trench and laterally locked in its horizontal position using a backfill and a protection layer (see Figure 2.3). After immersion, temporary post-tension is deactivated by cutting the tendons at the joints. As a result, a continuous flexible system is created and at the joints shear forces must be transferred between segments (see Figure 2.4).

The shear keys that connect the segments provide a vertical shear capacity. The capacity depends on the size and material of the key. In this research, a traditional reinforced concrete shear key is assumed (see Figures 2.5 and 2.6). The adjustment of the key has limitations. For example, as mentioned before, the tunnel needs to be buoyant in the construction phase, adding material like thickening the key will influence this process. Furthermore, the key itself is limited by the height of the tunnel.

Considerations of other materials have financial consequences. At the location of the shear key, a flexible joint is constructed. Flexible joints are ”weak” points in terms of the water tightness of the tunnel and its amount should be limited. In the current design approach of alternating bedding scenarios, longer distances between joints will increase the forces in the shear key. An optimal design would meet a segment length in which the shear key is loaded to its maximum capacity. The research presented in Chapter 4 focusses on the spatial variability of the tunnel foundation and its relation to the forces in the shear keys. The analysis is based on an analysis of a rectangular tunnel section using a gravel foundation, although the same approach as presented here can be used for a sand flow foundation.

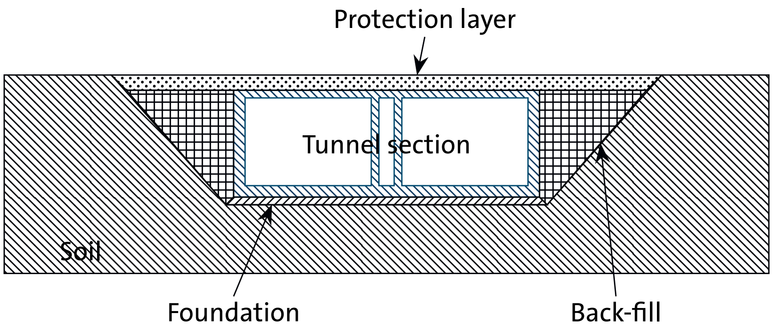

Figure 2.3: Typical cross section of an immersed tunnel section

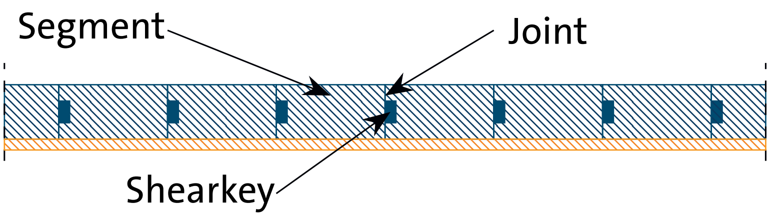

Figure 2.4: Typical longitudinal section of an immersed tunnel section - side view

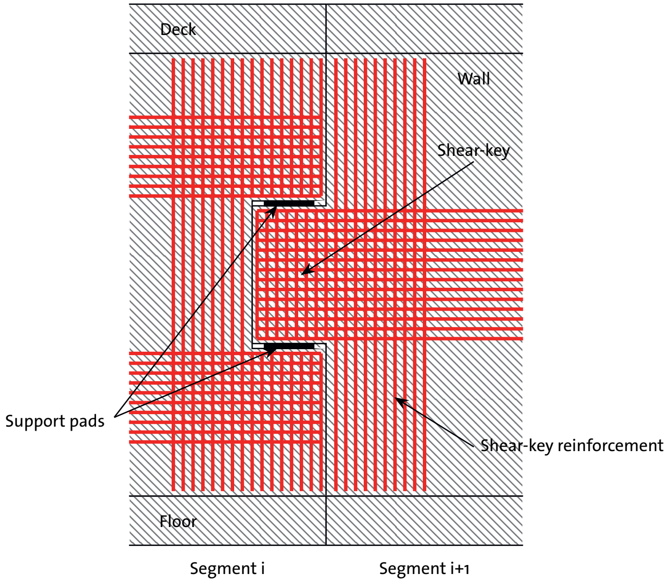

Figure 2.5: Joint layout - cross section

Figure 2.6: Concrete shear key in IMT

2

2.4. Bivariate copulas

A copula is a multivariate cumulative distribution function with uniform margins [0,1]. Sklar's theorem (Sklar 1959) [48] states that a multivariate distribution function of a random vector is expressible by the marginals of the individual variables and a copula function C. For a 2 dimensional case see eq. 2.1.

$$H_{XY}(x, y) = C(F_X(x), G_Y(y)) \tag{2.1}$$

The function $H_{XY}(x, y)$ represents the joint distribution of the continuous random variables $(x, y) \in \mathbb{R}$, with individual marginal distributions $F_X(x)$ and $G_Y(y)$ both using the range $[0, 1]$. The copula is defined on the unit square $I^2 = ([0, 1] \times [0, 1])$, ensuring compliance with eq. 2.1. When F_X and G_Y are continuous, the copula C is unique.

In order to use copulas successfully, variables must be transferred from marginal distributions to the uniform distribution [0,1]. Figure 2.7 shows a hypothetical joint distribution of the variables U_1 and U_2 with a respective Guassian ($\mu = 10$, $\sigma = 5$) and Gumbel distribution ($\mu = 7$, $\sigma = 15$). Individual variables are transferred to the uniform distribution, described by y, using a quantile transformation. On the right side in the figure the joint copula distribution is presented. The data show a larger dependency on the lower values of both variables. This dataset with tail dependency in the lower left corner can be described using the Clayton copula with parameter. $\theta \approx 3$.

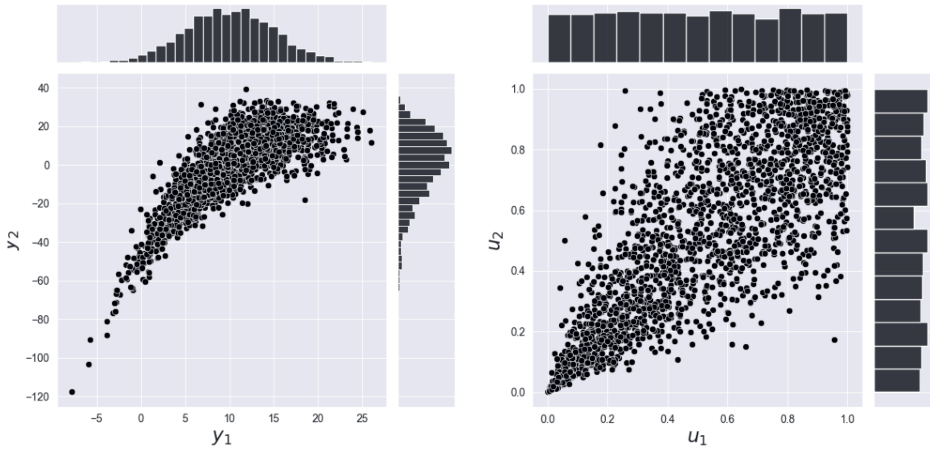

Figure 2.7: Data and copula representation

For different datasets, different copulas can be applied to describe the bivariate distributions of the data. The research conducted using VC uses `PyVineCopulib` [49]. In this package a large variety of the most used copulas and their rotated versions are used. In this thesis, only parametric copulas have been used. Parametric copulas describe the bivariate distribution using a function defined by parameters. The copulas available in `PyVineCopulib` using one parameter are:

- Guassian
- Clayton
- Gumbel
- Frank
- Joe

In Figure 2.8 samples from the 5 five bivariate distributions are shown. In this example, the marginal distributions of the variables are the same as those presented in Figure 2.7. The two parameter copulas are the student-t and the BB family copulas. In the research presented, one-parameter copulas are used in VC in Chapters 4 and 6. In Chapter 5 mainly one-parameter vine copulas are used and some two-parameter copulas are used. The non-parametric Bayesian network approaches rely only on the Gaussian copula.

The used datasets are fitted to parametric bivariate copulas by maximum likelihood, while the allowed copula family is restricted to one-parameter copulas including their rotated versions. More information and aspects on copulas are published by Nelsen (2006) and Joe (1997) [50, 51] for example.

2

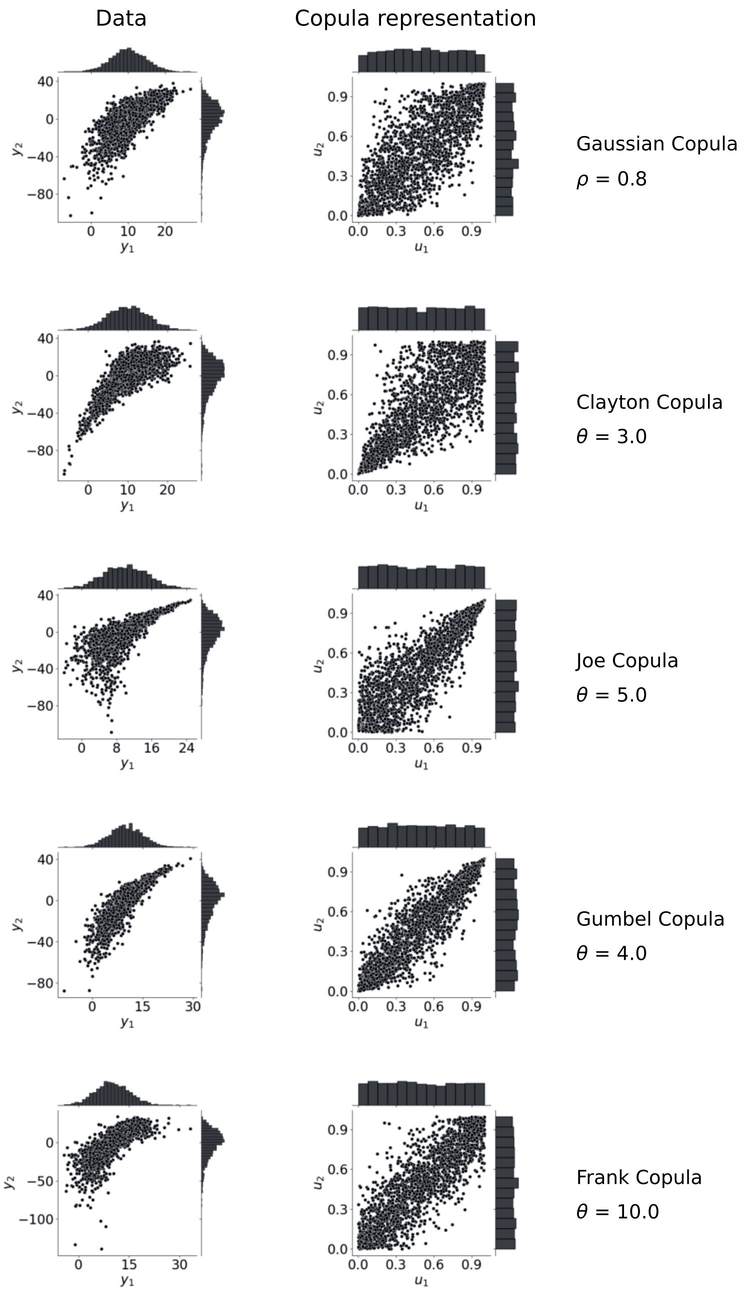

Figure 2.8: Data and copula representation - different used copulas - one parameter

2.5. Non parametric Bayesian Networks

A Bayesian Network (BN) is a graphical model that represents a joint distribution in a compact way. A BN consists of a *directed a-cyclic graph* (DAG) whose nodes represent random variables and arcs represent probabilistic dependence between the nodes. This research is restricted to the class of NPBNs which are well described by Hanea et al. (2015) [52]. NPBN in this research is implemented using the toolbox `BANSHEE` which is available in `Python` and `MATLAB` ([53, 54]). NPBNs have been used in different fields of application such as hydrology (Paprotny, 2017 [55]) and flood risk (Paprotny et al., 2017 [56] and Couasnon et al., 2018 [57]). In order to assess the civil structures, NPBN are applied in [26, 58, 59] to model the weight in motion data as a result of traffic load. An application of this weight-in-motion model is used in the reliability assessment of an SFT, published by Torres et al. (2022) [38] and presented in 5, and by Mendoza-Lugo et al. (2019) [25] to assess the reliability of bridges.

This specific class of BNs, NPBNs, is based on copulas, which are briefly explained in Section 2.4. One attractive feature of copulas is that they allow one to separate the dependence from the influence of the margins. Many types of copulas are available and are described in detail by Joe (2014) [60] and in Section 2.4. In the NPBN framework, bivariate Gaussian copulas are used to assemble the joint distribution. The bivariate Gaussian copula is $C_\rho(u,v) = \Phi_\rho\left(\phi^{-1}(u), \phi^{-1}(v)\right)$ where $(u,v) \in \mathbb{R}^2$, ϕ^{-1} is the inverse standard normal distribution and Φ_ρ is the bivariate Gaussian distribution with correlation coefficient ρ. An NPBN is an BN where the nodes are associated with a (typically) continuous random variable (X_i) with an invertible distribution function. Discrete random variables which preserve order may also be used in some cases. The direct predecessors of a particular node in the DAG are the "parents" of the "child" node. Arcs are directed from parents to children. The arcs of the BN are associated with (conditional) Gaussian copulas which are parameterised by (conditional) Spearman's rank correlations. The Spearman's rank correlation coefficient is the usual Pearson correlation coefficient computed with the ranks of the variates (instead of the original units). For every node X_i with a non-empty ordered set of parents $pa(X_i) = \{i_1, \dots, i_p\}$, conditional rank correlations are assigned according to the following equation 2.2.

$$\begin{cases} r_{i,i_{p-k}} & \text{if , } k = 0 \\ r_{i,i_{p-k}|i_p,\dots,i_{p-k+1}} & \text{for , } 1 \leq k \leq p-1 \end{cases} \tag{2.2}$$

Due to its construction, a rank correlation in [-1,1] can be assigned to any of the arcs of a NPBN. This assignment will lead to a valid rank correlation matrix. Once the NPBN has been configured, a unique joint distribution is determined. Using this joint distribution, efficient sampling is possible. In addition, exact inference or conditioning (analytical updating of the joint distribution) is also possible given the copula assumption.

2.6. Vine copula

Similarly to a NPBN, a Vine copula (VC) is also a graphical probabilistic model. VC consists of a vine structure, *Regular Vine* (RV) and bivariate copulas to model multivariate distributions. In many fields of applications where complex probabilistic dependencies occur, VCs are used in many publications [61–66]. It is essential to select an RV structure that represents the dependencies in the data set. In this research, the selection of the RV that best represents the dependencies is based on Akaike Information Criteria scores, which is explained later in this section by Equation 2.3. The number of variables dictates the number of possible unique RV structures, Morales (2010) [67] presents the relation between the number of variables and possible RV structures: $\#RV = \frac{d!}{2}2^{\binom{d-2}{2}}$, in which d is the number of variables. To use brute force to test all RVs for the given dataset, the Atlas *Chimera* containing all RV up to eight variables, including their permutations, has been compiled and presented by Morales et al. (2023) [35]. By itself, an RV structure V on d elements (variables or edges) is built up out of d-1 sequential trees($T_1, \dots, T_{d-1}$). Each tree is built up out of d variables and $d-1$ edges, with the sequence between the trees arranged by:

1. T_1 is a tree with the initial variables set $N_1 = \{1, \dots, d\}$ and edge set $E_1 = \{1, \dots, d-1\}$,

2. For sequential trees: $j \geq 2$, T_j is a tree with variable set $N_j = E_{j-1}$ and edge set E_j is defined,

3. For the edges in the sequential trees: $j = 2, \dots, d-1$ and $\{a, b\} \in E_j$ it must hold that $|a \cap b| = 1$.

Property 3 ensures that if there is an edge e connecting variables a and b in tree T_j, $j \geq 2$, then a and b (edges in T_{j-1}) must share a common variable in T_{j-1}, this can be referenced as the *proximity condition*. As a consequence, an RV on d elements is only valid if an edge in tree $j+1$ shares a common node in tree j. For $e \in E_j$, the subset of $N_1 = \{1, \dots, d\}$ reachable from e by the membership relation can be considered as the *constraint set* associated with e and is the complete union U_e^* of e. For $j = 1, \dots, d-1$, $e \in E$ if $e = \{i, k\}$ then the *conditioning set* associated with e is $D_e = \{U_i^* \cap U_k^*\}$ and the *conditioned set* associated with $e = \{C_{e,i}, C_{e,k}\} = \{U_i^* \setminus D_e, U_k^* \setminus D_e\}$. Note that for $e \in E_1$, which is the edge set for the first tree, the conditioning set is empty. Note also that the order of an edge is the cardinality of its conditioning set. For $e \in E_j$, $j \leq d-1$, $e = \{i, k\}$ $U_e^* = U_i \cup U_k^*$ is found. In summary, the variables of T_1 reachable from a given edge through the membership relation are elements of the constraint set of that edge. When two edges in sequential tree T_j for $j = 2, \dots, d-1$ are joined by an edge in T_{j+1}, the intersection of the respective constraint sets forms the conditioning set. The symmetric difference of the constraint sets is the conditioned set of this edge. Figure 2.9 shows a graphical representation of an RV with 5 variables as an example. Individual RV are represented by upper triangular matrices. The database *Chimera* contains all RV up to 8 variables. The matrix representing the RV is the *matrix representation of a regular vine* and can be called *regular vine matrix*. As mentioned above, `PyVineCopulib` is used and between different packages the notation of the

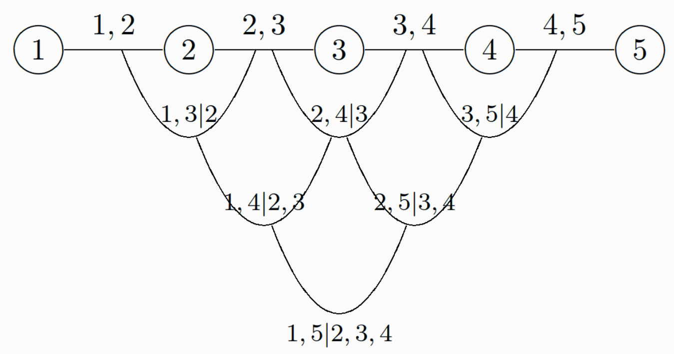

Figure 2.9: Regular Vine with 5 nodes

matrix varies in orientation. The matrix M represents the RV of Figure 2.9.

$$M = \begin{bmatrix} 2 & 3 & 4 & 5 & 5 \\ 3 & 4 & 5 & 4 & 0 \\ 4 & 5 & 3 & 0 & 0 \\ 5 & 2 & 0 & 0 & 0 \\ 1 & 0 & 0 & 0 & 0 \end{bmatrix}$$

RVs are categorised in a systematic way and are classified according to their tree equivalent class. As each regular vine structure is built out of trees, the trees itself have a shape. This principle is used to categorise the RV. Morales (2010) [68] shows in Appendix A a catalogue of trees and tree-equivalent regular vines up to 8 variables. A regular vine on 8 variables is built up by a tree of 8 nodes in the first tree, 7 nodes in the second, and up to 2 nodes in the last tree. The sequence of sequential trees results in equivalent vines and uses the naming convention of Tx + Tx + Tx + Tx + T3 + T2, in which x refers to the shape of the tree. All tree equivalent regular vines differ up to the fifth tree, which has four nodes, because all vines with three and two variables are equally shaped, respectively, T3 and T2. For regular vines with 8 variables, 1464 different tree equivalent vines can be defined. A more detailed description of the RV structure is published by Morales et al. (2023) and Cooke et al. [35, 69].

Selection of Regular Vine

As presented in Section 2.6, an RV consists of subsequent trees built out of copulas. More precisely, a RV consists of 3 elements:

- RV structure, consisting out of the sub-sequential trees
- Bi-variate copulas for each of the edges in the RV structure
- Estimation of the parameters of the bi-variate copulas

The RV that performs ”best” in describing the data is measured by the Aikaiki Information Criterium (AIC) score as presented by Akaike (1998) [70]. The AIC score is calculated by the number of parameters in the model and the maximum likelihood of the model, as presented in 2.3. In which k is the total number of parameters and $\ln(\hat{L}$ the log-likelihood of the model. The model is considered by the lowest (most negative) AIC. If a model uses copulas with more parameters, it will result in a penalty in the AIC score (less negative).

$$\text{AIC} = 2k - 2\ln(\hat{L}) \tag{2.3}$$

As the number of possible structures increases extremely quickly with the number of variables, algorithms have been developed to estimate an RV structure. The most widely used method, which has also been implemented in `PyVineCopulib` and used in this research, is known as the sequential method and is presented by Dissmann et al. (2012) [33]. In this method, the first tree is selected by considering data-pairs with the strongest dependencies. For all pairs, empirically the absolute Kendall τ values are used. From this information a spanning tree is obtained in which the sum of the absolute values of Kendall's τ is maximised. For the next tree, the same sequence is used in which Kendall's τ is conditionally calculated. After finding the complete RV structure, the bivariate copulas are fitted to the pairs, completing the definition of the RV. For the first tree, the copulas are fitted and for the next tree the conditional observations are calculated using the conditional distribution functions of the parents of the previous tree. Sequentially, all other vines are fitted for the higher trees. This procedure is presented by [61]. Due to the independence between trees in this method, it is not guaranteed that the best RV is found in terms of AIC, this is already concluded by Dissmann et al. (2012) [33], stating that the lowest trees have the greatest influence on the overall fit and thus it is important to have the largest dependency early in the RV. In addition to this method, alternative methods, which are less commonly applied, have been developed. Csazo et al. (2013) [71] uses fitted pair copulas based on the highest p-value[1] of a goodness-of-fit test; in this method, first all copulas between the variables must be estimated. The p-values are used as edge weights for the sequential R-Vine selection procedure. Kurowicka (2010) [72] uses an opposite approach to the common algorithm, starting with the highest tree with the lowest dependency and sequentially working to the first tree. In this research, to find the RV that fits best with the data in terms of the AIC score, a brute-force approach is used. The RV atlas for up to eight variables is presented by Morales et al. (2023) [35]. The database is made publicly available for `Python`, `Mathlab` and `R` [3]. In 6, data sets of eight variables are fitted and compared with the most widely used method. Both methods have in common that after an RV is found the bivariate copulas are fit. The main difference is that using the algorithm, only one RV structure is tested based on dependency, while in the BF approach all RV structures are tested.

[1]The p-value indicates the difference between the empirical data distribution and a theoretical distribution. Lower p-values indicate a low fit, and higher values closer to 1.0 indicate a well fit

2.7. Gaussian random fields

Spatial covariance indicates that a local value of a particular parameter is correlated with neighbouring values of the same parameter depending on the spatial distance between locations. The distance between two points dictates to what extent the values at the two locations will vary. Abrahamsen (1997) [73] gives an overview of the properties of Gaussian Random Field (GRF) properties, which is based on Vanmarcke (2010) [74]. Recent developments and advances are presented by Liu et al. [15]. In this research, GRFs are applied to simulate spatial variability in tunnel foundation of immersed tunnels. If the distance between two points increases, the covariance (statistical correlation) decreases exponentially. The covariance between two points in a grid is defined by the covariance length (L_{cov}) as expressed in equation 2.4, in the example with 0.5, 1 and 2, which shows these different covariances over the distance between points. To illustrate this dependency, for 3 hypothetical situations, three covariance length functions over distance have been plotted in Figure 2.10.

$$cov((x_1, y_1), (x_2, y_2)) = e^{-\sqrt{\pi}/2 \frac{\sqrt{(x_2-x_1)^2+(y_2-y_1)^2}}{L_{cov}}} \tag{2.4}$$

$$f_X(x_1, ..., x_n) = \frac{e^{-\frac{1}{2}(x-\mu)^T \Sigma^{-1}(x-\mu)}}{\sqrt{(2\pi)^n |\Sigma|}} \tag{2.5}$$

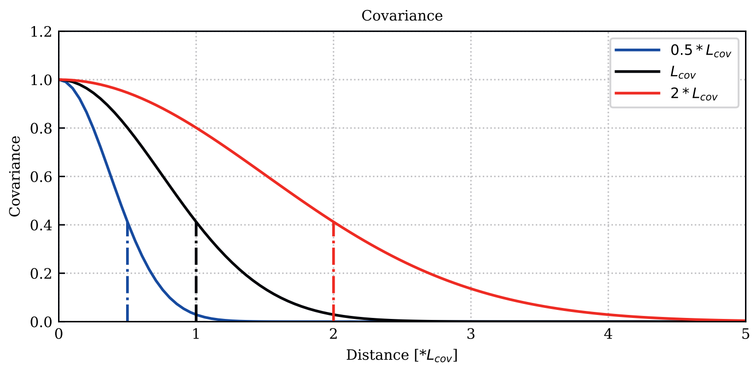

Figure 2.10: Covariance based on covariance length

The actual covariance between individual locations is dictated by L_{cov}. If the covariance length is halved, the covariance between two points decreases faster; in contrast, if the covariance length is doubled, the covariance between two points decreases more slowly.

For a hypothetical surface, which is discretised to n_x times n_y in which n_x is the number of points in the longitudinal direction and n_y in the lateral direction, the total number of points n is defined as $n = n_x \cdot n_y$. The covariance matrix Σ contains information on the covariance between all points within the grid defined by n_x and

n_y. The factor $\frac{1}{2}\sqrt{\pi}$ in the equation 2.4 is the scaling factor that can be adjusted for the representation of the model.

If all distances between all points are available in a distance matrix, the covariance matrix Σ can be found in which the covariance is defined for each connection. Using eq. 2.5 a multivariate Gaussian distribution can be found and samples can be generated given L_{cov}. A sample of the field can then be transferred to any other distribution using a quantile transformation in which the quantiles of the normalised Gaussian distribution map to the quantiles of the target distribution. For a 100x100 grid, four different GRFs ($\mu = 30, \sigma = 10$) have been generated ($L_{cov} \in [1, 10, 10, 1000]$), and is presented in Figure 2.11. If L_{cov} is small compared to the dimensions, a spike pattern can be observed, if L_{cov} is large compared to the dimensions a low variation over the area can be observed. For the generation of GRF in this research, the `GSTools`, a toolbox for geostatistical modelling in `Python` is used [75].

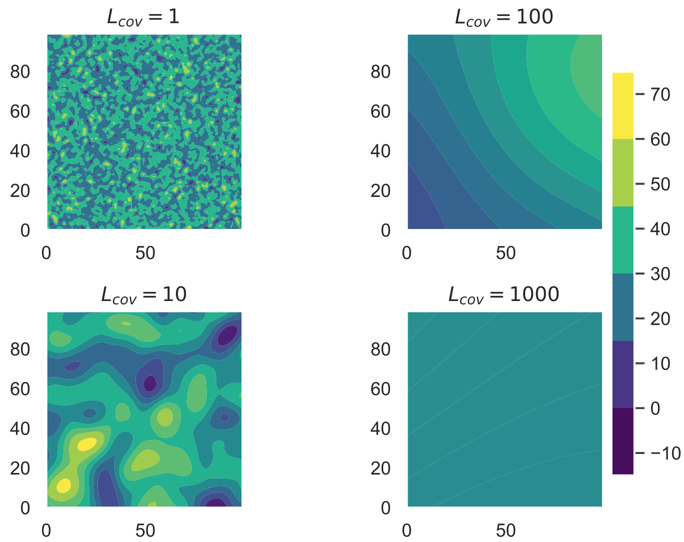

Figure 2.11: Hypothetical Gaussian Random Fields

The application of GRF is still uncommon in the designs of tunnel foundations. By nature, the soil parameters will develop continuously throughout the area. Special circumstances like faults and other exceptions will give rise to discrete transitions but are not considered in this research. The trench is dredged to immerse the tunnel in it, and by itself the dredging process has a tolerance. After dredging, a gravel layer is applied to the required level or a sand foundation is applied using a sand-flow operation. In Chapter 4, a gravel layer is used, while the method can be adopted, with other requirements and specific installation issues, for sand-flow foundations. Soil variables, such as stiffness and level of dredging, which are directly related to the thickness of the foundation layer, are spatially correlated and can be described using GRF.

3

Target reliability of submerged floating tunnels

3.1. Introduction

In this chapter, an outline of the reliability of SFT structures is presented and the contrasting elements that can be found in defining requirements. SFTs have not been built on a functional scale yet, let alone a relatively small demonstration project at Qingdao Lake with a length of 100 m [6]. Obviously, this structure is a new kind of structure, but it has elements of other types of long term existing structure types:

- Road bridge
- Road tunnel (land or river crossings)
- Fixed off-shore platforms
- Floating off-shore structure (platform or bridge)
- Passenger ship
- Submarine
- Dike ring

All of these applications have different types of load, consider failure in different ways, and in some cases use different types of buoyancy balance. Typical loads which will act on the structure are:

- Dead and live loads
- Hydrostatic and hydrodynamic loads
- Static buoyancy
- Responsive buoyancy
- Active (de)ballasting

Table 3.1 gives a brief overview of these structural types and their mutual differences. The structures face different risks and for reliability analysis the following risks might become relevant, but are not applicable to all of them:

- Structural failure
- Flooding
- Fire
- Explosion
- Collision inside and outside the structure

Table 3.1: Type of structures and their differences

Type of structure	Structural loads	Hydrostatic loads	Static buoyancy	Responsive buoyancy	Risk of structural failing	Risk of flooding	Risk of structural loss through flooding	Static buoyancy	Length effects	Length effect in reliability
Road bridge	x				x				x	
Road tunnel (land)	x				x	x	x		x	
Fixed off-shore	x	x			x					
Floating off-shore	x	x			x					
Passenger ship	x	x		x	x					
Submarine	x	x		x	x			x		
Dike ring	x	x				x			x	x
SFT tethered	x	x	x		x	x	x	?	x	x
SFT pontoon	x	x		x	x	x	x	?	x	x

The risks of an SFT structure can be seen in parallel with a regular tunnel. PIARC [76] published a road tunnel manual and gives an overview of safety principles, hazards, measures, and tools for safety management. Figure 3.1 shows an overview of typical incidents, which affect the tunnel and tunnel users, and the relationship with failure. In this figure, all incidents are considered, even incidents that are not significant. Significant incidents are categorised as events that have the potential to develop into events with serious consequences to the health, life of people, the environment, or the tunnel. In the figure, fires and collisions are specifically highlighted and get also specific attendance in the manual of PIARC. The definition of significant incidents differs globally from country to country. The failure of the tunnel can be identified as the non-availability for a certain period of the tunnel for the public. For example, in the case of fire or collision, traffic would be temporarily blocked, and after resolving the blockage, the tunnel is reopened for traffic. In specific cases, the tunnel could also fail structurally, for example, due to an external collision, failure of the support system, or an internal cause such as an explosion causing mayor leakage. Additionally, incidents which are significant but do not lead directly to a failure (small collisions, for example) could evolve to a failure as non-availability. In addition, smaller significant incidents can even lead to structural failure; for example, a vehicle fire could result in a structural failure, as high-temperature load influences the structural behaviour (expansion) and the material behaviour of the tunnel (splash).

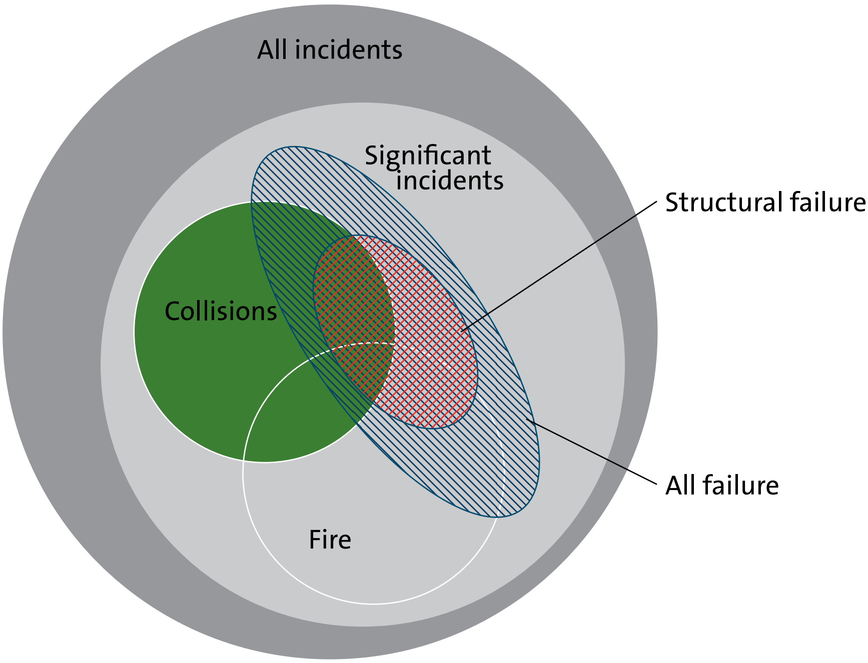

Figure 3.1: Schematic incident and failure overview

In general, non-structural risks can be more easily mitigated during lifetime, e.g., just by installing new Mechanical and Electrical systems (M& E) like ventilation and sprinklers for fire, but also traffic policies like platooning (driving in a convoy of trucks) with hazardous goods or even prohibiting certain traffic to pass the structure. Regular tunnels are currently designed and constructed for decades or more than a century, especially tunnels under water (immersed) or in soil (bored). The options to improve structural reliability during their service life are limited; for example, thickening the structure, adding reinforcement, or even repairing the structure is a complicated or even impossible task. When designing a structure, all future developments concerning structural reliability over the lifetime should therefore be considered. Currently, in Europe, most structures in the infrastructure system have been built in the period after World War II with an intended lifetime of 50 years. These structures have, in the meantime, exceeded their expected lifetime and assessment programmes are conducted throughout Europe. In this assessment, not only the original capacity is considered, but also changes in terms of magnitude and frequency of the loads, and the development of the traffic over time.

In this chapter, first, the distinction between the different types of structure with similar behaviour or applications is described. Sequentially, the deduction of the target reliability for these structures is explained followed by current reliability approaches. Finally, the different limit states and other relevant aspects in relation to the target reliability are presented. The chapter ends with a conclusion and an approach to derive the target reliability for an SFT.

3.2. Review of different fields of application

Road infrastructure

Road bridges and tunnels are infrastructure objects. The expected lifetime for these structures is currently 100 years or more and once they are part of the network the impact of a potential non-availability of failure will cause large economic consequences. In terms of standards, such as the Eurocode [1], the consequence class for this type structure is set to the highest class. Obviously, this kind of structure is subject to loads as defined, for example, by self-weight, other permanent loads, and variable loads from traffic. Immersed tunnels are experiencing permanent soil and water pressures, as well as deformations due to settlement. All loads are predominantly static and can be treated as static. Immersed tunnels are loaded with dynamic hydraulic loads only in the construction phase.

The 'failure' of road structures is strongly related to structural failure; on the other hand, a temporary non-availability of the structure can also be considered as failure. Non-availability is generally not considered in the structural reliability of tunnels. However, non-availability can be an important aspect in the total reliability of a road structure.

For immersed tunnels within the road structures, buoyancy loads are taken into account in equilibrium limit states (EQU). Road structures like bridges and tunnels can have a considerable system length; however, in current engineering practice, this length effect is not considered in the reliability analysis other than in longitudinal force distribution such as span lengths. The failure of a cross section must meet the target reliability criterion. The fact that there are many cross sections is not explicitly counted for in the target reliability definition.

The risk and reliability of road structures are prescribed by codes and standards, as in [77]. Depending on the consequences, a target reliability is set to the structure which corresponds to the probability of failure of the structure. Formally, the defined target reliability has no relation with other threats, leading to non-availability, but not leading to structural failure. The design of such structures is generally carried out using a Load Resistance Factor Method (LRFM), which is a basic approach in several codes and standards such as in [1, 78].

Off-shore structures

Offshore structures serve various purposes and can be fixed to the bottom in shallow areas or can be floating. Oil and gas depletion can be carried out at large depths. In these circumstances tether systems can be applied, or the structure can be structurally fixed to the sea bed with column structures. Off-shore constructions will experience hydraulic loads such as waves and tidal effects. For certain, this will have different effects on floating offshore structures than on fixed offshore structures.

The failure of offshore structures can be considered a structural failure. The consequences are different; environmental damage can be severe. The life-time of these structures is usually shorter than that of road structures. The risk related to a large number of direct fatalities is smaller. On the offshore structure, less people will be present than in or on a road structure and they are voluntary and economical dependent on it. The risk and reliability approach is similar to road structures, based on a consequence class, a target reliability is set, and it is found in different standards, such as [79].

Ships

Ships have been used over the ages to transport people and goods, not only in the inland, but also across the seas and oceans. The external loads on the structure are related to the weather and wave loads. Internally, ships are loaded with self-weight and cargo loads. The initial buoyancy is passive, the weight of the ship together with all vertical loads equalise the weight of the displaced water (Archimedes force). If the ship is loaded or unloaded, the buoyancy force will increase or decrease (responsive buoyancy). Ships can be equipped with ballast tanks to ensure equilibrium and for stabilising matters. By actively adjusting the contents of the ballast tanks, the buoyancy is changed reactively.

The risk acceptance criteria are established by the decision makers. The Marine Safety Committee of the International Maritime Organisation has published a Formal Safety Assessment (FSA) in [80]. In this assessment, the risk on ships in maritime circumstances can be objectified into two main parts;

- the risk of accidents with fatalities
- cost benefit optimisation

The risk of accidents is based on operations, weather, technical, and human errors, and other circumstances. Different kinds of hazardous and acceptable risks can be assessed. The acceptance of risk of a fatality is described by the so-called F-N curves. Conventionally in a Cost-Benefit Assessment (CBA), the benefits should be larger than the costs. In a CBA, all risks are described in monetary units. Often, also a Cost-Effectiveness Analysis (CEA) is conducted. A CEA describes the relationship between costs and benefits and does not quantify the benefit. The value judgment is up to the decision maker by implementing mitigation measures or risk control options (RCO).

One could argue the Cost Benefit Assessment, because of the question "how to value a fatality?". If that is related to age, for example, a child or an elderly person would be worth nothing (low replacement costs) related to someone just starting working after finishing his or her education (prepared to contribute to society). In CEA the Implied Costs of Averting a Fatality (ICAF) can be proposed, as presented in 3.1.

$$ICAF = \frac{\Delta Cost}{\Delta Risk} \tag{3.1}$$

With $\Delta Cost$ as the additional costs of the mitigation matter and $\Delta Risk$ as the reduced risk in terms of the number of fatalities. For this thesis the structural reliability of ships would be of interest. In ship designs strength of component is verified, including the strength of the complete hull. Apart from that the stability of ships is an important element in the design. Ships shall be able to righten themselves in severe dynamic sea states. Stability codes indicated that the stability of a ship is never sufficiently guaranteed by the properties of the 'structure'. The propulsion and navigation systems and a trained crew are indispensable to avoid loss (or failure).

Submarine vessels

Naval submarine vessels are designed to sail underwater and actively regulate buoyancy. People within the submarine will be in the vessel for a longer period than a vehicle on or in the road structure. Failure is considered if the structure fails, when it floods, for example, because of a failing buoyancy system.

The environmental damage might be severe in the event of failure in the case of the use of nuclear power resources within the vessel. Safety measures to mitigate risks and therefore influence the risks and reliability of the structure might be applicable to other types of structures. Incidents and vulnerabilities related to war and armed operations are excluded in this summary.

For security reasons, it was not possible to find any risk approach on these types of structure or vessels. In DNV's naval vessel classification [81], it is mentioned that an adequate risk analysis should be provided and sets the probability of failure or fatalities only qualitatively in terms of minimisation and leaves the decision to society. The use of mitigation measures used in naval submarines could be used in the safety design of SFT, but that is beyond the scope of this research.

Flood defences

A dike ring or a flood defence, in general, is a passive system that protects against floods of the area behind it. These structures can fail in several ways, such as hydraulic overload beyond the defined hydraulic limiting conditions, or geohydrologic, geotechnical causes. Over-topping of a gate is a failure mode that does not have a structural cause (but could lead to structural failure though), but the dike ring fails in its function.

The dikes are geotechnical structures that experience hydraulic loads. The dike structures are stretched over a certain length. Their structural safety is considered in cross sections. However, along the dike structure, a variation of different parameters can be expected. The soil conditions will vary over length and the load will differ over length. Therefore, spatial variation is relevant and is accounted for in the target reliability of the structure.

Damage caused by a failure of a dike could be large, because dike rings protect large areas and a lot of people behind it. The probability of failure for overtopping is related to water levels and their probability of exceeding during events with certain recurring times. The probability of failure in relation to the consequences defined as the number of fatalities is described by an FN-curve. With an increasing number of fatalities, the probability of failure should decrease, as presented in figure 3.2. For spatial variability, the reader is referred to Schweckendiek et al. (2017) [82] and Jongejan et al. (2020) [83].

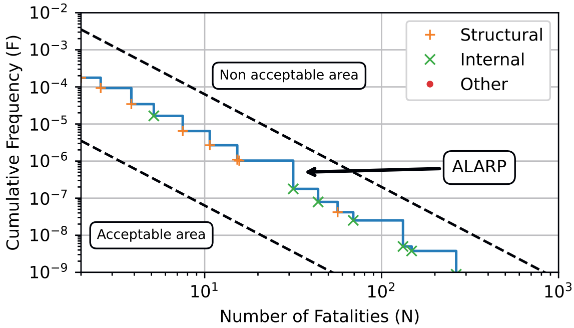

Figure 3.2: FN-Curve

Submerged Floating Tunnels

As for the structures mentioned above, the SFT structure is loaded by structural loads and by static and dynamic hydraulic loads. The tethered SFT only has a passive buoyancy by itself, and the underwater volume does not change when the structure is loaded. The buoyancy of the pontoon-supported system is responsive. Both systems could be used with an active buoyancy system with which the buoyancy could be regulated. Compared to a traditional immersed tunnel, the structural failure of a section of an SFT threatens the equilibrium of the structure, as it will influence the buoyancy weight ratio. All objects in the structure that contribute to this equilibrium and prevent leakage into the structure or threats to the support systems are potential hazards to the total failure of the structure. Considering leakage and ultimately flooding of the structure, typical threats are, but are not limited to, damage to the section such as cracking caused by overloading, collisions, earthquakes, and tsunamis. It is recommended to equip SFTs with responsive buoyancy systems to anticipate these events and mitigate the risks related to meeting the target reliability requirement. The support system is threatened by external hazards. Similarly, overloading the supporting structure due to collisions, waves, and currents, tidal effects, could hazard the system and ultimately result in total system failure. Considering the support system, redundancy will improve the robustness of the structure.

In the context of the Bjørnafjord feasibility study [39], the risk and reliability of SFT have been calibrated by Baravalle (2016, 2019) [84, 85]. The calibrations show that the results, which are based on optimisation, do not contradict [77], however, the acceptance criteria for fatalities are not covered.

Having presented the list of structure types as in Table 3.1, it is obvious that SFT structures in general are comparable in various aspects to the other types of structures. However, none of the other common types of structures is completely equal in terms of loading, buoyancy, structural failure, and considering the effect of length. Therefore, an SFT can be identified as a special structure that does not meet the standards specifically meant for any of the application fields. The usual approach prescribed by these standards is based on the Load Resistance Factor Method (LRFM). If the codes could be made applicable to SFT's, different boundary conditions could be used to determine safety or material factors. However, it is questionable whether an LRFM approach is achievable for the SFT structure.

In cases in which regular standards such as [1, 78], which usually uses the LFRM defined by [86], are not easily applicable, a different and more fundamental approach is needed for the design of such a structure. From a structural reliability point of view, the probability of failure for SFTs must match the probability of failure of structures that have a comparable user population and the same kind of service application. An SFT that serves as an infrastructure and is in that sense comparable to a regular bridge or tunnel. However, just applying the regular standards on SFT can be argued, the current standards are validated and calibrated for traditional wind and traffic-loaded structures. An SFT structure is a one-of-a-kind structure and will require a separate and dedicated validation of the reliability of the structure. This can be accomplished by using different approaches as described in ISO 2395 [86] and JCSS probabilistic model code [77], this will be further specified in the following paragraphs.

3.3. Target reliability

The reliability of a structure may vary in time but shall at all times be higher than the target reliability, this reliability is established by the reliability index (β) as a statistical measure. The reliability index is defined by the cumulative Gaussian distribution ϕ, which relates β to the probability of survival $(1 - P_f)$ (Equation 3.2 and Figure 3.3). In order to translate the reliability index to different reference periods, equation 3.3 is applicable in which β_1 and β_n the reliability indices are for respectively 1 year and n years.

$$P_f = \phi\left(-\beta\right) \tag{3.2}$$

$$\phi(\beta_n) = \left[\phi\left(\beta_1\right)\right]^n \tag{3.3}$$

The target reliability is the desired minimum reliability level, which can be determined on the basis of several considerations. For different applications, according to consequences, the target reliability differs. For different fields of applications, the different aspects are considered. For civil structures, the target reliability is prescribed by different codes and standards and varies for different geolocations and applications; a more detailed view of the target reliabilities is given by Schweckendiek et al. (2018) [87].

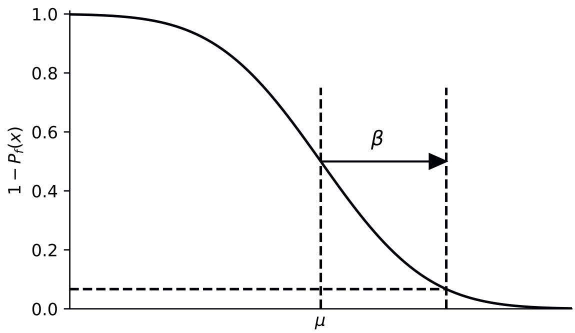

Figure 3.3: Reliability index in the cumulative distribution function for the probability of survival

A possible analysis for a choice of a target reliability is an economic analysis of risk of damage and/or failure and cost of repair and/or replacement. The target reliability based on this analysis is dependent on interest rates and inflation of monetary value. This method is a straightforward analysis if no large amount of injuries or fatalities are to be expected. As a result, building cheap structures deliberately not designed against high rare loads can be economically justified. When loss of a structure would impose the risk of a large number of fatalities, this must also be considered. Although this approach is debatable as the value of human life need to be quantified in a monetary value.

The risks themselves can be categorised by the economical risk, the personal risk, and the societal risk; these risks in relation to tunnels are discussed in Section 3.4.

For primary dikes in the Netherlands, the target reliability is regulated by law and is based on risk, costs, and societal acceptances. In high-risk areas (such as highly densely populated and important economic areas), the annual probability of failure (total failure leading to inundation) is set to 10^{-4}, for less vulnerable areas, this is set to 3.3^{-4}, and for low-vulnerable areas the probability is set to 1^{-3}. For buildings and infrastructure in Europe, the same kind of consideration is applicable. In Eurocode EN 1990 [1], there is a distinction in consequence classes 1 to 3, in which consequence class 1 has low consequences for the safety of people, class 2 considers normal risks for people, and class 3 considers a high impact on society in the case of failure. The deduction of the target reliability is based on the annual probability of failure, which are respectively for consequence classes 1 to 3, 4.2, 4.7 and 5.2.

As a base case for civil structures in general, consequence class 2 for a reference period of 50 years is used, a minimum target reliability of 3.8 is required. This corresponds to a probability of failure of 7.2^{-5} in 50 years. For class 1 and class 3, the required target reliabilities are 3.3 ($P_f = 10^{-3}$) and 4.3 ($P_f = 10^{-5}$) respectively. However, in the table, the required reliability indices are set for 50 years, while tunnels and bridges currently have a expected lifetime of 100 to 120 years. Today, tunnels in

Europe require a reliability index of 4.8 ($P_f = 10^{-6}$) for structural failure, as it is usually part of vital infrastructure with a long estimated lifetime of 120 years. Currently a new version of EN1990 is being developed, in this document there is a distinction into 5 consequence classes (CC0 to CC4). CC0 considers a very low probability of loss of life or personal injury or an insignificant economic, social, or environmental consequence. In contrast, CC4 considers an extreme qualification in fatalities and in juries and huge consequences for the economy, society, or environment. In the concept version, no quantification of the reliability index is given for CC0 and CC4. For CC1 to CC3, the quantification is similar in both versions. However, for the load factors for CC3, a distinction is made. CC3 is divided into CC3a and CC3b for bridges and associated geotechnical structures. CC3b is meant for situations where an increased level of reliability is needed, and CC3a is meant for bridges on and over railways and over and under major roads. Structures in consequence class CC4 are not covered, and additional provisions to those given by Eurocode may be needed. There is no specific distinction for tunnels in both EN1990 versions, but tunnels can be categorised equally as bridges, as they are part of the infrastructure system.

Table 3.2: Relation between target reliability and probability

P_f	10^{-1}	10^{-2}	10^{-3}	10^{-4}	10^{-5}	10^{-6}	10^{-7}
β	1.28	2.32	3.09	3.72	4.27	4.75	5.2

An overview of the reliability indices (annual and lifetime) for the ultimate limit states is presented in Table 3.3. In relation to these reliability indices, the requirements for the design of structures are specified in the applicable codes and standards. In the Eurocode standard, the Load Factor Resistance Factor method (LRFM, see also Section 3.5) is used and the different consequence classes are used to define load factors in the ultimate limit states, which are increased with the reliability index with multiplication factor $K_f i$ (CC1: $K_f i$ =0.9, CC2: $K_f i$ =1.0, CC3: $K_f i$ =1.1) . For specific circumstances, this method does not suffice, for example, if a structure has a consequence class larger than level 3. In addition, structures that do not fit within the boundaries set by actual codes and standards might require a different probabilistic approach than the LRFM. For example, high-rise buildings that have a length higher than heights covered by wind tables, but also structures to which unusual loads or load combinations apply, such as SFT structures.

3.4. Risks in tunnel structures

Arends et al. (2005) [88], Geyer et al. (1995) [89], Mashimo (2002) [90] and Diamantidis et al. (2000) discuss risks in tunnel structures. Typically, three types of risk can be identified; the personal risk, the societal risk, and the economic risk that can be related to the incidents shown in Figure 3.1. In current tunnel structures, risks can be identified internally and externally. Internal hazard refers to events in the tunnel, such as fire, terrorist attacks, etc. External hazards concern external loads on the tunnel, such as soil and water loads. Both might lead to identified risks. If related to failure, for example, a fire in the tunnel might lead to a large number of fatalities, but

Table 3.3: Lifetime target reliability indices for the ultimate limit state from literature

Source	Application	Consequence classes				
		A Low	B Some	C Considerable	D High	E Very High
ISO 2394 (1998) ISO 23822 (2010)	All All	Small 2.3	Some 3.1		Moderate 3.8	Great 4.3
EN 1990 (2002)	All		RC1 3.3		RC2 3.8	RC3 4.3
SANS 10160 (2010)	All	RC1 2.5	RC2 3	RC3 3.5		RC4 4
NEN 6700 (2005)	All		Class 1 3.2	Class 2 3.4	Class 3 3.6	
ASCE (2010)	All	I 2.5	II, III, I 3.0/3.25/3.0	IV, II, I 3.5/3.5/3.5	III 3.75	IV, II, III IV, II, III IV 4.04/4.0/4.25/4.5
NBCC (2010) CDHBDC (2014)	Buildings Bridges		Low 3.1	Typical 3.5	High 3.7	
STOWA (2011)	Hydraulic	QC I 2.3	QC II QC III 2.7/3.1	QC iV 3.4	QC V 3.7	
TAW (2003)	Hydraulic				River dike 3.8	Sea dike 4.3
ROM 0.5-0.5 (2008)	Geotechnical	Minor 2.33	Low 3.09		High/Very high 3.72	
CUR 166 (2012)	Sheetpiles	Class I 2.5		Class II 3.4		Class III 4.2
OCDI (2009)	Marine	Normal 2.19/2.67	Intermediate 2.67		High 3.65	
CUR (2003)	Quay walls		Class 1	Class 2	Class 3	
CUR (2013)	Quay walls		RC1 3.3		RC2 3.8	RC3 4.3

might not lead to structural failure. On the other hand, if a joint leaks and the tunnel slowly begins to flood but all people could escape, but the fully flooded tunnel could lead to collapse and structural failure of the tunnel, the failure is identified. Both situations consider failure, but only one of the concerns concerns structural failure. Of course, there are many scenarios that can be identified in all types of combinations of number of casualties and structural failure.

In regular codes and standards for building structures, such as Eurocode, structural integrity is the main focus. There is a difference in the approach considering the failure of the structure (structural reliability) and the acceptable personal risk. Thus, in the latter objective, the structure can still be reliable, but it cannot be safe. Man could think of situations such as fire, collision, or other types of failure.

Personal risk

The personal or individual risk is concerned with the probability of mortality of an individual. In case of tunnels, two different types of individuals can be identified; people who are voluntary using the tunnel (passengers, employees) and external people, people living in the surrounding of the tunnel facing consequences of a hazardous event. The acceptable probability of death differs depending on the location, but in the Netherlands the acceptable individual risk for a tunnel can be expressed as in equation 3.4. In this formula β indicates the degree of voluntariness (employees

$\beta = 1.0$, passengers or users $\beta = 0.1$, and external people $\beta = 0.01$).

$$\text{IR} < \beta 10^{-4} \left(year^{-1}\right) \tag{3.4}$$

The personal risk can be based on a significant incident like a collision or a fire, but does not necessarily cause a structural threat and consequently structural failure.

Societal risk

In the consideration of societal risk, the probability is related to the amount of casualties caused in the case of a hazardous event. Usually hazardous events to be concerned for societal risks can be categories as ”high impact with low probability”. The F-N curve as presented in figure 3.2 gives an indication of the probability of this kind of events. The figure indicates all types of failure as presented in figure 3.1, the area on the lower left part of the graph can be identified as acceptable risks and the upper right part as non-acceptable. Combinations of probability and number of fatalities can be identified as to whether they are acceptable or not. However, in some cases, it can be discussed and the risk level can only be as As Low As Reasonably Possible (ALARP). For societal risks in this tolerable region, the decision maker must consider whether risks have been reduced by ALARP, taking into account public concerns. Concerning (large) tunnels, the societal risk criteria based on ALARP are often referenced for new tunnels.

Societal risk can be based on a large and significant incident or event, such as a large fire or a flood by leakage. These incidents can be fatal to users and have a large effect on society. However, it does not necessarily develop to structural failure. But while an incident on a personal level or risk is usually small, these incidents are large and could eventually develop to structural failure if the risks are not mitigated properly, like fire protection or (redundant) pumping facilities.

Economical risk

The last risk criterion is the economic risk criterion, which focusses on the optimisation of the risk level based on economic considerations. Risk and consequences are quantified in monetary units. In this consideration, the optimal probability of failure is found when the incremental investment becomes larger than the reduction in the costs of the consequences of failure. It is obvious that this concerns the fact that all elements considered such as structural damage and closure costs, see also 3.5

While personal and societal risk focus on people, resulting in death or major injuries, economic risk is focused on property. As indicated, both personal and societal risk (for example, as a result of incidents as shown in Figure 3.1) could develop to a situation in which the structure is lost or the other way around; the personal risk or societal risk are conditioned by structural failure.

3.5. Reliability approaches

Different approaches for the analysis of the risk and reliability of structures can be found in literature [77, 86]. Structural design and design decisions can be approached with the following methods:

- Semi-probabilistic
- Reliability based
- Risk informed

Semi-probabilistic - Level I

The semi-probabilistic method is a simplification of the other methods and is validated by the higher level methods. It is also known as the LRFM (Load-Resistance-Factor-Method). It is applied to categorised and standard consequences, failure modes, and uncertainty representation. This approach is used in most codes and standards such as Eurocode [1]. In case structures are comparable, like buildings or bridges, the semi-probabilistic approach can be used conveniently. The codes are valid for this kind of structure based because they are calibrated and validated for these and compatible structures. The LRFM is used mainly and is practical for ordinary structures. In case structures do not fit within the application scope on which the probabilistic approach is based, more sophisticated methods need to be applied.

In the LRFM, neither the consequences nor the probability of failure are considered directly. The designer selects a design parameter by satisfying a design equation. In practice, the resistance must be larger than (all) the loading actions and combinations. The parameters are selected such that if the requirement set by the equation is met, the design will fulfil the requirement set by the target reliability. In practice, resistance parameters R are reduced by a resistance factor γ_r and loads L are increased by a loading factor γ_l (Equation 3.5).

$$\frac{R}{\gamma_r} \geq L\gamma_l \tag{3.5}$$

By optimising the resistance, the structure is optimised for this method and according to the same type of structures for which this method is calibrated. The structure itself with respect to the risks or the probability of failure is not optimised. The partial factors are validated by reliability based approaches.

Reliability based - Level II and III

The reliability approach is a simplification of the risk-informed method and can be used if the consequences of damage and failure are clear and understood. Reliability-based assessments are based on reliability theory and a probabilistic approach of random variables and stochastic processes. The Probabilistic Model Code [77] describes and standardises the approach. In this method the consequences of failure or non availability are not directly considered in the design. The probability of failure is specified directly or chosen based on the application. The probability of failure or target reliability is addressed with $\beta_t = \phi^{-1}(P_f)$, which is the standard normal cumulative probability distribution function. In this method, the target reliability is not varied for different engineering problems; the designer in practice will choose a design that satisfies the requirements set by the target reliability or a lower probability of failure set the requirements provided by or with the (future) owner. With the method a unique P_f is used and calibrated for a class of similar structures. Therefore, the structural design is not optimised but P_f will regulate the reliability-based approach.

Level III is a comprehensive method. Uncertain quantities are modelled by joint distribution functions. The probability is then calculated exactly by, for example, numerical integration. This method can effectively only be applied when a limited number of variables is used.

Level II is an approximation method. The uncertain design parameters or loading parameters are modelled by distributions based on a mean value and a standard deviation together with the correlation coefficients between the stochastic variables. The joint probability density is simplified and by linearising the limit state function (First Order Reliability Method), the computational effort is reduced. The reliability index for this method was defined by Cornell (1969) [91] as presented in Equation 3.6.

$$\beta_t = \frac{\mu_Z}{\sigma_Z} = \frac{1}{V_z} \tag{3.6}$$

In which Z is the joint distribution function and V_z is the coefficient of variation of Z. To have a design that fully meets the reliability requirements, the reliability index β must be larger than the target reliability index β_t.

Risk informed - Level IV

The risk informed method is an intensive approach. In this method, described in ISO 2394 [86], decisions are made based on full risk analyses. In the risk-informed method, also known as the level IV method, decisions are made based on minimising the risks. For this, the decision parameter p is introduced in Equation 3.7.

$$R(p) = C_c(p) + E(H) * P_f(p) \tag{3.7}$$

In which C_c is the cost of safety measures, if p increases, it reduces the likelihood of structural failure. $E(H)$ are the expected consequences in the event that a failure occurs. $P_f(p)$ is the probability of failure, which depends on the decision parameter. The product of $E(H)$ and P_f represents the risk. For example, a concrete beam in a structure is dependent on its capacity on the amount of reinforcement. If the amount of reinforcement increases, the costs will increase, but the probability of failure will decrease. $R(p)$ is the total risk related to the design parameter in monetary units. With this method, an optimised design can be achieved based on the consequences in case the derivative of $R(p)$ is zero.

The risk-informed approach is rarely used in engineering practice. Although it is the only method that relates the decision parameters to the consequences, from a reliability point of view, an optimal design can be achieved. But every individual limit state needs to be considered. Secondly, threats and related consequences are often not known or specified in advance during the design process. The lower-level methods can be standardised and lead to reasonable results close to the optimum for most cases.

3.6. Limit states

Various limit states need to be considered, some of these limit states are beyond the scope of design standards for some types of structures. Three types of limit states can be distinguished; Ultimate Limit State (ULS), Service Limit State (SLS), and the Accidental Limit State (ALS).

Ultimate Limit State

A Ultimate Limit State (ULS) is a situation in which the structure will physically fail and collapse as a result of excessive displacement damage. In the case of structures, men must think of plastic deformation or heavy cracking of the structure, which will ultimately lead to total failure of the structure. In case of an SFT, failure might occur when the displacement of the structure is excessive and the joints fail and the tunnel floods. This will have a massive influence on the buoyancy of the structure and will cause failure and even loss of the structure permanently. Every structure must meet the following Ultimate Limit States;

Equilibrium (EQU)

In this case, the structure fails to maintain static equilibrium. In this case, the strength of the structure of the foundation of the structure is not governing. In relation to the SFT structure, if the unbalance of the buoyancy of the system is associated, it does not meet the EQU limit state.

Structural (STR)

In this case, the structure fails due to a (local) structural failure, caused by the excessive strength of the materials used or large displacements, including the foundation and other directly related substructures. Component failure is generally considered as a limit state. STR failure may cause progressive failure of the SFT.

Geotechnical (GEO)

In this case, a structure fails due to geotechnical failure or large soil deformations. An SFT structure is either tethered to the seabed or hanging on pontoons. For pontoon SFT, GEO failure is inapplicable. For the tethered structure, geotechnical failure of the anchor point of the tether or the weight structures on the seabed could lead to the loss of a substructure (tether) and subsequently to the loss of the total structure.

Fatigue (FAT)

In this case, the structure fails due to (local) structural failure due to fatigue loads. During the lifetime of the SFT, the structure is cyclically loaded with hydraulic loads. The load interval and the expected number of cycles will define the fatigue load. Failing by fatigue will therefore occur after a (longer) period after the start of use.

For each of the ultimate limit states, the requirements will differ.

For regular civil structures, these ultimate limit states suffice. The stability of SFTs is based on the balance between permanent loads and buoyancy forces and will be vulnerable if the balance of the structure is lost. Tunnel leakage is usually classified as a service limit state, but for SFT-specific leakage it should be considered as an ultimate limit state. As a consequence, higher impacts need to be considered, while for the service limit state, representative loads are usually applied. Leakage itself can be related not only to the cracking of the concrete lining but also to all watertightness provisions such as gaskets.

Service Limit State

A Service Limit State (SLS) is a situation that could cause temporary unavailability of the structure. Large accelerations or deflections of the structure, which make the structure inappropriate to drive through. Also, situations which might threaten the structure on the long term are also considered to be an SLS situation. Service limit states can be set by codes and standards, for example, on specific criteria (such as cracking, displacements, maximum stresses, and strains) are set by applicable (material-specific) standards. In terms of usability, the limits can be set by standards, but could also be agreed upon with clients, (future) owners, or user(groups).

Accidental Limit State

An Accidental Limit State (ALS) is a situation caused by an ”accidental” action, but the ALS could be considered as a special ULS. Actions that might only occur rarely during the lifetime of the structure, while in regular ULS cases the actions are common. In the case of SFT structures, loads such as explosions in the tunnel, sunken ships, or earthquakes are typical examples of these loads. Special requirements related to these situations might be set. For example, the structure might fail structurally, but it must be possible to repair the structure to its original state. On the other hand, a probability approach can also be used on the frequency of the load over the lifetime of the structure. If the probability of such a load is of a very low magnitude, then the load could be neglected. However, this must be agreed upon between the (future) owner and the authorities.

3.7. Other topics of influence

Apart from the items addressed in the previous sections, other parameters also influence the reliability of the target or have a different objective. In this section, some of the topics and parameters are mentioned and discussed.

Economical lifetime

Structures are built with an intended service lifetime (buildings: 30 to 50 years, tunnels and other infrastructural works: 100 years or more). The intended lifetime is a given, based on technical feasibility and an assessment of the time that a structure can be useful in its initial form. If this lifetime is set, the economical value will indicate whether it is sensible to include the probability of failure during the service life. This deviates from economic analyses to optimise the economical lifetime of a structure. For example, a wooden house and a masonry house will have the same target reliability, while the intended lifetime of a wooden house will be less than that of the masonry house. For the renovation of civil structures, a lower reliability index can be applied because the economic value decreases over time. A discussion on the economic value of a structure in the infrastructure can be held. Normally, the economic value of the structure is actually greater than the redemption and interest costs. It will also represent the economic value of the physical link that has been constructed and, in many cases, cannot be easily replaced by a new structure. In the next paragraph, the influence of time in the different methods is presented.

Risk informed approach

In the risk informed approach, an optimising approach is needed for all different limit states. In this method, the time effect can obviously be inserted. Based on the development over the damage costs related to the failure can vary. The economical value might increase, and replacement costs can be reduced by the redemption costs. However, many parameters need to be derived and estimated over a longer period, which might introduce a large scatter on the outcome. As a base case, one could assume that the economic value will increase according to different scenarios. However, the assumption will be based on processes which might be unknown at the moment of design and/or construction and would be largely influenced by the global economic growth.

Reliability approach

The target reliability is based on the probability of failure with the distributions for both the resistance elements and the actions. In this approach, the two terms, the resistance and the loads, in the equation could be time dependent. The loading might increase over time, for example, by increasing traffic intensity or higher hydrodynamic loads, and the resistance might decrease over time, processes of corrosion and fatigue, or increase as concrete strength increases over strength, which makes the reliability approach time dependent.

Spatial variability

A continuous structure is as weak as its weakest link. The dike structures, as well as the SFT structures, span large lengths. If a dike fails at a cross section, the complete structure will fail because the threat of water will have a negative influence on the complete area behind it. In addition to the distribution of the actions and resistance, a continuous structure will have an increasing probability of failure with increasing length.

3.8. Target reliability framework for Submerged Floating Tunnels

The methods used for assessing risk and reliability in structural design vary depending on the type of object, such as fixed bottom structures, flood control systems, or vessels. It appears that the SFT has unique characteristics. It can be identified as a civil structure that facilitates traffic of all types in a hydrodynamic environment during its full service life. Civil structures rely on codes and standards for their design. These are developed and validated because civil structures are actually built. When the various structures are compared to SFT in Table 3.1, none of the structures has the same set of characteristics as an SFT and none of the current codes and standards will cover all the risks and design aspects of an SFT. However, the reliability assessment approach described in ISO2394 [86], could be used. Section 3.5 explains the different approaches. The lower levels can be validated by the higher level approaches. It will take time for the civil engineering community to build up design experience in SFTs before cross-validation could lead to a design practice that comprises, for example, the commonly used calibrated LRFM methods (level I), as presently used for other structures. Specifically for SFTs a proposed framework is given in this section.

Overview

For regular civil structures, the target reliability levels have been defined and can be found in several codes and standards around the world. Concerning SFTs, the question can be raised as to how the target reliability can be defined. Pandey et al. (2025) [92] discuss life safety in the reliability-based design of structures. In general, a civil structure needs to be designed and realised for a purpose. For SFTs, it would serve traffic passing a long, wide waterway. Structures cannot be built with the guarantee of absolute safety. Building a structure will come with a cost and construction budgets are never unlimited. Taking these elements into account, there is a balance between life safety and the societal affordability for the realisation of civil structures. Realisation of an SFT is in this matter not an exception.

The most common approach for life safety is the As-Low-As-Reasonably-Possible (ALARP) framework, which is typically used as a framework when it comes to life safety in design of structures. Within this framework, the acceptable risk is classified as intolerable, tolerable, or an area in which safety measures should be considered; see Figure 3.4. The intolerable risks need to be mitigated despite the associated costs as the risk is unacceptable. However, the tolerable risk can also be mitigated or reduced, and the mitigation should be based on the effectiveness of the measures.

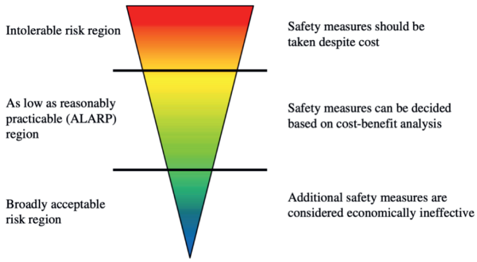

Figure 3.4: Risk categorisation, originated from Liu (2021) [93]

3

However, the majority of civil structures can be found in the category between the two extremes of this categorisation with moderate to high risks. In this categorisation, risks are only allowed if they are ALARP and in other words if the costs which are related to reduction of risks are out of balance with the risk reduction benefits.

Life safety in structural design can be distinguished as the individual risk and the societal risk and approached from an economical perspective. The **individual risk** is defined as a risk of death (P_d). For civil structures, the probability of death as a consequence of structural failure per year is expressed in Equation 3.8 if an annual value[1] of 10^{-5}. The probability of death related to the failure risk $P_{f,IR}$ can be found when the conditional probability $P_{d|f}$ is known (Equation 3.9). However, this probability is complex to derive and in [94] proposals can be found between 0.01 and 0.20 for buildings dependent on the consequence classes (where low classes consider low usage and high classes high usage). The question can be raised whether these values are applicable to SFT, as the probability of survival from an SFT in full structural failure is smaller than for buildings and $P_{d|f}$ will be closer to 1.0. [1]

$$P_d = P_{f,IR} \cdot P_{d|f} < 10^{-5} \tag{3.8}$$

$$P_{f,IR} \leq \frac{10^{-5}}{P_{d|f}} \tag{3.9}$$

The **societal risk** definition is found in the F-N curve, see Figure 3.2, in which the size of the group at risk is related to the probability of loss of life. The underlying theory is that societies are less tolerant to events in which large groups are involved than to cumulative consequences to events with the same probability. Basically, the society will respond differently to an event with 100 casualties compared to 100 events with 1 casualty. The F-N curve contains the probabilities of possible events and the allowable number of people involved. The requirement is set to a minimum relation between the probability of and the number of people involved, but the requirements could be unfeasible as indicated. The ALARP principle could be adopted in this relation as well.

[1]Value is used as an example. The concept of “acceptable” risk of human death resulting from structural failure varies in literature for different hazards and are subject of continuous discussions, for example by Reid (1999) [95] and Menzis (1995[96]

In general, individual and societal risks are considered the lower bounds for the exposure of unacceptable risks to individuals. The target reliability of structures is also governed by economical considerations and usually requires higher levels of reliability than life safety requirements.

Target reliability index β

Up to the 1970s, the common approach in designs was to use a global safety factor requirement given the ratio of the resistance and the loads or load combinations on a structure. Later, the concept of the target reliability index β was introduced. The target reliability index β is linked to the probability of failure of an object or a part of the structure. The limit state function defines when a (part of the) structure fails based on a given design. The target reliability sets the requirement for this limit function. Most modern codes and standard use a semi-probabilistic approach, known as the Load-Resistance-Factor-Method (LRFM) as presented in Section 3.5, in which a partial factor is defined for the actions or loads on the structure and the material definitions. However, the partial factors in the LRFM method are related to a specific β that is related to the probability of failure of the structure. As the safety of life for SFT will depend on a different conditional probability of death given structural failure than for other structures, this could influence the partial factors in this method. However, βs are commonly specified from a combination of an economical perspective and individual and societal risk requirements.

Reliability based design by economic optimisation

For SFTs, this approach of the LFRM could lead to uneconomical designs and the question can be raised if an SFT can be achieved with respect to the desired target reliability as specified by current codes and standards. The answer to this question can be found by relating design to economic design and life safety. The approach focusses on an economical optimum for the design of the structure. In other words, the optimal amount of investments is found if the additional investment on a specific part equals the reduction of the monetised risk of the structure. Figure 3.5 schematically shows this optimum. The decision parameter is the parameter that influences the design capacity or the resistance to failure. Examples of the decision parameters can be a material, a geometrical section parameter, a typical allowable loading scheme, etc. In Figure 3.5, the safety cost increases with increasing decision parameter (magenta). In this hypothetical example, a linear relation is assumed between the decision parameter and the safety costs influenced by it. For example, if a section is enlarged, more material is needed and requires an additional budget. In reality, this can be different, but the relation is positive. With an increase in the decision parameter, the structure will be more safe and the capitalised risk will be reduced (blue). The total cost (blue) is the summation of the capitalised risk and the safety cost, and the optimum for the decision parameter can be found at the lowest value (the derivative of the function is zero). The graph presented in Figure 3.5 is simplified, and the total cost consists not only of the initial building costs but also of multiple different aspects related to the structure, such as interest, maintenance, demolition costs and economical damage due to non-availability, for example. This approach focusses directly on costs and neglects the incorporation of life safety in the design. Discussions about the value of life have been conducted on several platforms. Life safety could be incorporated into reliability-based design and can be translated, considering the ALARP principle, as the amount of money a society is willing to spend to save an anonymous human.

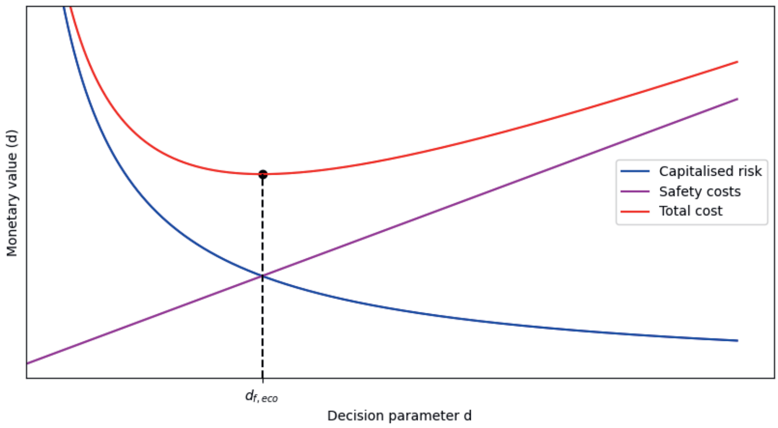

Figure 3.5: Cost optimisation in economical risk approach

The target reliability indicates the optimal relationship between costs and safety. For civil structures, this is found in codes and standards and involves calculation methods, characteristic material parameters, loading schemes, and different conditions and limit states. As mentioned, most recent codes use semi-probabilistic methods; however, many codes, such as Eurocode [1], also contain methods to recalculate this method using reliability-based methods with both linear (level II) or non-linear (level III) limit state functions.

Addressing the required safety in the design of SFT is challenging, as the classification of structures (consequence classes) is explicit in codes and standards, while failure consequences are only implicitly considered, such as the number of fatalities and non-availability of the structure. Implicit failure consequences are dependent on the utility rate of usage, but also on the exposure (with return time), warning, and self-rescue measure. The failure consequence in the economic risk approach is from a mathematical object far from complex, however, this contrasts with the estimation of failure consequences, which is a gathering of direct (building, maintenance, etc.) and indirect costs (non-availability, human life). As a recommendation, a guideline or method could be compiled to estimate these costs.

Obviously, to construct an SFT, a design must be made and should be based on a safety level. A civil structure is constructed out of different parts or components, and the design of the structure distinguishes different parts. For example, different 2 dimensional approaches can be considered instead of a large 3 dimensional approach. In addition, support systems can be evaluated separately and in parallel with structural approaches. In other words, the design of civil structures will be split up into different parts and elements and the target reliability is applied to each individual part, where there could be a distinction between the system and component level, and by using redundancy a lower reliability could be requested to components as the system would provide alternative safety measures such as an extra support facilitating a secondary bearing.

Framework

In summary, an initial framework as presented below can be used to arrive at a safe but also economical design for SFTs.

- Define an acceptable individual and societal risk to derive the maximum probability of structural failure. This must be assessed using the conditional probability of death or major injury given structural failure. For SFTs, it is important to note that the conditional probability of death given structural component failure could be higher than for other civil structures, which will lead to a stronger requirement on the probability of structural failure (larger β or lower P_f) than for other civil structures such as bridges.
- In codes and standards, the parameters belonging to LRFM are related to the required β, which is for SFTs expected to be higher due to conditional probability. In the Eurocode standard [1] and in other codes and standards available, methods are included to derive partial factors.
- Although this approach to derive partial factors is intensive and, even with increasing computer resources, it will be impossible to conduct all design calculations on a higher level, so a sophisticated selection based on the highest risks and most important failure modes is recommended.
- Based on the defined requirement (β or P_f), evaluate the design of the SFT structure using LRFM (level I) with common design practices, using the derived partial factors.
- Calibrate the design for different limit states than used to determine the partial factors and adjust the factors if needed.
- In addition, the design of the SFT can be further optimised with respect to investments safety using the economic risk evaluation, but should never be lower than the acceptable individual and societal risk.

4
Spatial variation in tunnel foundations

4.1. Introduction[1]

As expressed in Section 2.3, IMTs are structures that cross water and are immersed in a dredged trench and covered afterwards to protect the structure. IMTs are supported by a bedding which stiffness is dictated by the soil stiffness below the structure and a foundation layer of gravel or sand. Typically, an IMT is constructed as a segmented structure which can adopt settlements along the length of the structure. As the longitudinal alignment of the IMT needs to be ensured, the different parts, segments, are connected using shear keys. The research presented in this chapter focusses on an alternative method to estimate the design shear key force.

The most common current design approach is an alternating bedding scenario (reduction of stiffness in a single segment using a prescribed factor. This is defined by Dutch requirements [2] and is adopted for many tunnels worldwide; see Figure 4.1), along the tunnel axis is used as a conservative approach. However, it does not account for spatial variability in both the subsoil and the foundation of the tunnel. Instead, the current design approach is geometrically orientated, using the length of a segment in an alternating bedding, in the tunnel to find the largest possible shear forces and not in the variability of the bedding support.

In this research, a method to find the variability of forces in the shear key is presented. In the method Gaussian Random Fields (GRF), which are parametrised by a covariance length, are used. Next, the probability distribution of the force in the shear key is found by using two different probabilistic methods, Vine Copulas (VC) and Non Parametric Bayesian Networks (NPBN), in which the covariance lengths for the subsoil and dredging tolerances are related to the shear forces. Both methods differ but allow both for conditioning. These probabilistic methods are valuable and can be identified

[1]This chapter has been published as journal paper: *The influence of spatial variation on the design of foundations of immersed tunnels: advanced probabilistic analysis* 't Hart et al. (2024) [97]

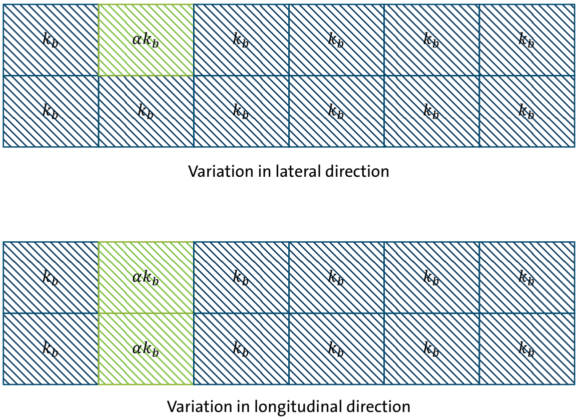

Figure 4.1: Bedding variation according [2]

as scientific engineering, because they connect variability in the subsoil and construction to estimate the forces in the shear key in both conditioned and unconditioned situations. Using these methods, both the GRF as well as a multivariate probability distribution for covariance lengths for (spatial variability of soil properties) and shear forces will result in a complete characterisation of the probabilistic relation between support conditions and the shear forces in the tunnel to be used in design. Secondly, more efficient and robust designs can be developed for immersed tunnels and can be identified as an alternative to the current design approach, which focusses on variability only depending on the length of the segments and can be considered as less close to the actual situation of the bedding variability.

The models and methods in this research also have limitations. For example, it assumes that the loads are uniform throughout the tunnel. Additionally, only two keys are considered per joint to transfer the shear forces, while in practice there could be more. On the other hand, only three variables are considered in the probabilistic methods. This can be extended by other variables, such as spatial variability of the sediment height on top of the tunnel site. Furthermore, this method clearly differs from the current design approach. To use this method in design practice, engineers should have a more than basic understanding of the probabilistic tools employed.

Tunnels, not limited to IMT, are based on geotechnical and structural analysis. Random fields have been applied in a comparison study by Cheng (2019) [10] of a pressurised tunnel face of a bored tunnel and provides a practical design tool. Gong (2018) [11] presents a probabilistic analysis based on random field generation for a longitudinal analysis of a bored tunnel. For a bored tunnel section, Yu (2019) [12] presents a 2D plain strain approach that includes random field generation, which confirms the reliability of the tunnel lining. The application of spatial variability or (Gaussian) random fields is yet to be uncommon in designs of IMT foundations. Random fields are stochastic processes in space, or in other words, random functions over a given domain as described by Adler (2009) [13] and Hristopulos (2020) [14]. Random fields are used in many research areas, such as environmental engineering, social sciences, finance, astronomy, and many others. Liu (2019) [15] shows the development in the research of these random fields. Within research in the field of civil engineering, the application of GRF is frequently observed in geotechnical analysis, for example, for levees and embankments as described by Hicks and li (2018)[16] and Li et al. (2017) [17] . The spatial variability of a soil continuum can be described using this method and is observed in literature; see, for example, [18–20]. In addition to geotechnical applications, random fields are also used in structural mechanical cases. Bucher (2006) [21] shows its application in material properties, such as the calculation of the modulus of elasticity or strength, as well as for geometrical properties, such as thickness in shell models. The application of random fields to trusses was researched by Bocchini (2008) [22] and discusses the application in the reliability analysis of cable-stayed bridges. In these examples the concept of random fields in Finite Element analysis is used. A description of this approach is given by van Marcke et al. (1986) [23]. In this research, two different probabilistic methods are used, Non-Parametric Bayesian Networks (NPBN) and Vine Copula (VC). Both are graphical models and represent probabilistic dependence between nodes and are explained in more detail in 2. The combination of spatial variability and a probabilistic approach to estimate the shear key forces in immersed tunnels is a topic that is not yet addressed in the literature.

4.2. Model and analysis

In order to research the influence of the covariance length of both the subsoil and the depth of the trench as a result of dredging operations, a hypothetical representative model is constructed. An IMT is supported by a bedding, consisting of a subsoil and the foundation, and loaded with various loads acting on the tunnel. These loads will result in a bedding reaction under the IMT. The IMT is a concrete structure and has a significantly higher stiffness than the soil bedding. As a result, the force distribution within the tunnel segment itself will be insensitive to bedding variations. The flexibility is induced into the tunnel in the longitudinal direction by the segments and the immersion or element joints.

A base model of a part of an IMT is used. The model has a length of 120m and a width of 30m. The segments are equally distributed over the length of the element and have individual segment lengths of 20m (L_s). A schematic overview is presented in Figure 4.2.

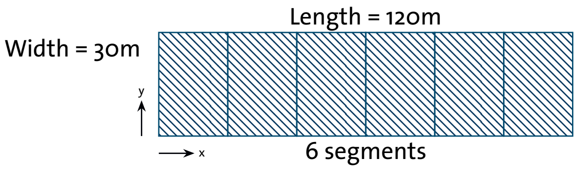

Figure 4.2: Covariance length validation model - top view

The six segments of the IMT are assumed to have a constant vertical displacement throughout the length of the tunnel part considered. Segments are considered rigid bodies, and joints are flexible. Figure 4.4 shows the loading principle of the tunnel in the longitudinal direction.

The bedding is assumed to be elastic, but due to the spatial variability not constant over the contact area of the tunnel. The linear stiffness of the subsoil is derived by a geotechnical[1] analysis and the bedding stiffness is based on the following parameters (see Figure 4.3 and Equation 4.1):

- Thickness of the foundation material (h_f in m)
- Stiffness of the foundation material (k_f in $\frac{\mathrm{N}}{\mathrm{m}^3}$)
- Dredging tolerance (Δt_d in m)
- Placement tolerance (Δt_p in m)
- Subsoil stiffness (k_s in $\frac{\mathrm{N}}{\mathrm{m}^2}$)

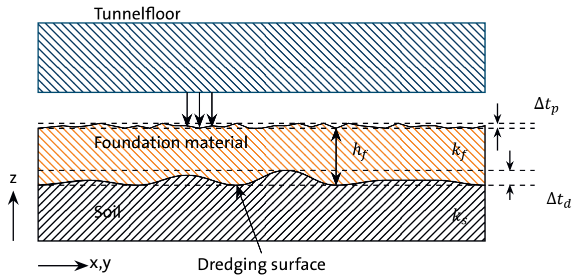

Figure 4.3: Bedding definition (cross-section)

$$k_b = \frac{1}{\frac{1}{k_s} + \frac{h_f}{k_f}} \tag{4.1}$$

An IMT is loaded by distributed loads, inside and outside of the tunnel. The total load is adjustable by adding ballast weight and is based on the vertical stability requirement. This requirement specifies the minimal total downward force that results from preventing the tunnel from floating due to the buoyancy force. In the final situation, after immersion and after the ballast concrete, the protection layer and soil cover are applied to ensure the downward force. The resulting force acts on the tunnel and in case there is no variation in the load, an average compressing pressure is supplied to the foundation beneath the tunnel (σ_a, see Figure 4.4).

Because the stiffness of the bedding varies underneath the tunnel, the response of the bedding (σ_b, see Figure 4.5) and therefore the load on the tunnel will vary. In this study, the vertical position of the tunnel is prescribed and adjusted in an iterative process until the total response force on the contact area A_b is equal to the total load (both σ_a and σ_b integrated over the area) as described by Equation 4.2.

[1] A separate geotechnical analysis is required to derive the subsoil stiffness based on the geological layers, the soil characteristics and the influence depth of the tunnel

It is assumed that the total element will have the same vertical displacement and remain undeformed, as this is a conservative approach. In reality, the tunnel will deform slightly by small rotations of the segment and in the joints, and as a consequence, stresses will distribute between the segments. If stresses are redistributed, the shear forces will reduce accordingly.

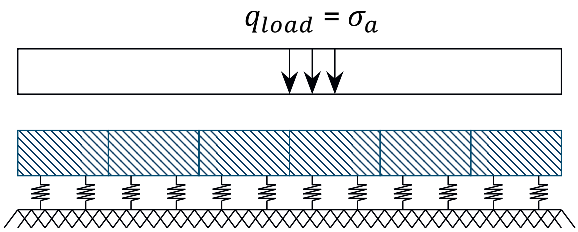

Figure 4.4: Structural tunnel system

$$\int\int \sigma_a dxdy = \int\int \sigma_b(x,y)dxdy \tag{4.2}$$

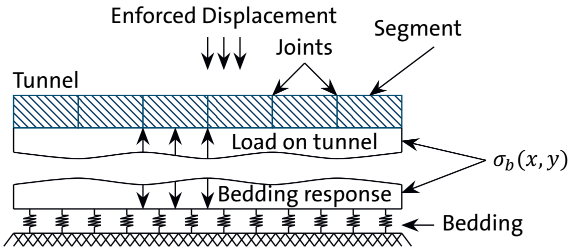

Figure 4.5: Tunnel and bedding response

The variation in the bedding response leads to different stress distributions in the different segments. A shear force in a joint can be derived between two segments. Using a stiff IMT, the stresses will not be redistributed between the segments underneath the IMT, and the maximum shear forces between segments will be found. In this research, an IMT with a two-shear key layout in the outer walls is assumed, and therefore each segment has four shear keys. The sequence to derive the shear forces at a shear key after finding the equilibrium of the bedding response is presented in Figure 4.6 and is obtained by:

- Integration of stresses underneath each segment to get the total force on a segment (F_i)
- Find the centre of gravity of the total force (red dots)
- Distribute the force to the shear key locations linearly (green dots)
- Define the shear key force as the absolute difference in forces between segments at the shear key locations ($F_{k,2-3}$ and $F_{k,1-4}$)

- Find the maximum shear key force of all shear keys

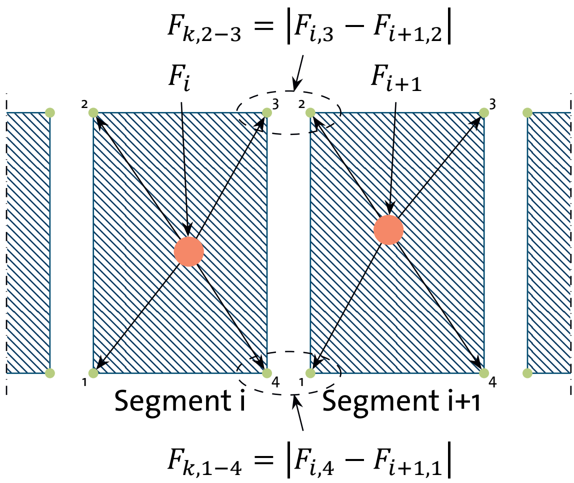

Figure 4.6: Force at shear-keys, shearkeys located at the corners 1 to 4 - Top view

In design, the maximum shear key force is used to compile a reinforcement layout for the shear key. In Section 4.3, this sequence is repeated for both different covariance lengths and different geometrical tunnel layouts and is the covariance length related to the shear key force. With this method, spatial variability of the rigidity of the bedding is considered beneath the tunnel. The variability differs not only in the longitudinal direction of the tunnel, but also in the lateral direction. In the presented model, only a spatial variation in subsoil stiffness and dredging depth are considered, besides that, the model also considers non spatial correlated variations such as variations in the top surface of the gravel and in the gravel stiffness. More parameters, spatial or non-spatial variated, can be considered in the model, such as settlements over time and gravel placement equipment.

The model serves 2 different goals, the first (Section 4.3.1) is to present the influence of the covariance length on the shear forces for different segment lengths. Secondly in section 4.3.2, the structural model is used to gather a dataset to create a NPBN and VC. With these probabilistic models, multivariate probabilistic analyses can be conducted and interactions between variables can be found. As a result, probability distributions of variables, in this case the shear force, can be found to conduct extreme value analyses.

4.3. Results

4.3.1. Spatial variability

In this section, Monte Carlo analyses (n = 1000) are performed in which the covariance lengths for both soil stiffness and trench dredging are considered equal and fixed in each analysis. The generation of the variability of the subsoil stiffness and dredging depth is independent. An even stronger effect would have been found if the same generated GRF had been used for both parameters, but this was considered less realistic as an independent generation and having two different GRFs based on the same covariance length. In reality, not only will the variability be independent, but also the covariance lengths of both parameters will be independent. However, to find a relation between covariance lengths and the shear key force, both are kept equal. Using this approach, the distribution of the shear force is given the covariance length.

In Section 4.3.2, the covariance lengths are considered independently. For bedding variations, the variable distributions as described in table 4.1 are used. These parameters are hypothetical and are based on experience in several designs of various tunnels. In order to demonstrate the method, the quantity of parameters is important, as long as they are representative. For each sample, GRF are generated for both the subsoil stiffness and the thickness of the foundation layer based on the considered covariance length. The size of the GRF corresponds to the dimensions of the base model as shown in Figure 4.2. As an illustration, for soil stiffness, the generated spatial distributions after the quantile transformation for different covariant lengths are presented in Figure 4.7.

Item	μ	σ	Distribution	Remarks
Gravel stiffness [kPa]	2000	300	Truncated Gaussian	uncorrelated min = 1000 max = 3000
Soil stiffness [kPa]	5000	1600	Truncated Gaussian	min = 1800 max = 8200 L_{cov} = varies
Trench dredging / Gravel thickness [m]	0.7	0.15	Truncated Gaussian	min = 0.35 max = 1.05 L_{cov} = varies
Gravel placement tolerance [mm]	0		Triangular	uncorrelated min = -10.0 max = 15.0

Table 4.1: Parameters and distributions

Using the sequence specified in Section 4.2, the maximum shear key force can be found in each sample of the analysis and the total set results in a distribution of the maximum shear key force for a specific covariance length. The results are presented in Figures 4.8, 4.9, and 4.10. The following trends can be identified:

- The maximum shear key forces (up to 4.8MN) can be found if the covariance length is similar to the segment dimensions and the variation is greater.
- If the covariance length is small or large compared to the segment length, the maximum shear key force is small (with 1 to 1.5MN) and shows a low variation.

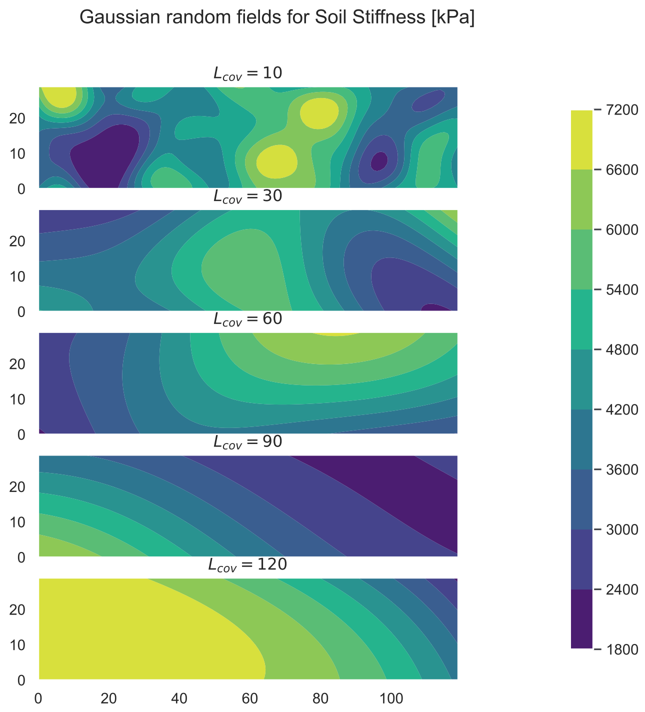

Figure 4.7: Contour plots of soil stiffness for different covariance lengths

In Figure 4.10 the relation between the shear key force at the 95^{th} percentile of the distribution and the covariance length is shown. The 95^{th} percentile is chosen as the characteristic design force (in design considerations for the evaluation of the ultimate limit state, this value is multiplied by a partial factor [1]).

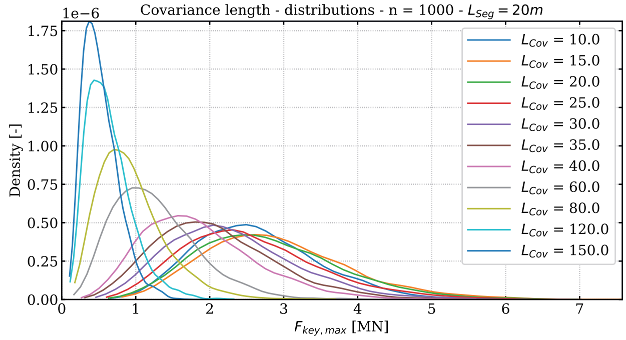

Figure 4.8: Distributions of the maximum shear key force for different covariance lengths

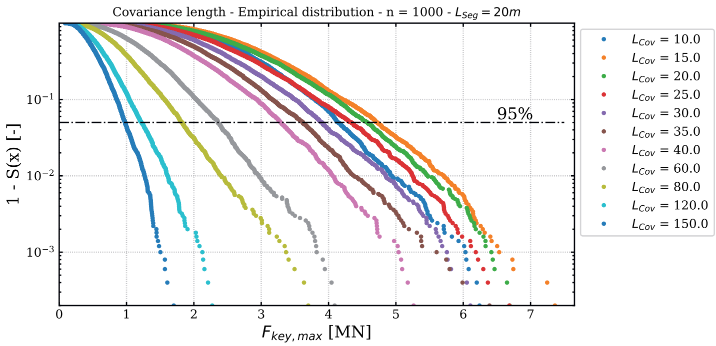

Figure 4.9: Exceedance probabilities of the maximum shear key force for different covariance lengths

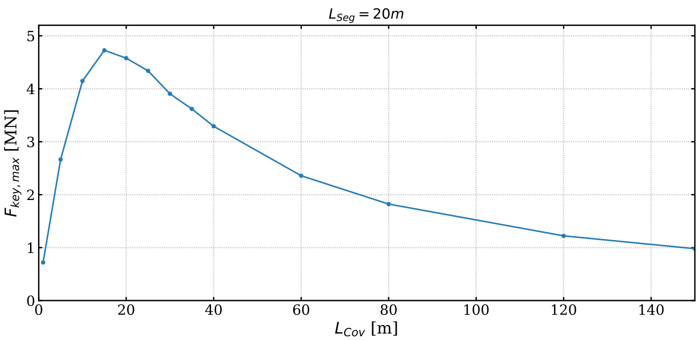

Figure 4.10: Shear key force at 95th percentile as function of the covariance length

In Figure 4.8 the number of segments and the width of the tunnel are considered constant. In Figure 4.11 the length of the segment L_s is varied from 10 to 60 metres, while the number of segments is kept equal to 6 (which changes the total length of the element), so the total contact area under the tunnel varies with the different length of the segment. On the horizontal axis the covariance length is divided by the segment length for comparison. The results are plotted for the covariance length over the segment length and the shear key force found at the maximum density as presented in Figure 4.8. Figure 4.12 shows the same figure as Figure 4.11, but for comparison, F_k is divided by the contact area under the segment. All individual graphs are presented in Appendix A.1.

The following observations can be identified from Figure 4.11:

4

- F_k increases with the segment length L_s. Larger integration areas, due to the increase of L_s, underneath a segment will cause higher shear forces, which can exceed the capacity of a shear key.
- The maximum F_k is found if the segment dimensions (length and width) and L_{cov} are similar.
- If L_{cov} increases to larger values compared to L_s, the F_k decreases.

There appears a strong relation between the covariance length and the shear key force. Secondly, as a geometrical consequence of a lower area below the segment, lower segment lengths show lower shear key forces. An optimisation of the segment length could be discussed, as joints are weaker spots in terms of water tightness. But in reality, the segment length depends on other factors as well, such as the casting sequence, seasonal temperature loads introducing longitudinal effects, and so on. However, the conclusion gives useful information in the early stage of the design of the geometry and structural solutions.

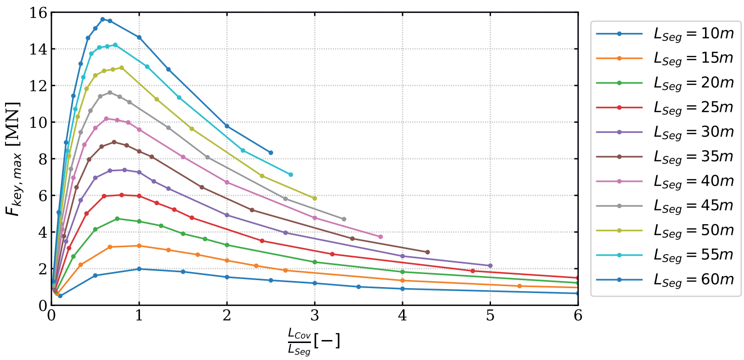

Figure 4.11: Shear key force at 95^{th} percentile as a function of the covariance length for different segment lengths

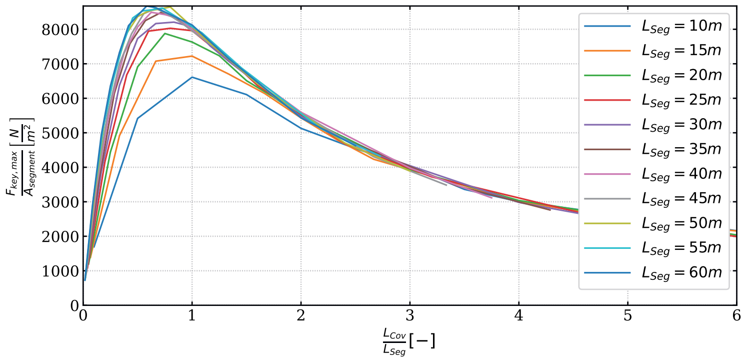

Figure 4.12: Relative shear key force at 95^{th} percentile as a function of the covariance length for different segment lengths

4.3.2. Probabilistic analysis

Probabilistic models

Using the physical model and the finding presented in Sections 4.2 and 4.3.1 a relation between the shear key force and the covariance lengths. In case covariance lengths are unknown, exceedance probabilities can be found for shear forces using probabilistic models such as NPBN and VC. With the application of Gaussian copulas only in NPBN while different copulas can be used in VC, tail dependency can only be considered in VC. Both models are used in this section. Both methods also allow for conditioning, so conditional probabilities can be derived to simulate different possible scenarios.

Figure 4.10 shows this relation for a model with a segment length of $20m$. The maximum shear key force is found at a covariance length of about 15 m. From the figure, it can be concluded that there is a positive relation between the covariance length and the shear key force up to a covariance length of about 15 m and a negative relation for covariance lengths larger than 15 m. Rank correlations, which are often used to parameterise multidimensional models in statistical analysis, do not capture non-monotonic behaviour such as the one described in Figure 4.10. Therefore, the model is split into two parts.

The correlation length on which the model is split is found by additional analyses between the interval of 10m to 24m with an increment of 2m. For this interval a quadratic interpolation is derived to find the maximum value, which appears to be $16.3m$, as presented in Figure 4.13. The dataset is divided into two parts at this value and results in two separate datasets at the split value, the lower part (part 1) that contains covariance lengths of up to $16.3m$, and the upper part (part 2) that contains covariance lengths of $16.3m$ and larger. Both parts show similar exceedance probability distributions. As this probabilistic approach focusses on the maximum shear key force, it can be conducted from parts 1 and 2. In Appendix A.2 and A.3 contain the results for both parts, in this chapter only part 1 is presented as the methods are equal for both parts.

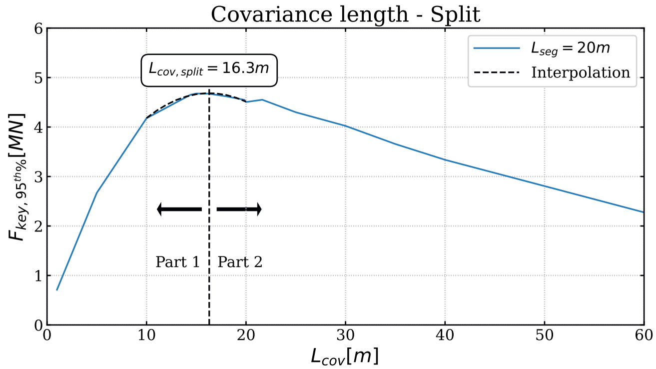

Figure 4.13: shear key force at 95^{th} percentile as a function of the covariance length - splitted

4

Data for probabilistic analysis are generated using the base model in a Monte Carlo simulation (n=3000). The covariance lengths were independent uniformly distributed between $0m$ and $16.3m$, and the total data contains 3 variables: both the covariance lengths and the maximum shear key force. The fitting is conducted by a `Python` package `SciPy` ([98]) using the most common distributions. The best-fit distributions are selected on the basis of the lowest sum of the square error between the observed value and the value based on the distribution. For this analysis, the area of interest is in the tail of the data and it appears that the log-normal distribution fits best for part 1 (and the gamma distribution for part 2), as presented in Figure 4.14. The parametric distribution for the shear force will be used together with uniform distributions for the covariance lengths in the simulations using the NPBN approach to find probability distributions.

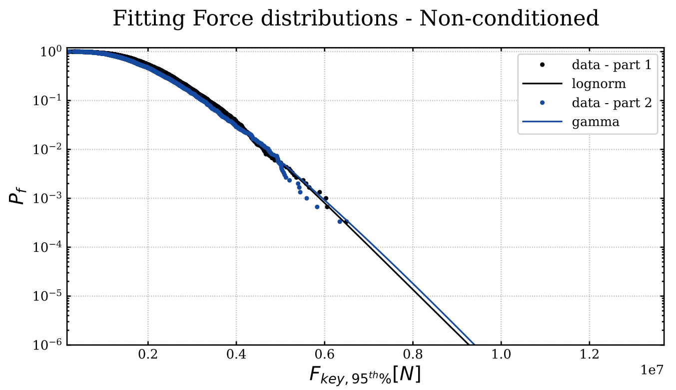

Figure 4.14: Cumulative distribution function of shear key force at 95^{th} with the best fit for both parts

A unique joint distribution is determined between the lengths of the covariances ($L_{cov,soil}$ and $L_{cov,trench}$) and the shear force. In table 4.2 the empirical rank correlation matrix is presented. The matrix shows only a small correlation between covariance lengths as these are considered independent. The correlation between the shear key force and the shear key force is 0.36 to 0.43.

	$L_{cov,soil}$	$L_{cov,trench}$	F_{key}
$L_{cov,soil}$	1	0.006	0.355
$L_{cov,trench}$	0.006	1	0.426
F_{key}	0.355	0.426	1

Table 4.2: Empirical rank correlation matrix for part 1 (lower)

Using the rank correlations, an NPBN is constructed with 3 nodes, representing both covariance lengths and the shear force, and 2 arcs, representing the correlation between the force to each of the correlation length. The NPBN is presented in Figure 4.15 and the conditional rank correlation matrix is presented in table A.2. In order the

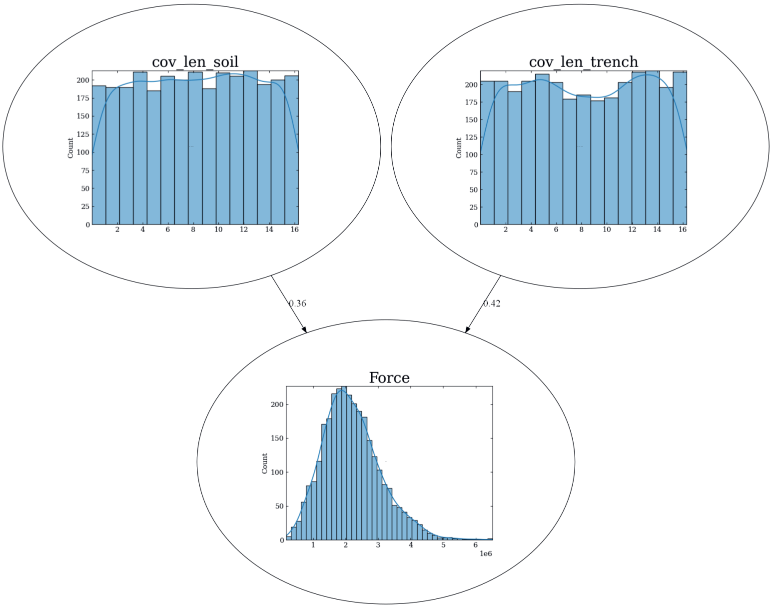

Figure 4.15: NPBN - part 1

validate whether the Gaussian copula represents the bi-variate pairs closely, a diagnostic tool is used. Appendix A.2 contains the validation of the NPBN. The Cramèr-von Moses statistic (CVM), which is related to the sum of square differences between the empirical copulas and the parametric copulas, is used. Figure A.8 shows the results of this validation. The graphs indicate, by the relatively small differences, that the Gaussian copula (maximal 0.2) is a fair representation of the bi-variate distribution.

Figure A.9 presents the empirical cumulative density of the d-calibration scores, based on the Helliger distance as described by Morales and Steenbergen (2014) [99].

The d-calculation scores are the distance between the empirical and empirical normal rank correlation and the empirical normal and normal rank correlation matrices. If these matrices are equal, the d-calibration score is 1. For both parts, the d-calibration score is within the uncertainty bounds if, respectively, 5000 and 25000 samples are drawn.

The complete output for the probabilistic approach using VC is presented in the appendix A.3. For 3 nodes, only 3 different RVs are applicable. The differences in AIC between the three possible VC are small, less than 5. The best fitted VC for part 1 is presented in 4.3 and has an AIC score of -1261. In the overview in A.24, a small tail dependency can be observed.

As stated above, the VC approach uses different copulas and is able to account for tail dependency. In Figure A.24, the joint plot of the results is presented. In this graph, tail dependency is visible. In the VC with the smallest AIC score for both parts, although the correlation is not strong with 0.35 to 0.43, tail-dependent copulas are found. Compared to the NPBN approach, in which it is concluded that the Gaussian copula give confident predictions of the dependencies, it is also seen in the CVM scores that the Gaussian copulas can be used, but that in some cases the tail-dependent copulas show a slightly better score. Based on these findings and assumptions for both approaches, the VC approach is better while the results are still comparable.

Tree 1:	Copula	Parameter
$L_{cov,soil}$ - $Force$	Gaussian	0.37
$L_{cov,soil}$ - $L_{cov,trench}$	Joe	1.01
Tree 2:		
$L_{cov,trench}$ - $Force \mid L_{cov,soil}$	Gumbel 180°	1.46

Table 4.3: Best fitted VC

Conditioning

With the best models found for both NPBN and VC, simulations are possible. The next step in the process is to condition the simulations. If inference or conditioning is applied to the models, uncertainty distributions of the remaining unknown nodes can be determined given a condition on one or more of the remaining nodes. In practice, this is valuable; If a certain variable is deduced from field research such as CPTs or by applying measures to reduce the tolerance on dredging, the influence on the shear key force can be found and accounted for in the design, or the design can be optimised based on these findings or measures. It is also possible to use an opposite objective. So, conditioning on the shear force in this matter is also possible. That will give the engineer the distribution of the covariance lengths of the soil stiffness and the dredging depth given a certain shear force.

In this research, the distributions are compared between the non-conditional distribution and different conditional situations. For both models, the lengths have been conditioned on different lengths. In addition to the conditioning of the lengths, the shear force has also been conditioned, giving the following scenarios:

- Both covariance lengths conditioned on $16.2m$, $0.1m$ from the split value

	Original dataset	Conditioned on 2 lengths L = 16.2[m]		Conditioned on 2 lengths L = 8.15[m]		Conditioned on $L_{cov,soil}$ = 16.2[m]		Conditioned on $L_{cov,soil}$ = 8.15[m]		Conditioned on $L_{cov,trench}$ = 16.2[m]		Conditioned on $L_{cov,trench}$ = 8.15[m]	
		NPBN	VC	NPBN	VC	NPBN	VC	NPBN	VC	NPBN	VC	NPBN	VC
1.00E-02	4.70	7.35	6.90	4.14	4.05	6.07	5.93	4.32	4.45	5.73	5.67	4.47	4.40
1.00E-03	5.89	8.73	8.05	4.98	4.84	7.34	7.12	5.24	5.49	6.92	6.83	5.46	5.35
1.00E-04	7.03	10.02	9.09	5.73	5.56	8.53	8.20	6.07	6.48	8.00	7.87	6.37	6.22
1.00E-05	8.15	11.27	10.06	6.43	6.23	9.69	9.21	6.85	7.45	9.01	8.84	7.22	7.04
1.00E-06	9.27	12.49	10.98	7.09	6.87	10.84	10.17	7.59	8.41	9.98	9.77	8.03	7.82

Table 4.4: Shear forces in [MN] for different conditions

- Both covariance lengths conditioned on $8.15m$
- Only one covariance length conditioned on $16.2m$, the other covariance length unconditioned
- Only one covariance length conditioned on $8.15m$, the other covariance length unconditioned

The outcome of the maximum shear force of the VC simulations is limited to the maximum value of the original dataset, as a result of the reverse quantile transformation. However, a difference between NPBN and VC is that in NPBN the fitted distribution functions have been applied, while in the VC simulation, the outcome is based on the simulation data. As a consequence, a dataset is created using the best fit VC (n = 1E7) and a conditional dataset for VC is created by specifying a small interval around the conditioned variable (in this case $0.2m$) and selecting a sub-dataset from the total simulation data based on this interval (or intervals if applicable, if conditioned on more variables).

In Appendix A.2.2 and A.2.4 the conditional exceedance probabilities are presented together with the unconditioned results for the NPBN and in Appendix A.3.2 and A.3.4 the equivalent results for VC are presented.

In general, the results differ slightly between the NPBN and the VC. The main differences in the approaches of both methods are already specified in the previous sections. In table 4.4 the uncertainty distribution for the forces have been derived based on fitted distributions. If the conditioning of one of the covariance lengths is $16.2m$, the shear forces increase compared to the original dataset and when the lengths are conditioned to $8.15m$, the forces decrease. If the conditioning for the 16.2m cases are compared, it can be observed that in case both lengths are conditioned, the forces are larger than when only one length is conditioned. Both observations are validated by the findings in 4.3.1. The difference between the covariance length for the subsoil and for the trench are compared, the forces are higher in case the covariance length for the subsoil is conditioned. It can be concluded that the influence of the stiffness of the soil on the bedding is larger than the depth of the trench (and the related thickness of the foundation layer). However, this is case specific; if the thickness of the layer differs and the stiffness of the subsoil stiffness differs, the conclusion can be otherwise.

Additionally, for NPBN also conditioning have been conducted on the forces. Using the approach, the probability distributions for the covariance lengths can be derived. The method is the same as for the conditioning on the covariance lengths, as described previously. Figure A.13 shows the probability diagram for the covariance lengths when the shear force is conditioned. The black line in the diagrams shows the distribution of the original sample, and the other lines show the distributions for a conditioned shear force of $2.0MN$ (blue), $5.0MN$ (green), and $7.0MN$ (red). In all graphs, the blue line is below the black line, which indicates that the probability of the covariance length is not close to the split value. In contrast, the green and red lines are above the black line. The probability that the covariance length is closer to the split value is higher than in the original sample. The red lines indicate that when a shear force of 7.0MN is conditioned, a covariance length closer to the split length is more probable than in the case of a shear force of 5.0MN (green line). With this perspective, the designer has the option of a different objective and to use the capacity of the shear key as a starting point. If the covariance lengths of the subsoil can be derived, the design can be adjusted to the circumstances.

4.4. Relation to traditional design

In the more traditional design approach with an alternating bedding, the stiffness is considered uniform underneath a segment and a segmented beam on an elastic foundation is used to describe the behaviour of the model in a 2 dimensional space. Using this approach, torsional effects cannot be found; to account for torsional effects and, consequently, varying shear forces in the keys in one joint, a factor is used, which is usually taken as 20% to 25%, which is based on experience. The variation of the bedding along the tunnel is accounted for by an alternating bedding, which is specified by a factor depending on the foundation method. In the alternating bedding approach, spatial variation in the subsoil is not considered and is independent of the dredging method. In reality, this will vary by method and consequently by the marine environment and depth.

The method presented in this research varies substantially from the current design approach. In that approach, the tunnel is modelled in a 2D space. Both methods require soil investigation and interpretation of these results. If the soil investigation is intensified, both models will have increased accuracy, but only in terms of the stiffness of the subsoil. However, if a covariance length or an interval of covariance lengths can be derived, subsequently a distribution of shear forces can be derived using conditioning on this extended knowledge. In case the covariance length cannot be derived based on the available soil investigations, an upper bound for the covariance lengths can be found in estimation of the split value of the covariance length. Conditioning on an interval on this value will give an upper bound distribution of shear forces.

In Eurocode [1] and ROK [2], the design is based on the Load Resistance Factor Method (LRFM).In short, in this method, the probability of both forces and resistance are accounted for by partial factors. For the service limit state (SLS), the loads are applied in frequent combinations, and for the ultimate limit state (ULS), the loads are combined and multiplied by a partial load factor. These load factors differ for different load cases. The limits states together will result in a "frequent" load and a maximum considered load. These are in fact 2 quantiles in a load distribution. Here, the SLS can be considered as the mean value and a characteristic value at the tail of the distribution. In the presented method using representative loading, a distribution of the shear force is found, which can be considered equivalently. For SLS, which focusses on durability in design, the mean or $50^t h$ quantile of the distribution can be used. In ULS design, which focusses on structural capacity, the force can be found by selecting the quantile relating to the required reliability index for the tunnel.

4.5. Discussion

In this research, only covariance lengths for soil stiffness and dredging depth are considered, and both lengths are considered independent parameters. The latter could be the topic of discussion, if the top part of the soil influences the dredging process, a correlation between both could appear. However, if the soil consists of a multi-layer profile, this influence of the top layer on the total stiffness of the soil will reduce. In order to use this method in the tunnel design process, even parts of the method can be used. The GRF model can be used to derive bedding stiffness to adopt in longitudinal and transverse analyses. Using the derived subsoil stiffness and the designed thickness of the foundation layer, including their covariance lengths or the most conservative covariance lengths (close to a derived split value), distributions of average bedding stiffness per segment can be derived. Using 5% and 95% of these distributions as design values for the stiffness for an alternating bedding approach. More advanced would be the derivation of the maximum shear force using the total method. When the covariance lengths are unknown or only known as bandwidths, probabilistic methods will be valuable, as conditioning can decrease the variation on the shear forces.

In reality, the soil will also vary in the support area of the tunnel. The application of the method needs adjustment, where the applicable distribution of the soil parameters develop over the area. Usually, different CPTS are taken over the area. Different stiffness subsoil characterisations can be found in the support area. It is up to the designer how to account for these differences as the characterisation of the subsoil stiffness can be assumed to be continuous or with discrete transitions. Both options can be served using the quantile transformation to the quantiles of the local subsoil distribution.

Summary

Summarising, in order to apply the method in design, if no covariance is known, first the split value needs to be found using a Monte Carlo approach, as the approach only captures monotonic behaviour in the distributions. With the split value found, multivariate distributions with NPBN or VC can be found for the interval below the split value and above the split value. Conditioning the multivariate distribution models can be applied either below the split value or above close to the split value. This will result in a conditional probability distribution for the shear key forces to be used in design.

A design can be optimised in terms of reduction of the number of joints as it will directly effect the shear key force, although the lengths of the segments are dependent on more circumstances than the shear key force. If field research results in more information on the actual covariance length of the subsoil stiffness or if the dredging process is supplied with quality measures to have a very large covariance length, a better understanding of the shear key force can be obtained than by application of the alternating bedding approach.

5

Reliability analysis of traffic in submerged floating tunnels

5.1. Introduction[1]

As mentioned in Section 2, an SFT is a buoyant structure that can be stabilised differently. In this chapter a reliability analysis is conducted on an SFT that is stabilised by floating pontoons at the surface.

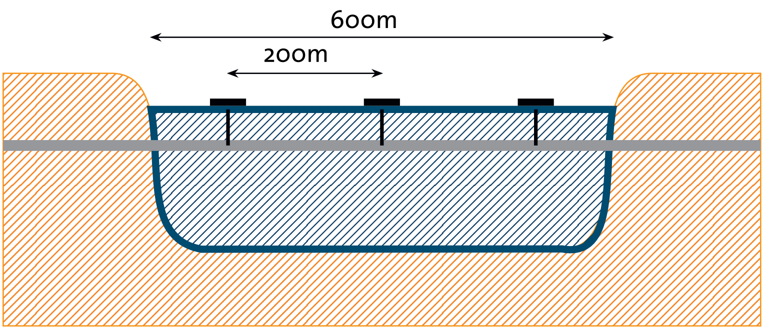

Figure 5.1: SFT supported by floating pontoons

An SFT is similar to an IMT. For example, both depend on gravity-induced vertical loads such as dead weight, vehicle weight, the self-weight of the structure, and its buoyancy. However, an IMT is supported on the seabed, whereas an SFT is floating. This makes an SFT a structure in a dynamic hydraulic environment and will thus be differently (externally) loaded than an IMT. An IMT is usually covered with a protective layer of soil and is continuously supported by soil bedding. An SFT structure is

[1]This chapter is based on journal paper: *Structural reliability analysis of a submerged floating tunnel under copula-based traffic load simulations* - Torres et al. (2022) [38]

floating during its lifetime and relies on the balance between the up and down-ward vertical forces and is discretely supported along the alignment by pontoons or tethers. Flooding due to leakage of both types of tunnels will result in a significant loss. In case an IMT floods, it will get a larger vertical load and would under go settlements. However, after sealing the leakage and emptying the IMT, it is still in place and could still be an option to recover the structure although massive repair operations might be required as described by Tveit (2010) [100]. In case an SFT floods, the buoyancy balance is lost and large displacements could lead to a progressive behaviour of multiple leaks along the alignment. In case of flooding, the risk of losing the structure without an option to repair is significantly high. Therefore, it is essential to avoid large leakage of SFTs. It can be discussed that tether supported SFTs are more vulnerable, but Grantz (2010) [101] also concludes that pontoon structures are vulnerable to total destruction by flooding. In this chapter is focused on flooding by leakage of the tunnel lining, worth to mention is that flooding of the hinterland might be a consequence if the hinterland's elevation is lower than the tunnel's entrance as described by Luniss (2013) [102], so the risk might also relate to consequences outside the tunnel structure; this is not limited to the SFT structures but also to IMT and bore tunnel structures.

An SFT will be subjected to several different loads over time, such as wind and wave loads, the risk of collisions, tidal loads, and internal loads. Together with these loads, other failure mechanisms can also be considered. The method presented in this chapter is based on a hypothetical single tube tunnel supported by pontoons with an outer radius of $5m$, a wall thickness of $1m$, and spans of equal size of $200m$ (see Figure 5.1. The focus in this chapter is on the relationship between traffic load over time and resistance to leakage due to cross-sectional failure. A first design guide for SFT structures was published recently [103]. This guide describes several other design and loading situations in addition to the one considered in this chapter. The method presented here focusses on traffic-induced bending failure and static buoyancy loads (resulting forces from self-weight and dead load and the Archimedes forces), other loads and failure mechanisms are beyond the scope of this research.

The traffic load is defined as a fluctuating load in both magnitude, occurrence, and position over the structure. A traffic model based on Weight-In-Motion (WIM) data of heavy vehicles (heavier than 3.5 tons) is used to represent traffic at the tunnel. This data contains measurements for vehicle types, lane, speed vehicle length and weight, individual axle weight, and inter-axle distances. In a pontoon-type SFT, the weight loads are larger than the buoyancy load of the structure, and the traffic loads act in the same vertical downward direction as the resulting forces of the permanent loads. Thus, traffic loads will add to the resulting forces caused by permanent and buoyancy loads. An SFT must have sufficient reserve capacity to be able to carry the traffic load as described by Ingerslev (2010) [104]. However, in a tethered-type SFT, permanent loads act in the opposite direction. The traffic loads and the resulting forces of the permanent loads compensate for each other. A schematic overview of the loading on a pontoon-type SFT is presented in 5.7.

The methodology presented in this chapter is based on probabilistic modelling (copula-based models) of input parameters, mathematical calculation methods, and structural design principles. The approach results in a more realistic approximation of the structural response of the SFT. The SFT is tested for one failure mechanism: leakage failure due to longitudinal bending of the SFT tube. Approximately, this methodology consists of:

i. simulating the traffic passing through the SFT using a copula-based model in which WIM data are the input,
ii. computing the resulting bending moments, shear forces, and displacements of the SFT through a finite element method (FEM) model,
iii. performing a reliability analysis on the bending moments obtained in the previous step.

Traditionally, the requirements on structures are based on the target reliability, which is related to the consequences. The target reliability requirements increase if the consequences become larger; see also 3. This chapter presents a design adaption related to uncertainty and less predictable loading over time that is independent of the required target reliability. The method presented in this chapter results in reliability in terms of the return period of a design. It is up to the designer to validate the reliability requirements, and if it fails, the design needs to be adapted.

A similar approach to the one presented in this chapter was used to investigate bridges under traffic and earthquake loads by Medoza-Lugo et al. (2019) [26], where only heavy vehicles are investigated. The methodology presented by Tabatabai et al. (2017) [105] uses empirical copulas to characterise the WIM data to assess the load effect of heavy trucks on bridges. Copula models have been used in the past in transportation studies. Spissu et al. (2009) [106] proposed a copula-based model to study the relationship between vehicle type choice and usage (miles travelled). In Bhat and Eluru (2009) [107] analyses the effects on travel behaviour by studying the dependence between residential neighbourhood choice and daily vehicle miles of use by the household (VMT). In relation to traffic variables, Zou & Zhang (2016) [108] used a copula-based model to characterise the dependence between vehicle speed, headway and length.

Industry can benefit from this research to better understand the response of SFT to traffic loads. The flexibility of this methodology also allows them to study different configurations of SFT (pontoon, tethered, or supported by underwater piers). Moreover, this methodology can be applied to other variables of interest that may affect the structure under investigation, such as metocean loads (waves and currents), among others. Finally, this research can be used as a reference when data is scarce, since copula models can produce simulations that retain the probabilistic dependence between the variables.

This chapter starts by describing the modelling approach in Section 5.2. A brief description of the traffic data and simulation is presented in Section 5.3. After the results in 5.4, the chapter is closed with conclusions, discussions, and recommendations.

5.2. Modelling Approach

5.2.1. General Overview

In this section, the methodology is presented to perform a SFT reliability analysis using a combination of copula-based models and structural FEM models. The reliability analysis is conducted by the definition of the Limit State Function. An SFT structure is a buoyant structure where leakage will cause imbalance of the structure and could initiate progressive collapse. In this research, the limit state function is based on leakage caused by bending moments as a result of traffic loads. SFT structures can be affected by different types of load, and leakage due to bending failure is just one of the many failure modes. However, other failure modes or the influence of other loading variables are considered beyond the scope of this investigation. The modelling approach used in this chapter consists of the following steps (Figure 5.3):

- First, simulation of traffic passing through the SFT is carried out by using a copula-based model that characterises the distance between vehicles (intervehicle distance).
- Simulation of traffic is carried out for a determined "period of time" based on an average number of vehicles per unit time (i.e. one year). The result is a "train" of vehicles that will include the number of axles, axle weights, inter-axle distances, and inter-vehicle distances, see Figure 5.2.
- Then, the resulting time series of traffic are used as input in a FEM model, based on the Direct Stiffness Method (DSM) and the Differential Equation Method (DEM), to test its effect on the structure of the SFT in terms of cross-section results, like bending moments, shear forces, and displacements.
- From the bending moments, a stress distribution can be derived in order to validate the compression zone of the section.
- Finally, a reliability assessment is performed on the limit state (leakage failure mechanism due to bending moments in the longitudinal direction). The findings of the assessment can lead to adjustment or optimisation of the watertightness of the SFT section.

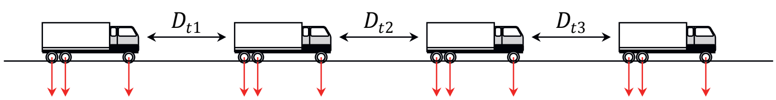

Figure 5.2: Train of vehicles, $D_t i$ refers to the intervehicle distance [m]

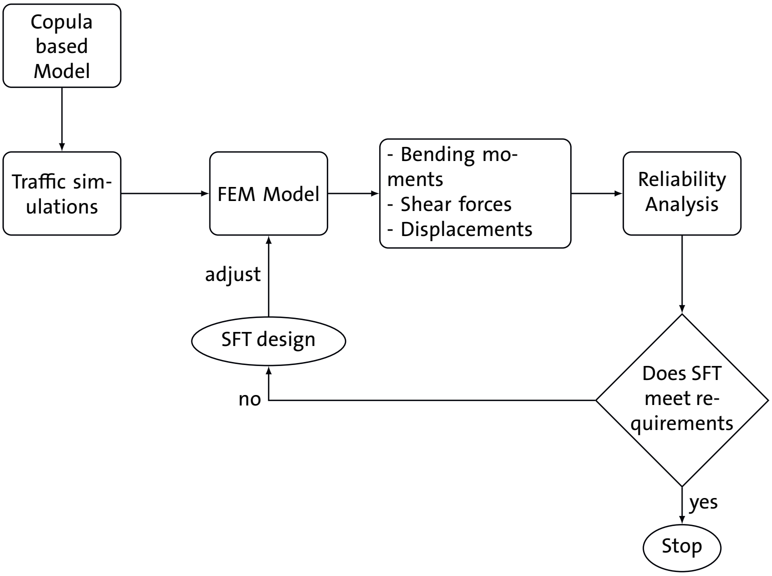

Figure 5.3: Modelling overview flowchart

5.2.2. Copulas for inter-vehicle distance

The traffic load passing through the tunnel is defined by four main variables (Figure 5.4),

- axle weight ($AX1, AX2$),
- distance between axles, ($DTF1, DT12, DTLAE$),
- inter-vehicle distance (X_t)
- number of axles per vehicle

In this research, a copula-based model is used to characterise the inter-vehicle distance by estimating the autocorrelation of this variable. The bivariate copulas were explained in 2.4. This allows us to create a more realistic modelling of the traffic passing through the SFT. The distinction between inside and outside congestion hours is also considered for this analysis.

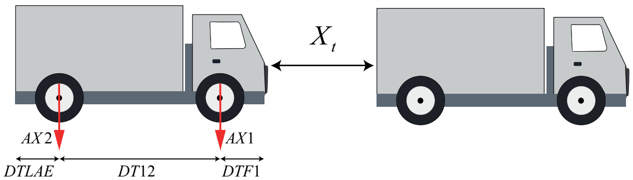

Figure 5.4: Traffic variables

$$H_{XY}(x, y) = C\{F_X(x), G_Y(y)\} \tag{5.1}$$

Here, $H_{XY}(x, y)$ is the joint distribution of the two continuous random variables $(x, y) \in \mathbb{R}$ with marginal distribution $F_X(x)$ and $G_Y(y)$ in the interval $[0, 1]$ and a copula taking values from the unit square $I^2 = ([0, 1] \times [0, 1])$, so that for all (x_1, x_2) Equations 5.1 are satisfied. If F and G are continuous, then C is unique. For a complete treatment of copula modelling, the reader is referred to Joe (2014) [109] and the references therein.

In order to estimate the parameters, select the model and simulate the bivariate copula models, the VineCopula package [110] is used. This tool is developed in R, a free software environment for statistical computing and graphics [111]. The package includes copulas such as Gaussian, Gumbel, Clayton, t, Joe, BB1, BB6, BB7, BB8, as well as their rotated versions. The parameters are estimated by pseudomaximum likelihood, and the copula families were selected on the basis of Akaike's information criterion (AIC). Let X denote a random variable (for example, the distance between vehicles) with distribution G_X. The time series of interest is $\{X_t\}, t \in \mathbb{N}$. The transition distribution is given by Equation 5.2. where $C_{\theta_X}(u|v)$ is the conditional copula. Notice that the parameter θ_X would model autocorrelation of order 1 for the time series of interest. In this study, for a sequence of intervehicular distances, the formulation in Equation 5.2 is used to simulate the values of the distance between vehicles. The graphical representation of this process is presented in Figure5.5.

$$H(x_t|x_{t-l}) = P(X_t \leq x_t|X_{t-1} = x_{t-1}) = C_{\theta_X}(G(x_t)|G(x_{t-1})) \tag{5.2}$$

$$\ldots \qquad X_{t-1} \longrightarrow X_t \longrightarrow X_{t+1} \qquad \ldots$$

Figure 5.5: Graphical representation of the process for inter-vehicle distance.

This model has been proposed before by Morales and Steenbergen (2014,2015) [59, 112] for the modelling of traffic loads in bridge reliability and for the modelling of time series of hydrological variables by Torres and Morales (2020) [113].

5.2.3. Simulating traffic

An algorithm was developed to simulate traffic through the SFT. The main goal of this algorithm is to capture the daily characteristics of different traffic scenarios, which will be explained in Section 5.3.1, while maintaining the proportion of vehicles per traffic scenario and category. The main steps are the following.

i. simulating the number of vehicles (per day, lane, traffic scenario and vehicle category),
ii. simulation of inter-vehicle distances (X_t) using a copula-based model (per traffic scenario),
iii. random sampling of axle weights and respective inter-axle distances from a vehicle data base (VH),

iv. combining the results from the previous steps to form a ”train” of vehicles

The algorithm starts by loading the required variables and the fitted copulas corresponding to each traffic scenario. The simulation is performed daily, where the number of vehicles per lane is randomly sampled from its corresponding empirical cumulative distribution function (ecdf). Then, the number of vehicles per traffic scenario and category is obtained by multiplying the total number of vehicles per lane by its corresponding vehicle proportion. This operation is carried out until the desired number of days is reached.

Next, for each traffic type, the simulation of inter-vehicle distances is executed from its corresponding fitted copula. And, since the vehicle category proportion per traffic type is known, the random extraction of axle weights and inter-axle distances from the VH data set is carried out.

Finally, the inter-vehicle distances (X_t), axle weights, and inter-axle distances are put together in a vector to form a ”train” of vehicles (Figure 5.4) that is used as input for the structural model. A simplified flow chart of the traffic simulation algorithm can be found in 5.6.

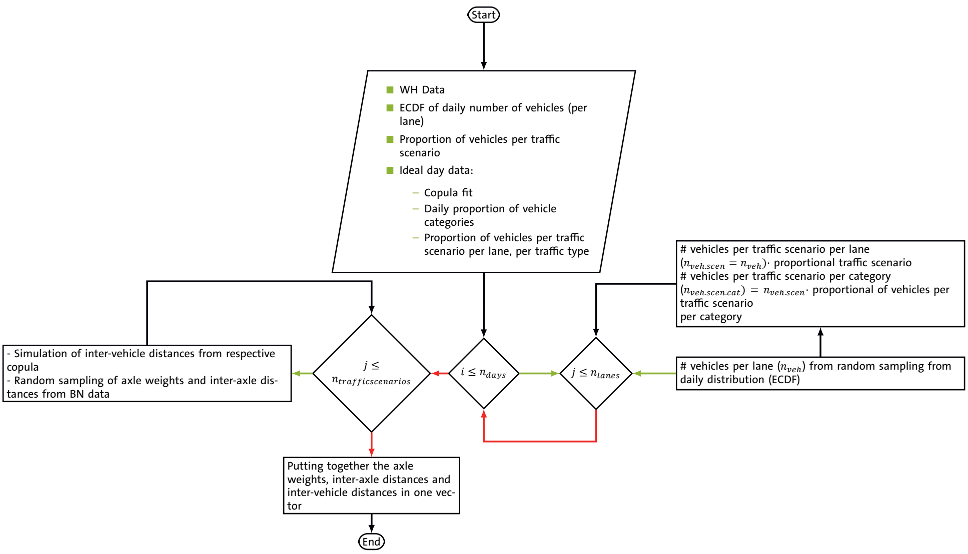

Figure 5.6: Traffic simulation model

5

5.2.4. Structural model

The structural system of the SFT is characterised by beams supported by pontoons. The methodology for the structural model is based on the Direct Stiffness Method (DSM) and the Differential Equation Method (DEM). This methodology is used to analyse the structure and determine the structural response in terms of cross-sectional results, such as bending moments. The application of these methods is focused on computational efficiency. The selected structural system of beams that suffices for this analysis. However, if the structure is loaded by 3D and dynamic loading, such as wave loads, impact loads, and others, a different modelling approach is required, using shell or solid models. With this slender implementation, the same geometrical model can be used for multiple load cases with arbitrarily located discrete loads without the need to split the model into many elements. In this way, a performance penalty is avoided. The SFT model has spans of equal size ($200m$) and the stiffness of the tethers is the same for all pontoon connections. The pontoons by themselves are considered hinged supports. A graphical representation of this model is presented in Figure 5.7. The model is simplified by considering only two full spans and two half side spans with symmetry supports (fixed rotations, free vertical translations). The system has a total length of $600m$ and is considered a monolithic structure without flexible joints or hinges. In total, the structural system consists of eight nodes and seven beams.

The system is loaded with traffic loads that represent the axle weights of vehicles driving through the SFT. These traffic loads are the result of the methodology presented in Section 5.2.2. The loading is defined as axles with an intermediate distance (inter-vehicle distance). More details on loading characterisation are given in Sections 5.3 and 5.4.

Since the load represents the axles of moving vehicles, the single axle load can therefore be positioned anywhere on the structure. For this reason, a grid is defined throughout the structure with a grid size of 1 m, resulting in a total of 600 individual positions along the structure. For each of the 600 individual positions, a unified axle load can be used to calculate the individual influence on the system cross sectional results (bending moments, shear forces) as presented in Figures 5.7b and 5.7c.

In general, in global design analyses, linear structural behaviour is used to find the global response of the structure. Nonlinear effects such as cracking or plasticity are considered in local cross-sectional analyses to design reinforcement or validation of the section. In this research, leakage of the SFT is considered as the limit state function. For simplicity, unfactored loads are considered. Partial load factors could be applied, but they will differ for different standards and different scenarios.

Due to the assumption of an elastic response of the global structure, the superposition principle can be used. Therefore, a discrete unit load is applied at each point in the grid along the structure to gather the results of a single-point load, resulting in 600 individual unit load cases. These cross-sectional results and displacements for each unit load case are gathered in matrix R_u that represents a point load at each point in the grid along the SFT model. Then, this resulting matrix is multiplied by each vector subtrain of vehicles $\vec{F}_t$ using the superposition principle, which contains the factors related to the axle weight.

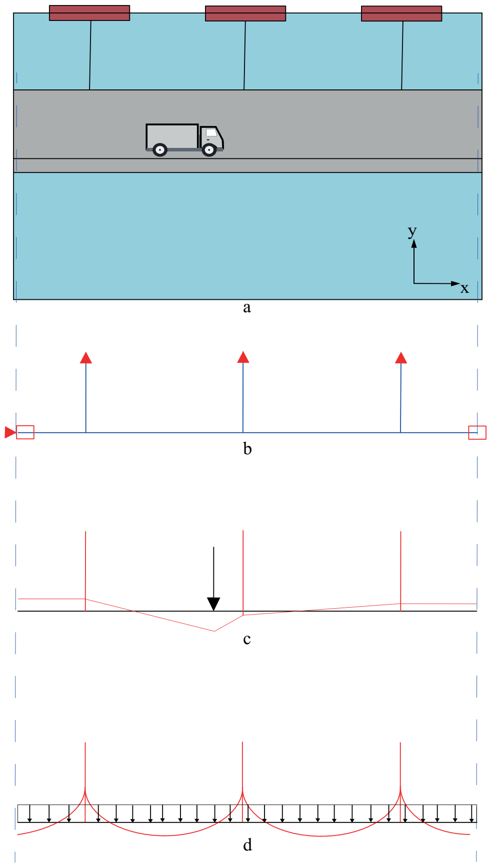

Figure 5.7: From top to bottom: (a) SFT scheme, (b) Structural system, (c) Bending moments due to a unit force load, (d) Bending moments due to buoyancy weight ratio (BWR) load.

In this way, the axle loads can act in any of the 600 grid points, and if for each situation a FEM analysis was performed, the analysis time would increase significantly. For each situation, the unit loads are multiplied by factors based on the axle weights and can be considered as the axle loads. The sum of all axle loads for the situation leads to the cross-sectional results for the situation.

The structural response due to each situation is obtained and added to the response caused by the BWR (R_{BWR}), as presented in Equation 5.3. By applying the subtrain vector $\vec{F}_t$, the loads on the end fields are excluded from the vector $\vec{F}_t$ due to symmetry. This symmetry acts as a mirror for the loads in the support condition. A single load on an end field will then be considered as a double load but mirrored over the support condition. The envelope of all situations including the results from the BWR will present the maximum cross-sectional forces.

For the case of a pontoon-SFT, the total bending moments are the result of the upward buoyancy force and the permanent loads acting on the structure (self-weight and dead weight). The relationship between permanent loads and buoyancy load is described as the Buoyancy Weight Ratio (BWR) and can be influenced by changing the ballast of the structure. The resulting distributed force (BWR load) has a downward direction that coincides with the traffic load. For simplicity, the BWR is considered constant over the length of the system. For example, for a BWR of 1.1, the permanent load acting on the structure is 10% higher than the upward buoyancy force. The bending moments caused by the BWR are presented in Figure 5.7d.

The axle loads (or axle weights) and their corresponding inter-vehicle distance are treated as a long train of axle loads. Each axle load has a different magnitude. 'Subtrains' (situations, smaller portions of the axle load train) can be derived by moving the 600m model over the vehicle train. All "subtrains" of loads are combined in a matrix F_t on a grid position. However, the number of subtrains ($\vec{F}_t$) is substantial and the use of DSM and DEM for each subtrain leads to a time-consuming process.

5

$$[R_t] = [R_u] \cdot \vec{F}_t + [R_{BWR}] \tag{5.3}$$

From the cross-sectional results and displacements for each subtrain in (R_t), the envelope of the results (R_e) is found. The minimum and maximum values of the results, such as bending moments and shear forces, can be distinguished along the structure. The resulting envelopes of the bending moments and shear forces are presented in Figures 5.8 and 5.9. If the traffic model (Section 5.2.2) generates a longer data set, then different distributions for R_e are found. For each data set generated by the traffic model, a different R_e is found.

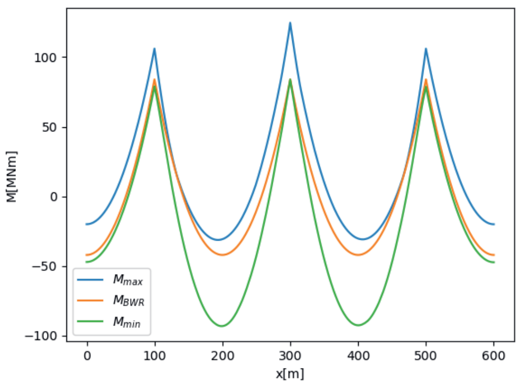

Figure 5.8: Envelope of bending moments

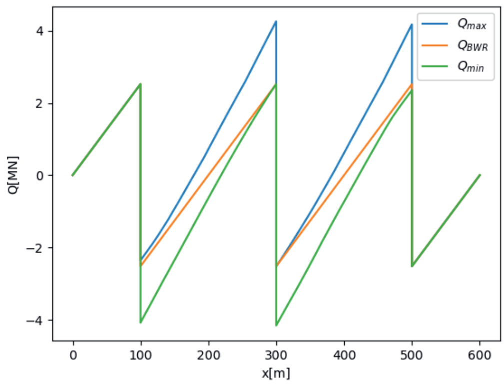

Figure 5.9: Envelope of shear forces

5.2.5. Limit state

The cross section of an SFT can be of different shapes; in this chapter, a tubular cross section is used (Figure 5.10). If necessary, this cross section may be post-tensioned in an asymmetrical manner.

One of the main threats of an SFT is the large ingress of water (leakage). This could lead to changes in the BWR. Should this be the case, the loads acting on the structure will be larger, i.e. the structure becomes heavier due to the presence of water. As a consequence, the distributed load (q_{BWR}) and R_{BWR} will increase significantly. Consequently, the design might not meet the requirements in terms of bending moments, forces, and displacements. In a worst-case scenario, this may even cause a progressive collapse of the SFT, because leakage can lead to the appearance of other failure mechanisms (whose investigations are out of the scope of this research).

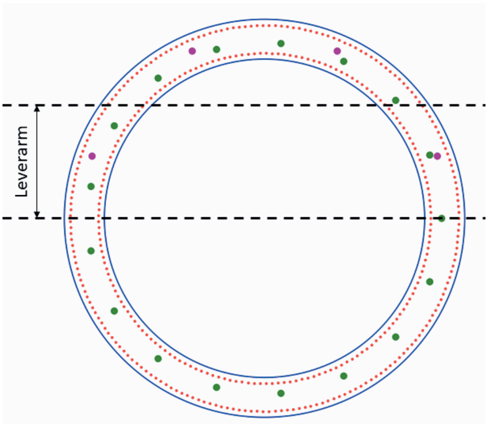

Figure 5.10: Tubular section with post-tensioning and regular reinforcement

Concrete is considered to be watertight when it is in compression; therefore, tensile stresses could lead to cracking that could facilitate leakage. If the concrete is in compression, leakage can not occur. In Eurocode 1992 [114], there are requirements for liquid-retaining and containing structures that are based on liquid passing through cracks. Different classes of liquid tightness are defined. In classes 2 and 3 (which are the highest requirements), it is required that cracks do not reach the full thickness of the structure. The requirement is set as a minimum compression zone in a section. For the SFT, this is the thickness of the tubular cross section. If part of the thickness remains in compression (the compression zone), the tightness of the liquid is guaranteed. The minimum value required for this compression zone is the maximum of 50mm or $0.2h$, where h is the thickness of the section. In other words, failure is considered if the compression zone at the thickness of the tubular cross section of the SFT (t_s) is smaller than $0.2h$. The location of the compression zone in the full cross section is presented in Equations 5.4, 5.5 and 5.6. If this water-tightness requirement is applied to the SFT structure (Section 5.4.1), the minimum compression zone of the section is defined by x_c, while the fibre location in the cross section (x_{fi}) is defined by the inner radius (R_i) and the compression zone. The sectional modulus (w_f) can be found by dividing the second moment of the area (I_z) by the vertical location of the fibre (x_f). See Figure 5.11.

5

$$x_c = 0.2t_s \tag{5.4}$$

$$x_{fi} = R_i + x_c \tag{5.5}$$

$$w_f = \frac{I_z}{x_f} \tag{5.6}$$

The pontoon-SFT is loaded with the BWR load and the traffic loads, resulting in cross-sectional forces and moments as found in the resulting envelope (R_e). With these sectional forces and moments, the stress distribution over the section can be derived. Post-tensioning will introduce a normal force ($N_{ax,pt}$) which is found by multiplying the post-tension stress times the area of the symmetric post-tension cables. If post-tensioning in a section is applied asymmetrically (purple dots in Figure 5.10), an additional bending moment (M_{pt}) is introduced as $N_{as,pt} \cdot a$. Where $N_{as,pt}$ is the post-tension stress multiplied by the area of the asymmetric post-tension cables and a is the lever arm defined as the location of the resultant of the asymmetric post-tension force ($N_{as,pt}$). When using a superposition principle, the stress state (σ_f) in the specific fibre can be derived with Equation 5.7 for the maximum bending moment of the envelope.

$$\sigma_f = \frac{M + M_{pt}}{w_f} + \frac{N_{ax,pt} + N_{as,pt}}{A_c} \tag{5.7}$$

Where:

- σ_f : Stress at outer fibre

- M : Total bending moment $M = M_{tr} + M_{BWR}$
- M_{tr} : Bending moment due to traffic load envelope at the considered section
- M_{BWR} : Bending moment due to BWR load at the considered section
- M_{pt} : Bending moment due to asymmetric post tensioning defined as $N_{as,pt} \cdot a$
- $N_{ax,pt}$: Axial post tensioning
- $N_{as,pt}$: Asymmetric post tensioning
- a : Lever arm
- A_c : Section area

Similarly to Equation 5.3, due to the superposition principle, M_{tr} can be derived from M because M_{BWR} is a constant value for any cross section of the model. In the limit state function, the sign conventions should be respected. Thus, M, M_{BWR}, and M_{tr} will act in the opposite direction as M_{pt}. The structure fails if $\sigma_f > 0$ as shown in Figure 5.11 and the SFT suffers leakage.

5

Here, $\sigma_f = 0$ is considered the limit value of the total bending moment M. Thus, the bending capacity is defined by Equation 5.8. The structure fails if M (total bending moment) is greater than M_{cap}, defined as a limit for the bending moment. Thus, the probability of failure is defined as $P_F(M > M_{cap})$. Since M_{BWR} is constant for any cross section in the model, the limit state function for the maximum bending moment caused by traffic is Equation 5.9. In that case, the structure fails if M_{tr} is greater than $M_{tr,cap}$ and the probability of failure is defined as $P_F(M_{tr} > M_{tr,cap})$.

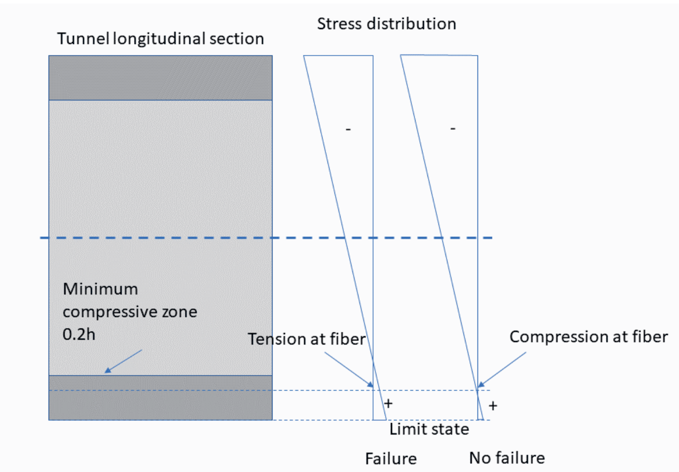

Figure 5.11: Longitudinal section with with respect to the limit state

$$M_{cap} = -N_{as,pt} \cdot a - \frac{(N_{ax,pt} + N_{as,pt}) \cdot w_f}{A_c} \tag{5.8}$$

$$M_{tr,cap} = -M_{BWR} - N_{as,pt} \cdot a - \frac{(N_{ax,pt} + N_{as,pt}) \cdot w_f}{A_c} \tag{5.9}$$

5.3. Traffic Data and simulation

Traffic data is formed by two data sets, namely WIM and VH. The WIM (Weight in Motion) data set consists of measurements of heavy vehicles on the National Highway A12 (km 42) in Woerden (The Netherlands) for two lanes (RW-12-L-2 and RW-12-L-3), described by Vervuurt et al. (2015) [115]. These measurements include time of measurement, vehicle category, lane, speed, the total length of the vehicle, the total weight of the vehicle, axle weight, and inter-axle distance. This data is available for 27 days in April 2013 (from 3 to 30) with a total of 157.000 vehicles roughly divided into 26 vehicle categories (B.1). All categories were considered for analysis and traffic simulation according to their proportion within the data set. For details on the accuracy of the data, the reader is referred to Vervuurt et al. (2015) [115]. In this data set, congestion was automatically filtered. In other words, the measurements were neglected if the traffic had a velocity lower than $40[km/h]$. This specific WIM data set was chosen because it is used as input to the model developed by Mendoza-Lugo (2022) [26] from which the second data set (VH) is obtained (Figure 5.12).

The second data set (VH) is the result of a Bayesian Network-based (BN) model developed by Mendoza-Lugo (2022) [26]. The data set is a collection of approximately 300.000 vehicles with their corresponding axle weights and inter-axle distances (the number of axles per vehicle is defined consequently) that were randomly generated using the BN model. This data set is discussed further in the next section. For the purpose of this research, the WIM data is defined by four variables;

i. axle weight,

ii. inter-axle distance,

iii. inter-vehicle distance

iii. number of axles per vehicle .

An overview of different vehicles and their number of axles is presented in Figure 5.4.

The aim of the traffic copula-based model is the characterisation of the inter-vehicle distance. In Figure5.4, X_t refers to the distance between vehicles (in kilometres). $AX1$, $AX2$ are the weights of axles 1 and 2 [KN]. $DTF1$, $DT12$, and $DTLAE$ are the distances between the axles (in metres).

In this research, the traffic model is focused on characterising the distance between vehicles (see Figure 5.5 and Figure 5.4). However, both data sets are used as a baseline to simulate the traffic variables that define the traffic load passing through the SFT.

5.3.1. Data Processing

The relationship between the WIM data set, the VH data sets, and the copula-based model is explained in this section. This link is visualised in Figure 5.12 and is discussed in the following paragraphs.

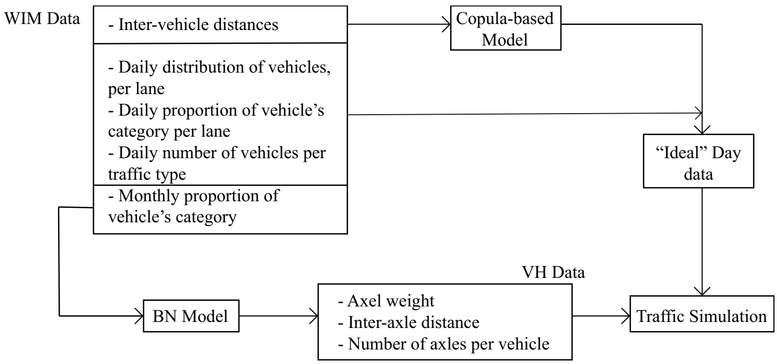

Figure 5.12: Data Overview for simulation of traffic.

For WIM data only normal weekdays are considered, and weekends and national holidays were excluded from the analysis. The "regular" days were analysed on three different time scales: hourly, daily, and monthly.

Hourly Analysis

The data sets are illustrated by histograms, so examination on a hourly scale became possible. With these visualisations, the congestion (large number of vehicles) and free-flow periods (low number of vehicles) could be distinguished. An example is presented in Figure 5.13 (April 4^{th}). The data were split into three different groups;

i. Free flow before congestion hour (Free Flow A),
ii. Congestion hour
iii. Free flow after congestion hour (Free Flow B)

This results in six different traffic scenarios: 3 groups for 2 lanes, namely, C_L2, C_L3, F_L2_A, F_L2_B, F_L3_A, and F_L3_B. Table 5.1 shows the meaning of this nomenclature.

Nomenclature	Traffic type and lane
C_L2	Congestion lane 2
C_L3	Congestion lane 3
F_L2_A	Free flow A lane 2
F_L2_B	Free flow B lane 2
F_L3_A	Free flow A lane 3
F_L3_B	Free flow B lane 3

Table 5.1: Nomenclature for hourly classification of traffic.

5

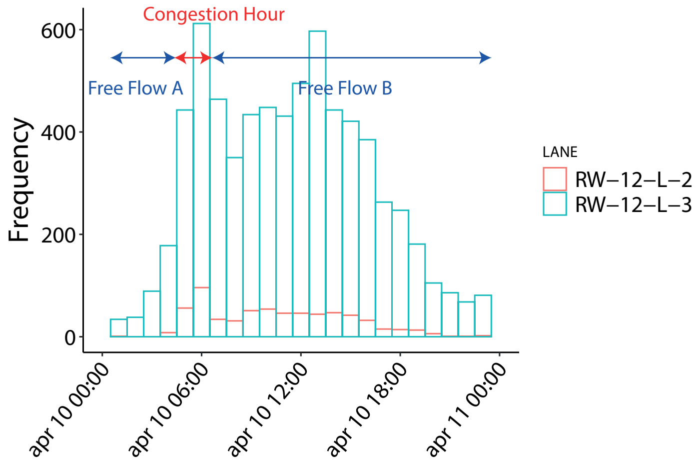

Figure 5.13: Hourly classification of traffic of WIM data [115]. April 4th, 2013.

For these six traffic scenarios, the corresponding inter-vehicle distances $\{X_t\}$ are obtained as shown in Equation 5.10 [115].

$$X_t = S_{t-1} * (i_t - i_{t-1}) \tag{5.10}$$

Where,

- X_t: Inter-vehicle distance at discrete time t [km].
- S_{t-1}: Vehicle speed at time $t-1$ [km/h]. The vehicle is assumed to travel at constant speed.
- i: Discrete time indices of the variable of interest (not calendar time).

Daily Analysis

On a daily scale, two variables are analysed: i) the daily distribution of vehicles per lane and ii) the daily amount of vehicles per traffic scenario. Empirical cumulative distribution functions (ECDFs) are constructed to characterise the daily number of vehicles throughout the month in lane 2 and 3. This is to gain insight into how the daily number of vehicles (on normal-condition days) varies. These ECDFs were not fitted to parametric distribution functions, since the number of normal conditions days is small. Consequently, the fit would not be reliable. Figure 5.13 shows that the number of vehicles in lane 2 is much smaller than in lane 3 at any time of the day. The average daily number of vehicles for lanes 2 and 3 is approximately 460 and 5150 vehicles, respectively.

Creating the "ideal" day

One single day was chosen to represent the entire month for calculation the daily number of vehicles per traffic scenario. This was the result of comparing the data for each day with normal conditions, considering factors such as the daily vehicle count and the existence of measurement errors. April 10^{th} appeared to have the highest number of vehicles and the lowest number of measurement errors. Thus, the proportion of vehicles per traffic scenario was obtained from the selected day (see B.2). The selected proportion is used to estimate the number of vehicles per category and traffic scenario given a daily number of vehicles. The definitions of vehicle categories are presented in B.1.

An ideal day is defined by combining i) the daily proportion per category and type of traffic and ii) the fitted copulas characterising D_t per type of traffic. This ideal day is a representation of the entire month and is the basis of the traffic simulation algorithm.

As mentioned previously, the daily proportion (%) per category and traffic type is represented by data from April 2013 10^{th} (Figure 5.13). The inter-vehicle distances (D_t) of all traffic scenarios (of each day of normal conditions) were fitted to bivariate copulas. This process characterises the dependence of the distance between vehicles and its lagged version (D_t,D_{t+1}). As a result, the autocorrelation of this variable is obtained.

Following a similar approach as for vehicle proportion, the copula that characterises the ideal day was selected by comparing the fitted copulas (and its parameters) of every normal-condition day among the six traffic scenarios. The criteria for choosing an appropriate copula include:

- The selected copula is the best fit for most of the normal-condition days of a given traffic scenario.
- The correlation value obtained from the simulated data (generated by the fitted copula) is similar to the correlation of the observations.

As a result, each traffic scenario is characterised by different copulas, each one belonging to different days of the month (Section 5.4.1).

Monthly Analysis

In this section, the number of vehicles per category and its corresponding proportion (%) relative to the monthly number of vehicles was calculated. The monthly proportion of vehicles is very similar to the daily proportion. This classification was applied to the entire data set without making any distinction between lanes.

The monthly proportion (B.3) is used as input for the BN model developed by Mendoza-Lugo (2022) [26] (Figure5.12). This model generates a vehicle characteristics data set (VH) according to its category while maintaining the same proportion of vehicles as input. In other words, the BN model provides the number of axles, axle weights, and inter-axle distances of the vehicles according to its category. For a complete overview of the BN model, the reader is referred to Mendoza-Lugo (2022) [26]. For this study, the VH data set contains 300.000 passing vehicles characterised by the proportion of categories presented in B.3.

5.4. Results

5.4.1. Copula-based model for inter-vehicle distances

As mentioned in section 5.3.1, traffic is characterised by six different traffic scenarios (Table 5.1). By combining the fitted copulas of each traffic scenario with the selected daily proportion of vehicles, an "ideal-day" data set is formed. This data set is the basis for the simulation of traffic through the SFT.

Table 5.2 presents the copulas that were selected for each scenario and its corresponding parameters (see Table 5.1 for nomenclature). Note that copulas of different days characterise each one of the traffic scenarios. The VineCopula package (in R), developed by Schepsmeier et al. (2018) [110] was used to fit the copulas to the data sets (Section 5.2.2). The parameters were estimated by pseudo-maximum likelihood, and the copula families were selected on the basis of Akaike's information criterion (AIC).

Scenario	Copula	Day	Copula parameter(s)	
C_L2	Gaussian	25	ρ = 0.148	-
C_L3	Frank	10	θ = -0.304	-
F_L2_A	Joe	17	θ = 1.519	-
F_L2_B	BB8	17	θ_1 = 1.717	θ_2 = 0.900
F_L3_A	Gumbel	17	θ = 1.137	-
F_L3_B	Joe	11	θ = 1.160	-

Table 5.2: Selection of copula and corresponding parameters for each scenario.

Table 5.3 shows the Spearman's correlation value for the observations (D_t,D_{t+1}). Note that the correlation values are relatively low, especially for C_L2 and C_L3. Nevertheless, the selected copulas are able to capture well the characteristics of the inter-vehicle distance for the simulation of traffic.

For the case of C_L3, the correlation value is negative. This means that the distance between vehicles at time t increases the inter-vehicle distance at time $t+1$ decreases or vice versa. Physically, this means that when a vehicle gets closer to the one in front of it, it gets further away from the vehicle behind. Similarly, a positive correlation means that the inter-vehicle distance behind a vehicle increases as the distance behind it also increases.

	Correlation
C_L2	0.103
C_L3	-0.093
F_L2_A	0.414
F_L3_A	0.289
F_L2_B	0.054
F_L3_B	0.10

Table 5.3: Spearman's Rho correlation value for observations of traffic scenarios.

Figure 5.14 shows the simulated inter-vehicle distances together with the observations for each traffic type. The data is presented as standard normal. The plots from both simulations and observations are very similar. Notice that the observations for congestion traffic scenarios (Figure 5.14a-5.14b) are clustered mainly in the centre with their shape resembling a circle. Although the plots for the free flow scenarios (Figures 5.14c-5.14f) are clustered in the centre, they present a slight asymmetry in the upper right corner of the plots. Nevertheless, the dependence structure of these copulas does not present great asymmetry, and the correlation values of the observations and simulations are very similar despite being relatively small. This is confirmed by the results presented in B.2.

The resulting simulated traffic series has an extent of 1 year (365 days) and represents traffic during regular weekday conditions, since weekends and national holidays were ignored in the analysis. This time series is used as input for the structural model.

5.4.2. Structural Model

In order to derive the structural response of the SFT, a model is proposed that combines the Direct Stiffness Method (DSM) and the differential equation method (DEM). A detailed description of this model is presented in B.5. The structural model is based on an arbitrary design of a pontoon-SFT structure that contains the basic elements for a design calculation of a single-tube tunnel layout. From this structure, two spans with two half-apart spans are modelled. The tubular section has an outer radius $R_o = 5m$, a wall thickness of $t_s = 1m$, and a BWR of 1.1 is assumed. When the structure is loaded with a BWR of 1.1, the resulting bending moments (M_{BWR}) at the tethers and in the centre of the span are $84MNm$ and $-42MNm$ respectively. To ensure water tightness, $200mm$ of the section must be compressed. For the middle section, a minimum axial compression force ($F_{ax,pt,centre}$) equal to $17.2MN$ is needed to ensure water tightness. For the section on the tethers, the force $F_{ax,pt,tether}$ must be at least $34.4MN$. Both of these forces can be accommodated by regular axial post-tensioning with equally distributed post-tension tendon around the circumferential. For a 15-strand tendon with an area of $150mm^2$ and a post-tension stress of $950N/mm^2$, a post-tension force of $2.14MN$ is found. Either 9 and 17 post-tension tendons will suffice for either of the two positions. In Figure 5.10, the green dots represent 17 tendons that are symmetrically distributed over the circumference.

The bending moments will increase due to the action of the traffic loads as presented in Figure 5.8. The design challenge is to provide post-tensioning to meet the reliability requirement of the system with respect to leakage and the minimum compression zone. If the requirement is not met, additional post-tension can be applied. If additional tendons are applied asymmetrically (presented in Figure 5.10 in purple), a counterbalancing bending moment is introduced. This is beneficial to the capacity of the particular axial section. The amount of asymmetry can be found in the lever arm (a) of the resulting force and the moment of posttension. If the lever arm (Figure 5.16) is increased, the counterbalancing bending moment will be greater. Therefore, a larger lever arm will provide a larger counterbalancing bending moment with the same number of post-tension tendons (Figure 5.16) . However, the lever arm is limited by geometric requirements such as the physical section, shape and the minimum dis-

5

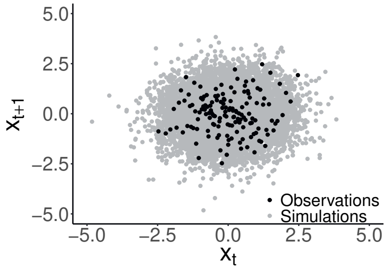

(a) C_L2

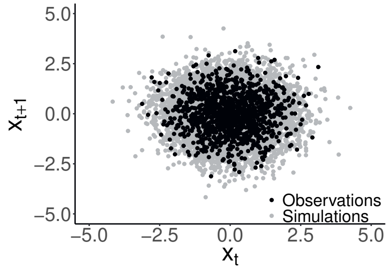

(b) C_L3

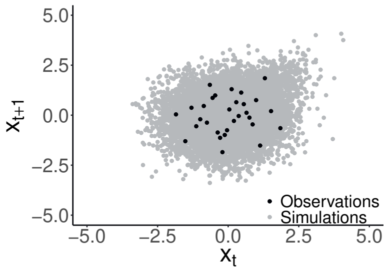

(c) F_L2_A

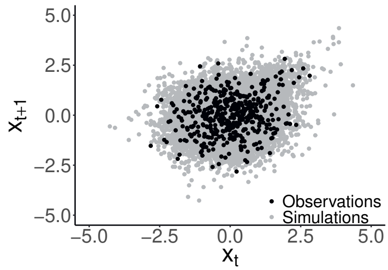

(d) F_L2_B

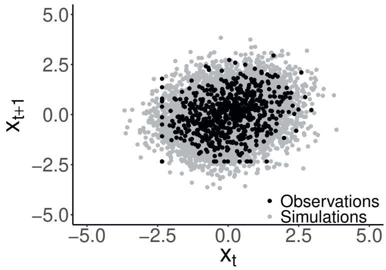

(e) F_L3_A

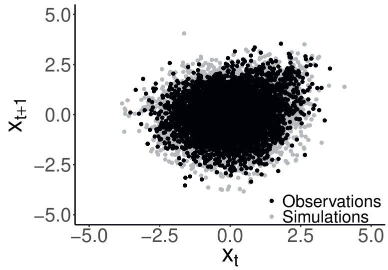

(f) F_L3_B

Figure 5.14: Observations and simulations for inter-vehicle distances (X_i, X_{i+1}) for all traffic scenarios from (a) Gaussian Copula, (b) Frank Copula, (c) Joe Copula, (d) BB8 Copula, (e) Gumbel Copula and (f) Joe Copula; parameters are estimated via maximum likelihood. The data is presented in standard normal units.

tance between two tendon heads. The centre-to-centre (ctc) distance between asymmetric tendons is estimated at 1 m; however, optimising this distance to a smaller distance could improve the design but is beyond the scope of this research. The relationship between bending moments and normal forces due to post-tensioning and the number of tendons for different lever arms is presented in Figure 5.15.

With the number of tendons, the normal force due to post-tensioning is found, and the bending moment is obtained by multiplying the total normal force due to post-tension by the lever arm. For simplicity, the same post-tension tendons were used in this analysis.

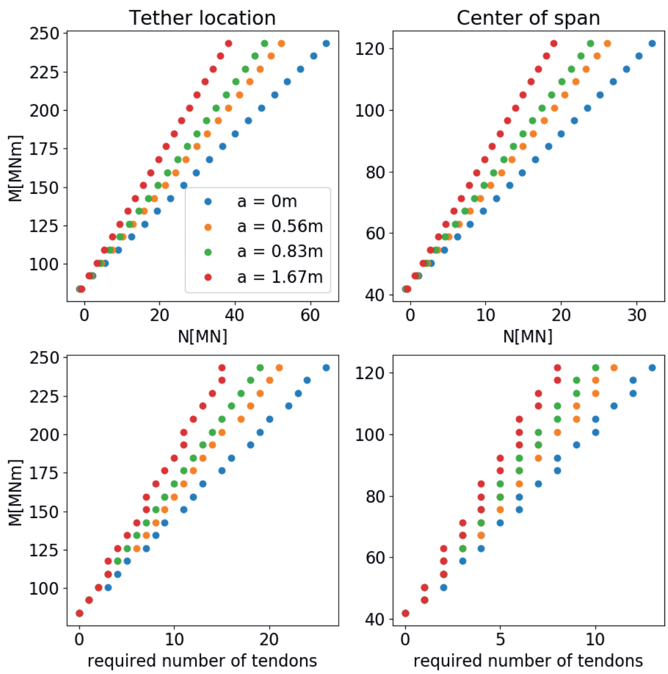

Figure 5.15: Bending moments related to the required normal force and number of tendons.

The geometry of the cross section is determined by many factors, such as the traffic envelope in combination with the BWR. Additionally, in an SFT, the hydrodynamic loads are directly related to the cross-section's geometry. For example, if the cross section is enlarged, then the capacity of the SFT will increase, but the effect of these loads will also be greater. Thus, adjusting the cross section geometry is not a straightforward solution as it might be for traditional structures, like bridges or buildings. However, to increase the structural strength, additional post-tensioning can be added. By varying the physical location of the tendons in the cross section, the lever arm can be changed. With a larger lever arm the bending capacity will increase.

In Figure 5.15 and Figure 5.16 different tendon layouts and spread angles are presented for the same number of tendons. By varying the spread angle, different lever arms can be obtained. The most efficient position of asymmetric post-tensioning is as close as possible to the outer fibre. However, post-tension tendons also have to meet construction requirements, such as the intermediate distances between the tendons and the ability to actually post-tension. These requirements may conflict with the most efficient location of the tendons. For this case study, a minimum distance of 1 m is considered from the centre to the tendons. Any optimisation that can be derived by changing this distance to a minimum value is out of the scope of this research.

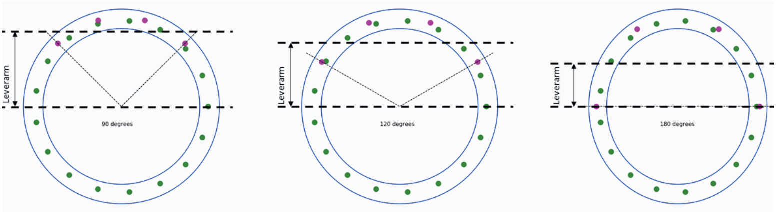

Figure 5.16: Different tendon layout for 60, 120 and 180 degrees spread (purple)

5.4.3. Reliability Analysis

The probability of failure (P_F) of the SFT was tested for bending failure of the SFT tube in the longitudinal direction. Its corresponding limit state is defined by Equation 5.7 when $\sigma_f > 0$, from which the bending moments due to traffic ($M_{tr,cap}$) are derived (Section 5.2.5).

The probability of failure of the SFT in this particular failure mode is defined as $P_F = P(M_{max} > M_{cap,max})$ or $P_F = P(M_{tr,max} > M_{tr,cap,max})$ or equivalent for the minimal moments $P_F = P(M_{min} > M_{cap,min})$ or $P_F = P(M_{tr} < M_{tr,cap,min})$ (Section 5.2.5). The limit state function is defined in Equation 5.11.

$$Z = P(M_{max} > M_{cap,max}) \tag{5.11}$$

M_{max} and M_{min} are, respectively, the maximum allowable capacity of the SFT in the centre of the span and at the tether location (Figure 5.8). In other words, failure is considered when the maximum bending moment exceeds the moment capacity M_{cap}, which can be positive and negative because of sign conventions. These limit values are directly dependent on the asymmetric post-tensioning.

The reliability analysis is divided into two parts. First, the resulting daily bending moments and shear forces obtained from the structural model are fitted to the probability distribution functions. From which their corresponding annual maximum frequency curves are derived. The second part is defined by the design of the post-tensioning. For a given SFT design, the limit bending moments are found. Consequently, the probabilities of exceeding these limit values are found through the annual maximum frequency curves.

Structural analysis was performed for different buoyancy-weight ratio (BWR) values ranging from 1.1 to 1.5. In this chapter, the focus was on a BWR=1.1 and the corresponding $M_{cap,max}$ and $M_{cap,min}$ to determine the probability of failure of the SFT. From a design point of view, a BWR close to 1.0 is the most economical. The BWR ratio results in a distributed load. By applying a lower BWR, the spans used in the structure can be larger. If larger spans can be used, less supporting pontoons are needed. The authors realise that other elements, such as loading or stability requirements, might cause the need for a larger BWR, but these are considered to be beyond the scope of this study. However, the results for other BWR values as well as their associated $M_{cap,max}$, $M_{cap,min}$, $V_{cap,max}$ and $V_{cap,min}$ are also shown.

Frequency Curves

The resulting daily values of the bending moments ($M_{cap,max}$ & $M_{cap,min}$) and shear forces ($V_{cap,max}$ & $V_{cap,min}$) obtained from the structural model (Section 5.4.2) were fitted to the probability distribution functions. The results are shown in Table 5.4.

BWR	M_{max} [MNm]	M_{min} [MNm]	V_{max} [MN]	V_{min} [MN]
0	Gamma	G.E.V. [1]	Lognormal	Birn-S[2]
1.1	G.E.V.	G.E.V.	G.E.V.	G.E.V.
1.2	G.E.V.	G.E.V.	G.E.V.	G.E.V.
1.3	G.E.V.	G.E.V.	G.E.V.	G.E.V.
1.4	G.E.V.	G.E.V.	G.E.V.	G.E.V.
1.5	G.E.V.	G.E.V.	G.E.V.	G.E.V.

Table 5.4: Distribution Fitting for bending moments and shear forces.

BWR	M_{max} [MNm]			M_{min} [MNm]			V_{max} [MN]			V_{min} [MN]		
	Shape	Scale	Location	Shape	Scale	Location	Shape	Scale	Location	Shape	Scale	Location
0	25.88	0.95	-	-0.04	5.39	22.81	-0.15[3]	0.22[3]	-	0.22	0.87	
1.1	-0.17	4.50	106.60	-0.05	5.63	63.74	-0.09	0.17	3.32	-0.06	0.11	2.75
1.2	-0.17	4.50	176.64	-0.05	5.62	98.62	-0.09	0.17	5.42	-0.06	0.11	4.85
1.3	-0.17	4.50	235.91	-0.05	5.62	128.19	-0.09	0.17	7.20	-0.06	0.11	6.63
1.4	-0.17	4.50	286.71	-0.05	5.61	153.56	-0.09	0.17	8.72	-0.06	0.11	8.15
1.5	-0.17	4.50	330.74	-0.05	5.61	175.56	-0.09	0.17	10.05	-0.06	0.11	9.47

Table 5.5: Parameters of the fitted distributions.

The criteria for selecting an appropriate probability distribution function were made based on maximum likelihood estimation (MLE) and visual inspection. Table 5.5 presents the parameters of the fitted distributions.

The corresponding annual maximum frequency curves for both the bending moments and the shear forces for a BWR of 1.1 are shown in Figure 5.17. From these plots it is possible to determine the return period (or probability of exceedance) of particular values for bending moments and shear forces. The corresponding values $M_{cap,max}$, $M_{cap,min}$, $V_{cap,max}$, and $V_{cap,min}$ for different return periods (or probability of exceedance) and BWR magnitudes are shown in Table 5.6. The results appear to be sensitive to the choice of BWR. As the BWR increases, the values for the maximum bending moments and maximum shear forces also increase. This highlights the importance of the choice of BWR when designing an SFT.

[1]Birnbaum-Saunders
[2]Generalized Extreme Value Distribution
[3]For the lognormal distribution, the parameters are: mean and standard deviation.

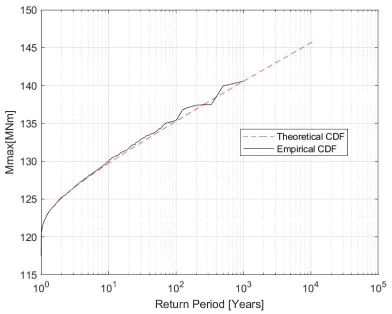

(a)

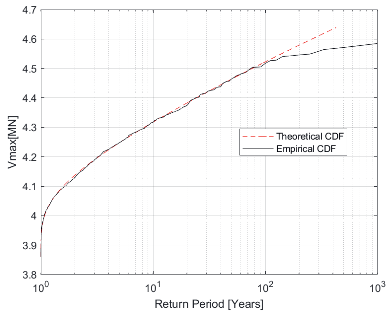

(b)

Figure 5.17: Frequency curves for (a) $M_{Max}[MNm]$ and (b) $V_{Max}[MN]$ for a 1.1 BWR

BWR	Variable	Return Period & P_F						
		5	10	20	50	100	200	500
		0.2	0.1	0.05	0.02	0.01	0.005	0.002
0		43	43	44	44	44	44	44
1.1		128	130	132	134	136	140	142
1.2	$M_{cap,max}[MNm]$	198	200	201	204	205	207	208
1.3		257	259	261	262	264	265	266
1.4		308	310	312	313	314	316	319
1.5		352	354	356	358	359	360	364
0		55	58	61	66	68	73	76
1.1		97	100	103	106	108	109	111
1.2	$M_{cap,min}[MNm]$	133	135	137	140	140	143	147
1.3		161	164	167	169	172	175	178
1.4		187	190	192	195	197	199	204
1.5		209	212	215	217	219	221	223
0		2	2	2	2	2	2	2
1.1		4	4	4	4	4	5	5
1.2	$V_{cap,max}[MN]$	6	6	7	7	7	7	7
1.3		8	8	8	8	8	8	8
1.4		10	10	10	10	10	10	10
1.5		11	11	11	11	11	11	11
0		2	2	2	2	2	2	2
1.1		3	3	3	3	3	3	3
1.2	$V_{cap,min}[MN]$	5	5	6	6	6	6	6
1.3		7	7	7	7	7	7	7
1.4		9	9	9	9	9	9	9
1.5		10	10	10	10	10	10	10

Table 5.6: Extreme values for $M_{cap,max}$, $V_{cap,max}$,$M_{cap,min}$, $V_{cap,min}$ for different return periods and a BWRs

Post-tensioning design

Post-tensioning is expensive in monetary terms. Thus, an economical design should limit the amount of post-tensioning. With the methodology presented in this chapter, the maximum moment due to traffic ($M_{tr,max,min}$) can be found more accurately and the design can therefore be economically optimised. The probability of occurrence associated with the resulting $M_{cap,min,max}$ is obtained from the frequency curves derived from Section 5.4.3. Thus, the probability of exceeding the limit values is translated as the probability of failure of the SFT.

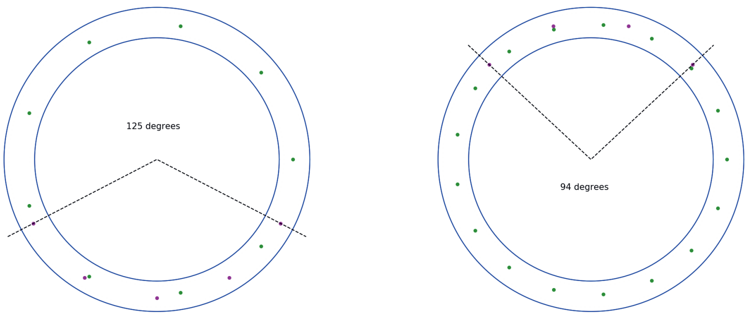

Figure 5.18: Layout of the post-tensioning for the cross section at the centre of the spans (left) and at the tether locations (right)

In Figure 5.18 the location of the post-tension tendons is presented for both the section in the centre of the span and the location of the tether. The proposed design layout is presented in Table 5.7 and the capacity for the maximum moment due to traffic is derived. According to Figure 5.17 and Table 5.6, the resulting M_{cap} in the centre of the span and in the tether location have a return period of 139 ($P_F = 0.01$) and 439 ($P_F = 0.005$) years, respectively.

The post-tensioning design can be modified to fit any probability of exceedance (or return period), specified by the target reliability index, presented in Figure 5.17 and Table 5.6. In this research, the presented layout is used as an example to show the application of the methodology.

Item	Unit	Centre of span	Tether location
Axial tendons	#	9	17
Asymmetric tendons	#	5	4
Spread angle	[degrees]	125	94
$N_{ax,pt}$	[MN]	-19.2	-36.3
$N_{as,pt}$	[MN]	-10.7	-8.6
a	[m]	3.31	-3.75
M_{pt}	[MNm]	-35.4	32.1
$M_{cap,max/min}$ = M_{BWR} + $M_{cap,max/min}$	[MNm]	108.4	-141.6
M_{BWR}	[MNm]	42.0	-84.0
$M_{tr,cap,max/min}$	[MNm]	66.4	-57.6
$M_{max/min}$ Return period	[year]	139	439

Table 5.7: Post tension specification and capacity

5.5. Discussion, conclusions and recommendations

Discussion

The methodology of the inter-vehicle model presented in this research combines univariate and multivariate models (copulas). This not only allows simulation of the distance between vehicles, but also models the number of vehicles per lane per day and their classification according to the different vehicle categories (B.1). Each vehicle category is defined by their axle weight and interaxle distance. The selection of each of the passing vehicles is random. In this way, it is possible to obtain a ”train” of vehicles that is closer to reality. One of the main advantages of this model is its flexibility. The model can be used for any number of vehicle categories, lanes, and traffic scenarios. In this case study, the model was developed on basis of one single ”ideal day”, nevertheless, the inter-vehicle model can be extended to encompass specific daily conditions (weekends and holidays) or seasonal conditions.

In the setup presented in this article, the geometry of the cross section and the length of the span are arbitrary choices. Higher BWR values lead to higher bending moments and shear forces, as shown in Table 5.6. This can influence other design decisions, such as shorter spans or larger tether sections, that could affect the stability of the system. In this research, the resulting bending moments and shear forces were computed for different BWR values. However, a BWR of 1.1 was chosen for further analysis. In any case, a design should be optimised for different circumstances. Possibilities to consider are (but not limited to):

- Using larger BWR values. This will lead to larger bending moments and shear forces. Consequently, other requirements for pontoons, tether systems, and foundations will be affected. However, a higher BWR could contribute to the stability of the system. Moreover, a longitudinal variation of the BWR might be applicable depending on local situations or specific design.
- In this research, a monolithic structure is considered. However, a more flexible structure with longitudinal rotational springs could be of interest depending on local circumstances, such as the action of hydrodynamic loads. This will help avoid local peak stresses or cross-sectional results. Yet, leakage at a flexible joint can be challenging from a design point of view.
- If larger diameter tendons are used in combination with a smaller spread angle, the mixed diameters of the post-tensioning tendons for both the axial and the asymmetric layout can be beneficial for the lever arm.
- In this research, the tendons are considered straight. It is a possibility to apply curved tendons in the longitudinal direction to benefit from the counterbalancing force provided by this curvature. However, curved tendons will generate an additional load in the radial direction.
- Although the SFT design presented in this chapter consists of a single tubular tube, the proposed methodology is applicable to different SFT designs (double tubes or different cross-section geometries as presented in [116]). Different geometries will influence the stiffness of the structure. If a double tube is used, the stiffness of the structure will be doubled and transversely aligned, and next

to each other aligned, it will double the stiffness and capacity if the tubes are structurally coupled. Larger sections, i.e. larger diameters, will increase stiffness but also capacity. Although the loading by traffic on the SFT will remain equal, it will influence the definition of failure. As the traffic load will act more asymmetrically, the effect of torsion will become more relevant and a more sophisticated model with 3D elements should be used.

- The current hypothetical model relies on concrete for its watertightness, if other methods, such as an external membrane that will ensure the watertightness, the failure mechanism will change from a crack criterion on the concrete to a strength criterion for concrete section or a service level criterion for the membrane. Note that a membrane on the outside of the SFT will introduce other issues, such as maintenance on the outside of the tunnel.

Conclusions

In this research, a methodology is presented to study the reliability of a pontoon-type SFT is presented. Considering that this structure has not been built yet, it is important that the variables of interest are characterised as close to reality as possible. For the purpose of this research, traffic loading is the variable of interest. The methodology is divided into two main parts, i) traffic simulation using a copula-based model, and ii) a structural model to test the SFT for a given failure mechanism (leakage due to bending of the SFT tube in the longitudinal direction). Finally, the reliability of the structure is investigated under the aforementioned failure mechanism.

5

From the original data set (WIM), several characteristics were extracted. Namely, i) the inter-vehicle distance, ii) the daily proportion of vehicles per lane, per category and per traffic type, and iii) the monthly proportion of vehicles. The first is used as input for the copula-based model, the second is used to create an "ideal" traffic day, and the third is used to create a large data set of vehicles per category. All of these were combined to finally simulate traffic flowing through the SFT.

The results of the copula model showed that the selected copulas can capture the inter-vehicle distance. Although the correlation of the intervehicle distance from the WIM data set is relatively small, the probabilistic model provides a great advantage since with just over a month of measurements it was possible to simulate a total of 1 year of data. However, longer data sets can be produced. The combination of the inter-vehicle copula model and random sampling from the VH data set (which provides the vehicle's characteristics) resulted in one vector that characterises daily traffic at the SFT. This vector was used as input for the structural model.

To simulate the response of the structure over long periods of time, the proposed structural modelling approach needs to be as efficient as possible. Thus, by defining the global DSM (Direct Stiffness Method) approach with long beams and a dedicated DEM approach for intermediate loading, the FEM model became as efficient as possible to avoid lag in the analysis. The analysis time was further reduced by applying the superposition principle.

The results of the structural model provided the maximum and minimum bending moments and shear forces under traffic load for different BWR values. From these results, the annual distribution of these variables and, consequently, their extreme values for several return periods were obtained.

Finally, the values of M_{cap} were obtained in the centre of the span and at the tether location. These values define the limit state function for failure due to tube bending in the longitudinal direction (Section 5.4.3). In other words, failure could occur only if the resulting bending moments exceed M_{cap}. The return periods for both M_{cap} of 108.4 MNm and -141.6 MNm are 139 and 439 years in the centre of the span and tether location, respectively. Their corresponding probabilities of failure are 0.01 and 0.005. These probabilities can be considered very high compared to international safety standards. For example, a structure with a RC3 reliability level (β=4.3) has an estimated probability of failure equal to 8.5e-06 [1] assuming that the lifetime of the structure is 50 years. For an SFT, the consequences of failure are much more severe than in regular buildings. For this reason, M_{cap} with longer return periods is needed. In such a case, changing the number and location of the tendons or using a different BWR could be appropriate, as mentioned above. As an alternative, modification of the section is also an option to consider, but the geometry of the section is usually earlier conducted in the design process and a given requirement when designing post-tensioning and/or regular reinforcement layouts.

Due to the lack of data regarding the structural response of an SFT, the combination of probabilistic modelling with structural analysis offers the possibility to study the design choices of this structure. This research shows an effective way to combine probabilistic modelling through copulas and structural analysis to simulate the traffic loads passing through the SFT and their effect on the structure. This methodology offers great flexibility because it can be used to test the reliability of the SFT considering other loading variables. For example, external environmental variables such as waves, currents, and their simultaneous action on an SFT. Moreover, this methodology is not restricted to use only on an SFT. It can be applied to other civil structures where the data is scarce.

Recommendations

The results were shown to be sensitive to the choice of BWR; therefore, this choice should be handled with caution when designing an SFT. Other limit states should be considered to assess the reliability of an SFT. For example, failure of the tethers, at the foundation or cross section. These failure modes could be considered as standalone limit states or in combination with each other. Assessment of combined failure modes could be executed through Bayesian networks.

6

Vine Copulas for Dynamic Response of Submerged Floating Tunnels

6.1. Introduction

In this chapter, a *dynamic mooring analysis* (DMA) is used for a hypothetical SFT supported by tethers. In these analyses, a diffraction analysis is conducted, sequentially followed by a time-history analysis. To describe environmental loads, real monitored data of wave height, period, and angle of impact are used from the Qiongzhou Strait. The structural responses of interest correspond to the maximum values of forces, displacements, and accelerations at the points of interest along the hypothetical SFT. The maximum values of structural responses are used together with the environmental input data, the wave height and period, to represent the multivariate probability distribution of the variables as a *Vine Copula* (VC) model. In total 14 different data sets of eight variables have been defined based on the combination of the input and the responses.

Probabilistic methods in structural design and specifically tunnels are rare, although Yu et al. (2017) [7] shows a probabilistic risk analysis in simulations of the construction of a diversion tunnel, Liu and Lu (2024) [8] shows a probabilistic seismic hazard analysis based on an enhanced Bayesian network in which information about frequency is used in inferencing and Pan et al. (2024) [9] shows a method to reduce costs and excavation-induced risks by proposing a probabilistic deep reinforcement learning framework to optimise monitoring plans.

Regarding VC, the fitting of RV structures to the data is done primarily with a popular algorithm based on maximising a function of the correlation matrix of variables or with *ad hoc* approaches. The fitting of all possible regular vines to the data has not been documented for multivariate probability distributions with 8 or more variables. The aim is to discuss the question of whether a particular vine-copula is suitable. Selection is based on the *Akaike Information Criterium* (AIC). Two methods are used to find the RV structure, using a common approach based on a *fitting algorithm* method (AL) and a *brute force method* (BF) by testing all possible regular vines of 8 variables. The number of unique RV increases rapidly and for 8 variables a total number of 660,602,880 different RV can be considered, a *High Performance Computer* (HPC) has been used in the BF method to calculate the AIC for each possible RV. After an RV and the accompanying copulas have been fitted, it can be used to sample and perform a conditional analysis, and with these results exceedance probabilities can be computed.

This chapter is a demonstration of how to compute exceedance probabilities in a sequential process of using a DMA together with VC and HPC to select an RV by using a BF method, and additional the difference between a commonly used selection method and the BF is presented by the differences in the computed exceedance probabilities. The probability of exceedance has a direct relation to the design of the structure. So, the most accurate exceedance probabilities are required to base design decisions on. Differences between both approaches can lead to too conservative and costly solutions in the design if the exceedance probability shows a higher value. But, on the other hand, if the exceedance probability is lower, it might result in a less reliable structures and even not safe enough with respect to the requirements.

6

The application of a DMA on SFT is a novelty, as SFTs are a novice and not yet built. DMAs are conducted by themselves, but the application is related to floating and mooring ships and their interaction and responses under wave conditions. Fitting data sets using an AL is a common probabilistic method, but using BF to fit data sets to RV with 8 variables is a novelty, as the Chimera database containing RV up to 8 variables has recently been released. Due to the amount of RV possible with eight variables, HPC has been used, which is uncommon in combination with VC and structural assessment of structural designs.

The chapter starts with a brief overview in Section 6.2 of the methodologies presented about the DMA of the SFT and some background of HPC. More explanation about VC, RV and the algorithm is explained in Chapter 2 In Section 6.3 the DMA model is explained in more detail, and in Section 6.4 the selection of the best RV is presented. In Section 6.5 the best RVs are used for conditioning and the differences between AL and BF are shown. The chapter is closed in Section 6.6 with conclusions and recommendations for future research.

6.2. Methodologies and components

6.2.1. Dynamic Mooring Analysis

To calculate the dynamic response of the SFT, commercial software is used for the DMA. This software is developed by `MARIN` and the analysis consists of two sequential parts, a diffraction analysis and a time history simulation of the model. `DIFFRAC` is a wave diffraction programme that is used to calculate the loads and motion responses of floating or moored multibody structures. `aNySIM` computes the motions of vessels resulting from non-linear hydrodynamic and mechanical loading. Initially, this software was developed for DMA on ships to find their responses and interactions. In this research, the SFT is divided into different elements and the interaction between the elements as well as the response of the elements. Both packages are used in different publications on wind turbines [27–31]. More detailed information on both tools can be found in [32]. The setup of the dynamic response model used in the DMA is presented in detail in Section 6.3.

6.2.2. High performance computing

The brute-force method requires a large computational effort to test all 660,602,880 RVs of 8 variables. To run this selection process, a high performance cluster (HPC) has been used [34]. This cluster of computers runs on a `Linux` operating system and is controlled using appropriate scripts. In Figure 6.1 an overview of the control is presented. First of all, the RVs are split into their tree equivalent classes, which for 8 nodes are in total 1,464. Their matrices were made available by a `MYSQL` database [117] using the RV database on up to 8 nodes `Chimera` [35]. The basis of the BF algorithm is to run over a subset of matrices as available, and for each subset the individual AIC scores and the elapsed times are saved together with the VC characteristics of the best VC in terms of the AIC score. The 1,464 scripts are sent to the queue, administered by SLURM [118] with the arguments related to the number of CPUs, the amount of memory to be used and the maximum running time. The actual job of the subset of the tree equivalent class of RV is split over the specified CPUs using `OPENMPI` [119]. After all CPUs have completed their task, the total results are collected and saved for the tree equivalent class. After all 1,464 individual jobs have been conducted, in an additional post-processing analysis, all results for a particular dataset are combined.

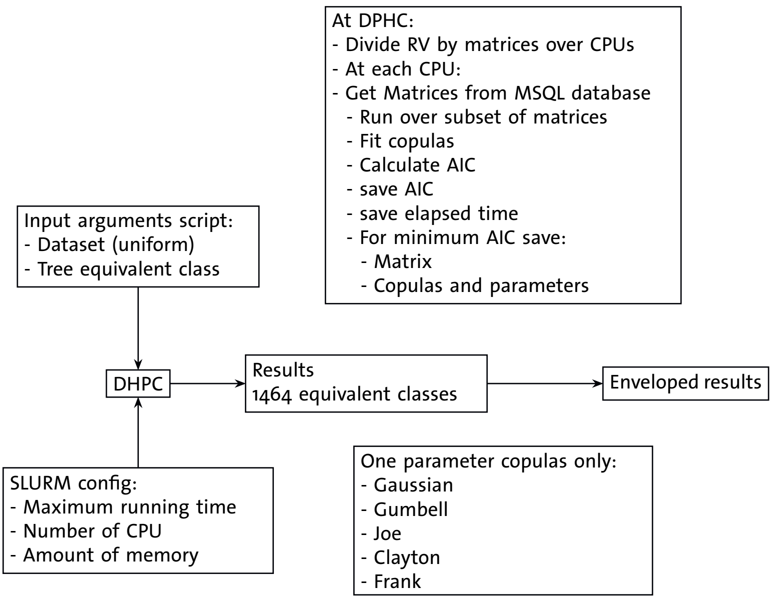

Figure 6.1: High performance cluster - Pyvinecopula diagram - configuration

6.3. Dynamic response model

The hypothetical SFT is represented by a model presented in Figure 6.3, the SFT is made up of 20 elements of 100 m length and is vertically supported by 5 tethers, and in the centre of the structure, the model is laterally supported by 2 mooring lines. The tethers and mooring lines are represented by spring elements and because the structure is positively buoyant, the tethers have an initial pretension stress. At both ends, the structure is supported by hinged connections.

The total DMA sequence is schematically visualised in Figure 6.4. The analysis is set up as a staggered analysis in which a diffraction analysis is combined with a time history analysis. The diffraction analysis is used to compute the hydrodynamic load on the structure based on a series of wave and current loads using a velocity potential around the structure as a function of the angle of impact and the wave period for a unified wave height. For the time history analysis, a wave load as a function of time is generated based on a JONSWAP analysis as described by Hasselmann (1973) [120], given the wave height and length characteristics. Combining the generated wave signal by the JONSWAP analysis and the diffraction result (velocity potential) to a time-dependent input on the structure gives a wave load over time. Using this wave load over time enables a time history analysis and the collection of a time history response of the structure (tether forces, mooring forces, displacements, rotations, and accelerations) based on a specified wave height, wave period, and angle of impact. For representative points in the structure and the tethers, the response over time is stored in a data set per analysis.

6

As input wave period (T_p [s]), wave height (H_s [m]) and angle of impact (ϕ [degrees]) for these analyses were used and based on monitoring data. The monitoring data was retrieved from ERA5 [121]. Torres et al. [122] give a description of how to obtain the input data set. ERA5 provides climate reanalysis data sets. For monitoring data, observations in the time span 2000 to 2019 have been used in the Qiongzhou Strait with a specific location in area 4, see Figure 6.2 (based on Torres et al. (2021) [123]). The wave data set was checked for outliers; an outlier was considered if it deviates more than 7 times the standard deviation of the monthly data from its mean. As SFTs are vulnerable to swell waves, a conditional draw from the monitoring data was performed by considering only wave periods greater than 7.8s. Furthermore, initially the structure is experiencing start-up distortion, and therefore only the results after $150s$ were considered.

A total time history analysis is intense in terms of computational effort and, within a limited time frame, 497 different analyses were performed.

Two types of samples are subtracted from the results for each analysis. For the first data set (denoted as corresponding and abbreviated by cor), the maximum tether force of all tethers per analysis is selected. The maximum tether force appeared to be found in tether 2. The first data set is compiled taking samples with the state of all responses at the moment of occurrence of the maximum tether force in tether 2. The sample contains the absolute difference between the actual response value subtracted by the average response of the value over time in the analysis. The second data set (denoted maximum and abbreviated max) is compiled by taking samples of the maximum amplitudes of the response of the points of interest subtracted

Figure 6.2: Overview of the grid at Qiongzhou Strait

by the average response value. As maximum values will not occur at the same moment in the time series, the dependencies between the variables in the corresponding datasets are smaller than in the maximum datasets.

From the two types of data sets, 7 subsets of data containing 8 variables are used. The subsets are presented in Table 6.1. The indices refer to the positions presented in Figure 6.3 and in which F is the tether force (in $[N]$), du displacements (in $[m]$) and da accelerations (in $[m/s^2]$). The y and z indices refer to the lateral and vertical directions, respectively. In the data sets of 8 variables, T_p (in $[s]$ and H_s (in $[m]$) are initially used as input to the DMA, and the remaining variables are responses from the model. The analysis itself is a hypothetical model, primarily to demonstrate this method. The DMA can be significantly improved, but this is beyond the scope of this research.

Table 6.1: Overview of datasets

#	var 1	var 2	var 3	var 4	var 5	var 6	var 7	var 8
1	F_2	F_3	F_4	du_{y2}	du_{y4}	du_{y6}	H_s	T_p
2	F_2	F_3	F_4	du_{z3}	du_{z5}	du_{z7}	H_s	T_p
3	F_2	F_3	F_4	da_{y2}	da_{y4}	da_{y6}	H_s	T_p
4	F_2	F_3	F_4	da_{z3}	da_{z5}	da_{z7}	H_s	T_p
5	F_2	da_{y2}	da_{y4}	du_{y2}	du_{y4}	du_{y6}	H_s	T_p
6	F_2	da_{y2}	da_{y4}	da_{y6}	da_{y3}	da_{y5}	H_s	T_p
7	F_2	da_{z2}	da_{z4}	da_{z6}	da_{z3}	da_{z5}	H_s	T_p

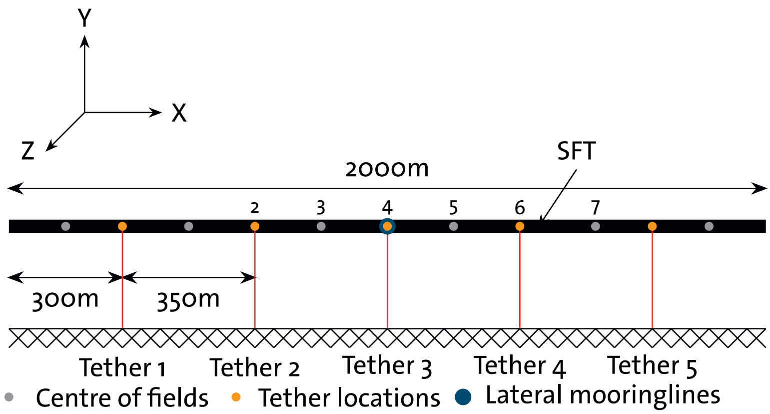

Figure 6.3: Schematic model

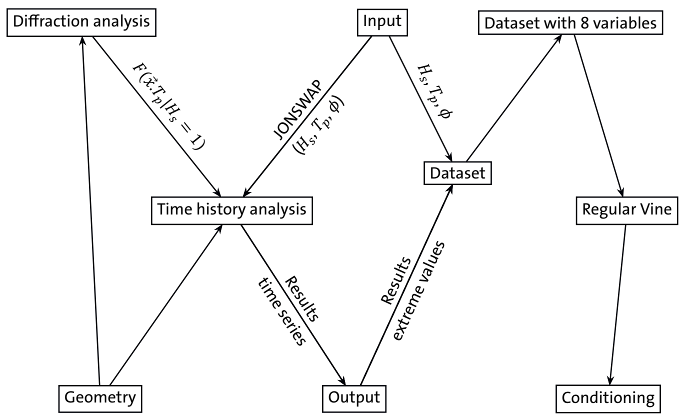

Figure 6.4: Diagram of analysis

6.4. Regular Vine selection

In order to apply the vine methods, the distributions of the variables must be transferred to the [0,1] domain of their *empirical cumulative distribution function* (ECDF). As mentioned, the RV which best describes the dependencies is considered and selected by the AIC score for both methods. Table 6.2 shows a summary of both approaches for the 14 datasets. In the table, the AIC scores for both methods are presented. The time is the sum of the elapsed time [days] of the individual subprocesses in the HPC. The total amount of time needed to find the best RV is around 5 to 6 years. It is obvious that the BF process is not feasible for 8 variables using a current regular commercially available computer. The BF analysis need to be conducted sequentially only using the parallel resources available by the cores in that case. In contrast, the RV found using the AL approach takes only a few seconds, which is easily achievable on such a machine.

As expected, the AIC scores for the BF RV are better than those for the AL RV, as the AIC AL RV can only be equal as BF RV as it is only one of the BF RV. If the empirical cumulative distribution of the AIC scores of all BF RVs is considered, the relative amount of RV that performs better on the AIC score than the AL RV can be found. Figure 6.7 shows this distribution of the entire BF RV and the AIC of the AL RV for dataset 6 maximum. This run shows that compared to the AL RV 29.6% of the BF RV perform better, as they show a lower AIC value and describe the dependencies better. The RVs of both are presented in Figures 6.5 and 6.6 and are, respectively, described by the matrices $M_{bf,6,max}$ and $M_{al,6,max}$. In the last column of Table 6.2, the percentage of BF RVs that have a better score than AL RV.

Tables 6.3 and 6.4 show the individual equivalent RV for all data sets for both BF and AL. Each individual data set shows a different equivalent RV for BF as for AL. For the same data set, the matrices $M_{bf,6,max}$ and $M_{al,6,max}$ are presented.

$$M_{bf,6,max} = \begin{bmatrix} 1 & 5 & 1 & 5 & 5 & 5 & 3 & 3 \\ 5 & 1 & 5 & 2 & 2 & 3 & 5 & 0 \\ 8 & 6 & 2 & 4 & 3 & 2 & 0 & 0 \\ 6 & 2 & 4 & 3 & 4 & 0 & 0 & 0 \\ 2 & 4 & 3 & 1 & 0 & 0 & 0 & 0 \\ 4 & 3 & 6 & 0 & 0 & 0 & 0 & 0 \\ 3 & 8 & 0 & 0 & 0 & 0 & 0 & 0 \\ 7 & 0 & 0 & 0 & 0 & 0 & 0 & 0 \end{bmatrix} M_{al,6,max} = \begin{bmatrix} 2 & 6 & 7 & 2 & 4 & 4 & 8 & 8 \\ 4 & 2 & 4 & 4 & 2 & 8 & 4 & 0 \\ 6 & 4 & 2 & 8 & 8 & 2 & 0 & 0 \\ 5 & 8 & 8 & 7 & 7 & 0 & 0 & 0 \\ 8 & 7 & 6 & 6 & 0 & 0 & 0 & 0 \\ 7 & 1 & 1 & 0 & 0 & 0 & 0 & 0 \\ 1 & 5 & 0 & 0 & 0 & 0 & 0 & 0 \\ 3 & 0 & 0 & 0 & 0 & 0 & 0 & 0 \end{bmatrix}$$

In the figures, the full RVs with all trees are presented. Figures C.3 and C.4 show the same RVs but split into their different trees. The definition of RV matrices is provided by Czado (2019) [63]. Differences in RVs can be observed while the BF approach results in T46 + T23 + T9 + T6 + T4 + T3 + T2 and the AL results in T34 + T22 + T10 + T6 + T4 + T3 + T2. Each connection in the presented figures is described by a bivariate copula distribution. Both methods fit the bivariates and, as mentioned before in this analysis, only 1 parameter copulas are used. In Appendix C.2 the copula definitions for this specific run are presented. Both RV with bivariate copulas can be used to sample and condition, which is a topic of Section 6.5.

6

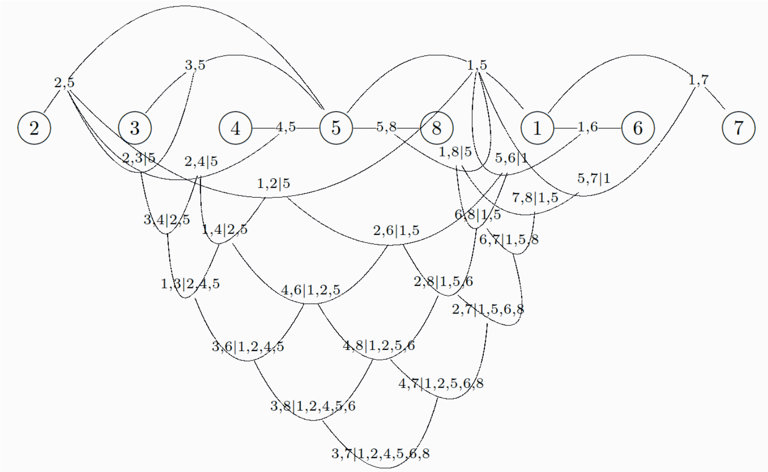

Figure 6.5: Maximum - Regular Vine - brute force 6

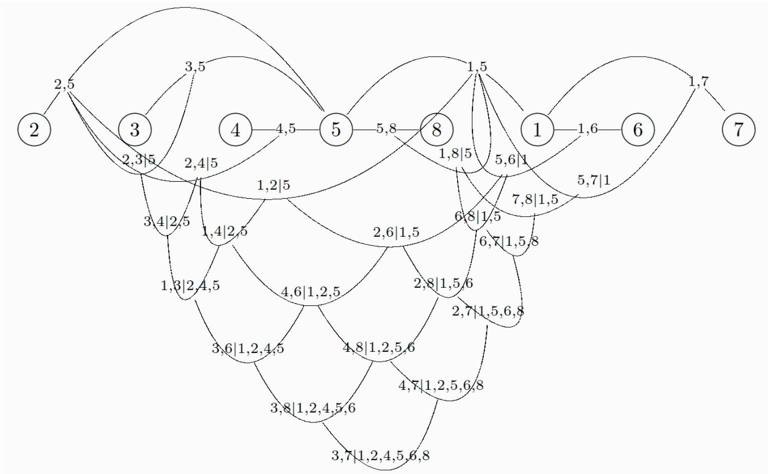

Figure 6.6: Maximum - Regular Vine - Algorithm 6

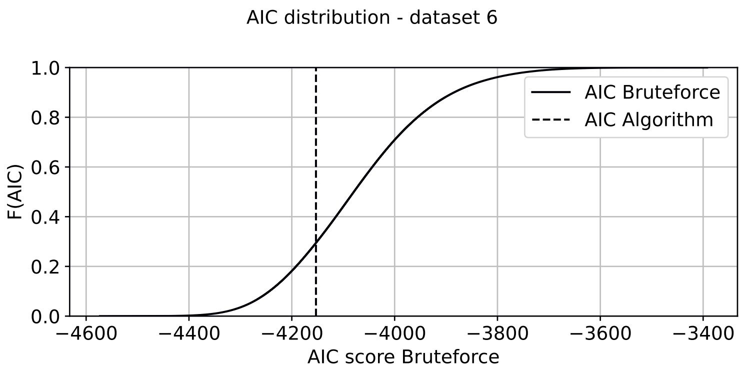

Figure 6.7: Distribution of AIC for run 6 - maximum values

Table 6.2: Comparison of method scores

#	Type	brute force AIC	Algorithm AIC	Time days	Algorithm score [%]
1	cor	-1797.2	-1548.0	1861.7	35.8
1	max	-6146.3	-5906.7	2182.0	2.0
2	cor	-2453.4	-2209.3	2051.3	9.9
2	max	-7777.5	-7139.8	2227.5	0.0
3	cor	-1790.8	-1562.5	1882.5	49.1
3	max	-5653.3	-5372.6	2204.3	2.2
4	cor	-1757.2	-1664.4	2147.2	3.6
4	max	-3622.0	-3552.3	2354.3	0.3
5	cor	-2924.0	-2557.5	1894.2	83.3
5	max	-5771.7	-5476.2	1935.9	1.3
6	cor	-2090.3	-1800.7	1868.6	69.5
6	max	-4573.7	-4153.0	1873.6	29.6
7	cor	-2749.6	-2429.6	2298.1	21.3
7	max	-998.8	-970.3	1991.8	0.2

Table 6.3: Best Vines of analyses - corresponding values

#	brute force vine	Algorithm vine
1	T45+T18+T11+T7+T5+T3+T2	T33+T16+T9+T6+T4+T3+T2
2	T38+T15+T9+T6+T4+T3+T2	T46+T17+T10+T7+T5+T3+T2
3	T46+T21+T13+T6+T4+T3+T2	T42+T20+T11+T7+T4+T3+T2
4	T44+T22+T10+T6+T4+T3+T2	T42+T22+T10+T6+T4+T3+T2
5	T46+T23+T12+T8+T4+T3+T2	T30+T17+T9+T6+T4+T3+T2
6	T34+T22+T13+T7+T5+T3+T2	T31+T18+T11+T7+T4+T3+T2
7	T35+T17+T11+T7+T4+T3+T2	T31+T17+T9+T6+T4+T3+T2

Table 6.4: Best Vines of analyses - maximum values

#	Brute force vine	Algorithm vine
1	T44+T20+T13+T7+T5+T3+T2	T28+T16+T10+T6+T4+T3+T2
2	T33+T20+T10+T6+T4+T3+T2	T27+T15+T9+T6+T4+T3+T2
3	T38+T17+T11+T6+T4+T3+T2	T28+T16+T10+T7+T4+T3+T2
4	T46+T19+T12+T6+T4+T3+T2	T34+T22+T9+T6+T4+T3+T2
5	T46+T21+T9+T6+T4+T3+T2	T30+T18+T11+T6+T4+T3+T2
6	T46+T23+T9+T6+T4+T3+T2	T34+T22+T10+T6+T4+T3+T2
7	T35+T21+T11+T7+T4+T3+T2	T30+T17+T9+T6+T4+T3+T2

6.5. Sampling and conditioning

The different VCs are used to sample multivariate distributions. The amount of possible samples is specified by the user. In this research, a sample size of 5000000 is used. As the RV represents the data set, the samples' distributions show a strong similarity to the original data set. Appendix C.1 shows the data set in pair plots of the data set of the maximum run 6 in the unit domain. Figures 6.8 and 6.9 show the empirical distributions of the same run for da_{y4} and da_{y6}, respectively. Five different distributions are presented, and in the graph the distributions of the original data set are presented (black), as well as both samples of the RVs (darkblue and lightblue). RVs sampled in the [0,1] domain are converted back to the original domain using their original ECDF linearly. Because of this linearisation, the maximum value will be equal between the samples and the original data set. The different VCs found enable the

6

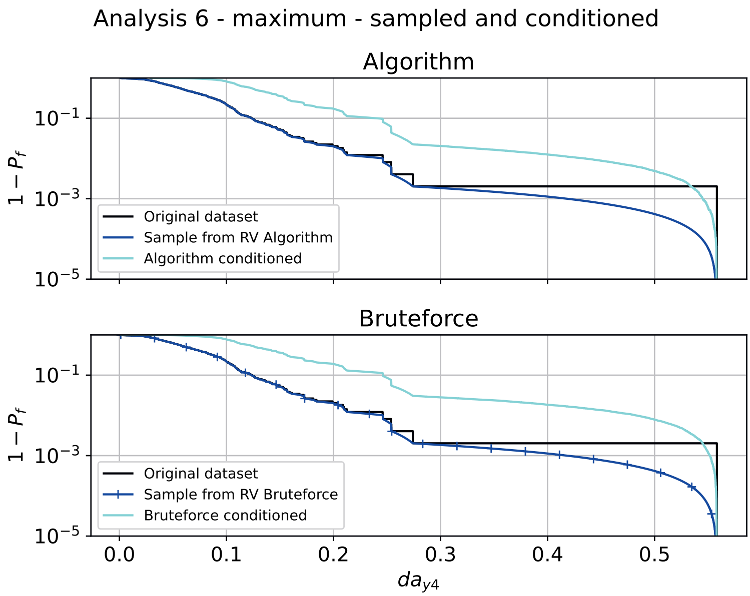

Figure 6.8: Empirical distributions for da_{y4} and run 6 - maximum

option of conditioning. Conditioning is performed by selecting part of the sample

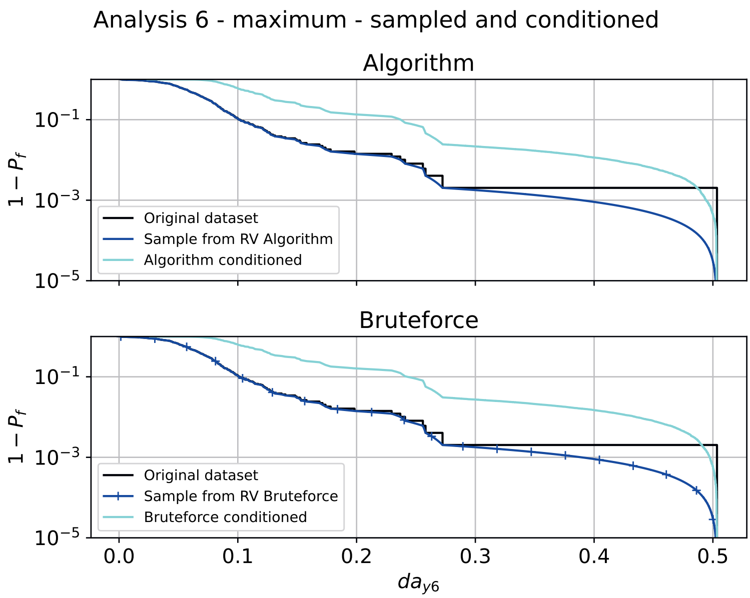

Figure 6.9: Empirical distributions for da_{y6} and run 6 - maximum

data by applying a filter. In this research, it is decided to define 2 scenarios to demonstrate the consequences of either the BF and the AL approach. Conditioning of the sample data is considered on all variables above the 70^{th} percentile except for the 2^{nd} and 3^{rd} variable individually (for run 6 these are da_{y4} and da_{z6}). The empirical cumulative distribution of both variables is presented in Figures 6.8 and 6.9. For completion, the ECDF for the original dataset and the unconditioned samples are visually displayed for both AL (top) and BF (bottom).

Within the empirical distribution, a difference between the RVs of BF and AL becomes visible. With the empirical distributions known, it is possible to quantify the values for different exceedance probabilities. The process for different probabilities is presented in Figures 6.10 and 6.11 and summarised in Table 6.5. Between both methods, differences can be found up to 11.78% in the case where variable 2 is considered and 3.45% in the case where variable 3 is considered.

If these results are related to the behaviour of the SFT during loading as specified by the conditioning above the $70^t h$ percentile, the prediction can in this case differ up to 11.78% and will influence a decision on a temporary closure if a certain threshold on accelerations is predicted to be exceeded. Similarly, different forces can be found in the tethers, mooring lines, as well as in the displacements between the AL approach and the BF approach. The result of all runs is presented in Appendix C.3.1 and differences can be found up to 20.37% for the corresponding runs and 14.08% for the maximum runs.

For smaller exceedance probabilities, the difference between values decreases to 0. This is an artefact of the process of the inverse CDF method. By definition, the conditioned data set can never have a larger value than the original data sample. To estimate extreme values beyond the maximum values of the original dataset, other techniques can be applied and discussed, but this is considered to be outside of the scope of this research.

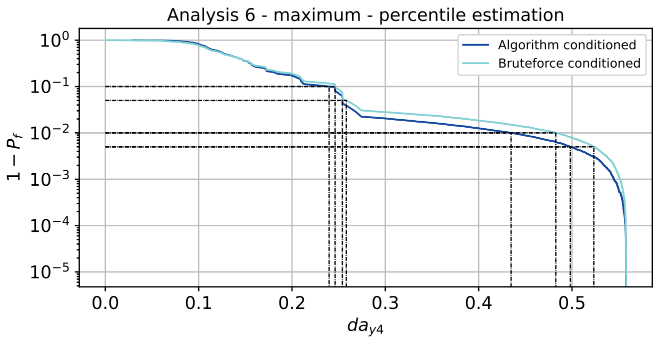

Figure 6.10: Conditional probability estimation for da_{y4} and run 6 - maximum

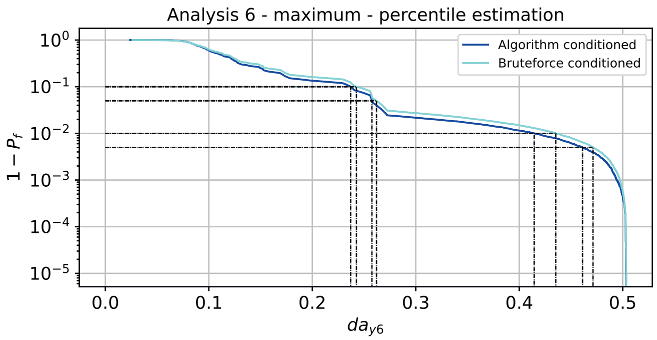

Figure 6.11: Conditional probability estimation for da_{y6} and run 6 - maximum

6.6. Discussion, conclusions and recommendations

Different conclusions can be drawn from this research. First, it is possible to describe the global response of an SFT using a sequential analysis. The combination of a diffraction analysis followed by a time history analysis gives an opportunity to analyse this complex off-shore structure. These combined sequential analysis are expensive in terms of calculation time, and not every possible scenario of combination of an angle of impact, a wave height, and period can be analysed individually. The individual simulations will show the maximum value that relates only to the input. In this demonstration, only three variables have been used; the angle of impact, wave height, and period. Using field data which were filtered for situations with only swell waves, a

Table 6.5: Run 6 conditioning on 2^{nd} and 3^{rd} variable

Run 6 P_f	Method	2^{nd} variable da_{y4}	3^{rd} variable da_{y6}
1.00E-01	BF	2.46E-01	2.43E-01
	AL	2.38E-01	2.37E-01
	Difference	3.37%	2.21%
5.00E-02	BF	2.58E-01	2.62E-01
	AL	2.54E-01	2.58E-01
	Difference	1.75%	1.64%
1.00E-02	BF	4.83E-01	4.33E-01
	AL	4.32E-01	4.18E-01
	Difference	11.78%	3.45%
5.00E-03	BF	5.24E-01	4.70E-01
	AL	4.97E-01	4.61E-01
	Difference	5.36%	2.02%

large series of potential situations have been simulated and from that filtered data, a limited set of is used to perform the analyses. The results of these analyses were used in a VC analysis. Selecting the best RV structure together with the copulas in terms of the best AIC score is essential to describe the data and assess the values related to exceedance probabilities. The selection of the RV structure in this research is the main topic, and it is shown that there is a clear difference between the AL and the BF approach.

As the BF solution will evaluate every possible RV given the number of variables, it will describe the dependencies between the variables in the data set more accurately than the AL solution, which can be concluded on the AIC cores of the individual runs presented. In general, the differences between the runs with the corresponding values show larger differences than with the maximum values. This can be explained by the fact that the maximum values are more correlated than in the case of corresponding values. Theoretically, the BF approach will always outperform the AL approach, since the AL approach will only present one of the BF solutions. One could conclude that the BF approach should always be used. However, the BF approach comes with a penalty which is related to the number of RV to consider, 660,602,880 RV need to be considered in case of 8 variables and require large computational effort, while the AL approach only uses a few seconds. The BF approach can currently take up to years on a regular computer. In order to apply the BF approach, it is essential to use HPC to identify the RV structure with the lowest AIC in combination with the fitted copulas. The differences in AIC scores between both methods show that in some cases there is a large amount of RV structures that describe the dependencies between variables better than the RV structure found by the algorithm (83% for the corresponding datasets and 30% for the maximum datasets). The effect of these differences appears in the case where conditional probability exceedance values are determined. In the specific case demonstrated, a relative difference in exceeding probability is found. Using the AL approach, one should consider that there could be a better RV structure describing the dependencies of the variables in the data set and in case of conditioning significant differences can be found. In order to find the best RV structure in terms of the AIC score, a BF approach should be considered; however, the current limitation is 8 variables.

In terms of the design of structures, the maximum probability that a failure is allowed dictates the design. So, if with a certain probability a force in the tether is found, the design in terms of the sectional properties can be chosen. In case this force is, for example, 10% larger than needed, it will result in more material use and, therefore, more costs. In contrast, if the force is 10% smaller, then the tether will have less capacity than required and the structure will not meet the reliability requirements. In parallel, for displacements and accelerations, the same conclusion can be drawn. Usually, analogous to bridges, there is a policy to close a crossing if there is a too large acceleration or deformation; if the predictions on these are not according to reality, the structure might close down more often in reality based on measurements than originally in the design found based on the exceedance probability. The requirement on the availability of the crossing might therefore not be met. As this research contains several components, each of them individually can be improved; therefore, the recommendations given are not limited. Regarding the DMA model, only one geometry has been used with a uniform length of the tethers. It is recommended to test more different geometries as well as different support conditions at the end of the structure. The most obvious recommendations for probabilistic analyses using VC are, in general, that the quality of a probabilistic analysis will improve if the initial dataset is increased. As in the current research, only 497 samples have been generated. The RV structures up to 8 variables are generated and available within the Chimera database [3], so the BF approach is limited to 8 variables and even with 8 variables, the amount of resources needed to find the best RV is substantial. Obviously, there are several recommendations on this issue; First of all, the Chimera database can be extended with RV structures with 9 or more variables. The amount of time needed in the BF approach can be reduced by using more resources; however, this will have a penalty on sustainability as HPC use a lot of energy. In order to reduce the amount of resources and/or reduce the amount of time needed, a better BF algorithm could be developed.

In these analyses, only copulas with one parameter have been considered; To improve the selection of the RV structure, more complex copulas with more parameters should be considered, but again the verification of RV structures would require more computational effort. As a last point, considering the selection of the best RV that describes the dependencies of the data, a new algorithm can be developed that would show a closer similarity to the BF approach.

When the best RV structure that best describes the dependencies of the data is found, simulation and conditioning can be performed. As a consequence of the application of VC, in which solutions are presented in the unit domain and transferred to the original domain, the extreme value estimation beyond the original interval should be explored and assessed.

7 Conclusions and recommendations

7.1. Conclusions

SFTs are structures which can be considered where long and deep waters need to be crossed. Although the construction of an SFT was already conceived at the end of the 19^{th} century, an SFT has not yet been built for several reasons, in the early years mainly due to a lack of technology. In recent years, the development of other fields of application has brought the feasibility of an SFT closer. Closer considerations of an SFT show that it has the underwater environment of a submarine vessel, the fixed positioning of off-shore platforms in marine environments, the dynamic behaviour of floating breakwaters while it will be used, loaded as a civil structure with an expected lifetime of 120 years. Although most civil structures such as large bridges and tunnels are unique structures, an SFT is a superlative. The design of traditional structures relies on codes and standards, which, in itself, are validated by the fact that these structures are actually built, and codes and standards are adjusted to new situations. SFTs can be considered as special structures to which no dedicated code or standard is applicable. One could state to use the conservative approach and use the upper bound of all standards of the fields of applications above when designing an SFT, but that could result in a uneconomical and even a safer structure than necessary. In order to come to a realistic design of an design, probabilistic methods can be a solution, as they can used in design in circumstances outside the scope of traditional codes and standards. The methods presented in this thesis are applicable not only to SFTs but also to other structures or even to other fields of application. However, the main topic of the study is founded in the design of SFTs This dissertation is therefore dedicated to the main objective:

Advancing probabilistic design of submerged floating tunnels

In order to develop a safe design for an SFT, probabilistic methods can be used, methods which are still uncommon in current design practices for civil structures. Conclusions are presented for the different secondary research objectives (as described in1.4).

How can the (target) reliability of an SFT be defined based on existing risk and reliability frameworks?

The reliability of a Submerged Floating Tunnel (SFT) can be defined based on existing risk and reliability frameworks by first establishing acceptable individual and societal risks. These risks are then used to determine the maximum allowable probability of structural failure. This probability is assessed using the conditional probability of death or major injury given structural failure.

For SFTs, the conditional probability of death given structural failure is expected to be higher than for other civil structures, therefore a more stringent requirement on the probability of structural failure (larger β or lower P_f) is expected. In codes and standards, such as Eurocode (EN 1990), the Load and Resistance Factor Method (LRFM) is related to the required β. Partial factors, e.g. for component failure and/or loss of failure, can be derived using reliability-based approaches (level II or level III), although this process is computationally intensive. Therefore, a sophisticated selection of failure modes based on the highest risks and the most important failure modes is recommended. Once the reliability requirement (β or P_f) is defined, the SFT structure can be evaluated using LRFM (level I) with common design practices and calibrated partial factors. The determined partial factors need to be validated for different failure modes with a back calculation and may need to be adjusted if they do not meet the required probability of failure P_f. Further optimisation of the SFT design can be achieved through economic risk evaluation, but the resulting reliability should never fall below the acceptable levels of individual and societal risk.

How can Gaussian Random Fields for the modelling of the foundation properties be used in combination with other probabilistic methods to estimate forces in IMT shear keys?

In this research, a method is presented to establish a relationship between the spatial variation of the subsoil and dredging parameters and the shear key forces in IMT and to find the exceedance probabilities using non-parametric Bayesian networks and vine copulas. Considering the relation between the covariance lengths and the shear key forces, the following conclusions can be drawn:

- If the covariance length is in the same order as the tunnel segment length, the largest shear forces will be found.
- The absolute shear key force increases with the length of the segment.

The latter conclusion is obvious; the area of a segment over which the stresses are integrated is larger and will lead to larger forces in case of increasing variability. Based on these conclusions, the design of the segment length can be optimised with respect to forces if the covariance lengths are known or estimated within limits, for example, by more intensive soil investigation using CPTs or quality measures and monitoring of the dredging process. If possible, it should be avoided in the design to have segment lengths comparable to the covariant lengths. However, the length of the segment depends not only on the shear force in the shear key. If the variation in dredging depth and subsoil stiffness are comparable, the design should anticipate higher shear forces. Estimation of a covariance length can be based on site investigations and CPTs, DeGroot et al. [124] presents a method for this. The thickness of the foundation material is related to the dredging tolerance. One could think of extending the quality measures on the dredging method to improve the dredging accuracy, because it would lead to a more constant thickness and stiffness and therefore a lower variability on the stiffness of the foundation layer. However, in daily practice, the selection of the dredging method depends on marine conditions and geology. The dredging method also dictates the dredging tolerance. As an additional option, by changing the thickness of the foundation layer, the influence of the subsoil stiffness on the bedding stiffness can be decreased. Using the results of a Monte Carlo analysis, datasets can be built that can be used in a probabilistic analysis using multivariate models. Vine copulas or non-parametric Bayesian networks can be fitted. The covariance lengths for the dredging depth and the subsoil stiffness are statistically coupled to the shear key. Rank correlations, which are used to parametrise multidimensional models, do not anticipate for non-monotonic behaviour. In the relation of the covariance lengths to the shear key force, there is a clear difference in behaviour between the lower covariance lengths and the higher covariance lengths, splitted by the peak value of the shear force, which enforces to split data at the covariance length peak value and conduct 2 probabilistic analyses. In case covariance lengths are unknown, exceedance probabilities can be found for shear forces using Non Parametric Bayesian Networks (NPBN) and Vine Copulas (VC). In this specific case, there is a small difference between NPBN and VC, where VC is more appropriate in the case of tail dependencies, as in this research. With this method, a better estimate of the probable shear key forces can be found using Gaussian random fields in combination with other probabilistic tools.

7

How can structural failure of an SFT through initial leakage caused by time-dependent traffic loads be evaluated using probabilistic methods?

In this research, a methodology is presented to study the reliability of a pontoon-type SFT. Structural failure through leakage caused by time-dependent loads is evaluated. The methodology is divided into two main parts, i) traffic simulation using a copula-based model, and ii) a structural model to test the SFT for a given failure mechanism (leakage due to bending of the SFT tube in the longitudinal direction). Finally, the reliability of the structure is investigated under the aforementioned failure mechanism.

From a monitoring dataset, several characteristics were extracted and translated into a traffic flow model using copulas. A simulation of this traffic flow model resulted in a "train" of traffic running through the SFT. To simulate the response of the structure over long periods of time, the proposed structural modelling approach needs to be as efficient as possible. Thus, by defining the global DSM (Direct Stiffness Method) approach with long beams and a dedicated DEM (Differential Equation Method) approach for intermediate loading, the finite element became as efficient as possible to avoid lag in the analysis. The analysis time was further reduced by applying the superposition principle. The results of the structural model provided the maximum and minimum bending moments and shear forces under traffic load for different values of BWR (Buoyancy-Weight-Ratio). From these results, the annual distribution of these variables and, consequently, their extreme values for several return periods were obtained.

Due to the lack of data regarding the structural response of an SFT, the combination of probabilistic modelling with structural analysis offers the possibility to study the design choices of this structure. This research shows an effective way to combine probabilistic modelling through copulas and structural analysis to simulate the traffic loads passing through the SFT and their effect on the structure. This methodology offers great flexibility because it can be used to test the reliability of the SFT considering other loading variables. For example, external environmental variables such as waves, currents, and their simultaneous action on an SFT. Moreover, this methodology is not restricted to use only on an SFT. It can be applied to other civil structures where the data is scarce.

How can the selection of regular vines be advanced with a brute force method and what are the advantages and disadvantages of such a method?

In this research, an advanced hydrodynamic analysis approach has been used to construct different datasets. It can be concluded that it is possible to conduct a dynamic mooring analysis to find the response of an SFT loaded by waves. Using field data which were filtered for situations with only swell waves, a large series of potential situations have been simulated and from that filtered data, a limited set of input is used to perform the analyses. The results of these analyses were used in a Vine Copula (VC) analysis. In essence, selecting the best RV structure together with the copulas in terms of the best Akaike Information (AIC) score is essential to describe the data and assess the values related to exceedance probabilities. The selection of the Regular Vine (RV) structure in this research part was the main topic, and two approaches, a commonly used algorithm and a brute-force method, were used and compared, finding the best RV in terms of the AIC score for datasets with 8 variables.

As the brute-force (BF) solution will evaluate every possible RV given the number of variables, it will describe the dependencies between the variables in the dataset more accurately than the AL solution in terms of the AIC score, which can be concluded on the AIC cores of the individual runs presented. For the two different types of datasets, the maximum values or the concomitant values, RV selection was performed. In general, the differences in AIC scores between runs with concomitant values show larger differences than with the maximum values. This can be explained by the fact that the maximum values are more correlated than in the case of concomitant values.

Theoretically, the BF approach will always outperform the AL approach, since the AL approach will only present one of the BF solutions. One could conclude that the BF approach should always be used. However, the BF approach comes with a penalty which is related to the number of RV to consider, 660,602,880 RVs need to be considered in case of 8 variables and require large computational effort, while the AL approach only uses a few seconds. The BF approach can currently take up to years on a regular computer. In order to apply the BF approach, it is essential to use a high performance computer (HPC) to identify the RV structure with the lowest AIC in combination with the fitted copulas. The differences in AIC scores between both methods show that in some cases there is a large amount of RV structures that describe the dependencies between variables better than the RV structure found by the algorithm (83% for the concomitant datasets and 30% for the maximum datasets). The effect of these differences appears in the case where conditional probability exceedance values are determined. In the specific case demonstrated, a relative difference in exceeding probability is found. Using the AL approach, one should consider that there could be a better RV structure describing the dependencies of the variables in the dataset and in case of conditioning significant differences can be found.

It can be concluded that the selection of RV structures in terms of the AIC score is advanced by considering a brute-force method. The current limitation given by Chimera [3] is 8 variables. Even the 8-variable limit can be extended, but even extending this database to 9 and more variables, there will always be a need to raise the limit and capture larger datasets.

When designing structures, the safety requirements (or the maximum probability of failure) dictate design decisions. Using the non-optimal fitted multivariate model based might lead to a non-economical or less safe design, as the structure might be too robust or have a lower safety. In parallel, for displacements and accelerations, the same conclusion can be drawn. Usually, analogous to bridges, there is a policy to close a crossing if there is a too large acceleration or deformation; if the predictions are based on a non-optimal fitted multivariate model, the structure might close down more often in reality based on measurements than originally in the design found based on the exceedance probability. The requirement on the availability of the crossing might therefore not be met.

7.2. Recommendations

This thesis touches on several research topics and did not aim to cover the full scope of probabilistic methods for structures or for the design of SFTs. In that way, there are several loose ends that can be a topic of further research. In this section, recommendations for further research can be found. Each part of the research individually can be improved, but the recommendations given are also not limited and can be seen as important initial directions. Furthermore, the methods developed and presented in this thesis are applicable in other applications.

Definition of a target reliabilities framework for SFT design

The design of civil structures is based on code standards that have been developed over decades. SFT is a novel structure type and it will take time for the civil engineering community to build up design experience in SFTs before cross-validation could lead to a design practise that comprises, for example, the commonly used LRFM methods (level I), as presently used for other structures. Specifically for SFTs a proposed framework was proposed in Chapter 3, to advance this framework the following recommendations, not only for SFT design, can be considered:

- The LRFM method prescribed by codes and standards does not consider a distinction between component and system level. If redundancy is concerned, differentiation the component and system level can be considered. For example, if by adding an extra support to the SFT, for the single component in such case a lower requirement could be used. As a second example, adjustable ballasting may be selected, which reduces the risk of imbalance but may introduce the risk of malfunctioning of additional components.

- An SFT is a novel structure with aspects from different fields of application. It is recommended to organise joint expertise teams for the design and involve the latest start-of-the-art knowledge from experts in the different fields of expertise.

- More research is needed to derive the acceptable levels of individual and societal risk specifically for SFTs as a basis for structural design.

- Safety measures will influence the conditional probability of death or major injury given structural failure. Adjusting or increasing measures on safety with exit strategies will decrease this conditional probability, and research on this topic for SFTs and the application of the findings will be beneficial.

- When assessing economical risk, the consequences of failure, direct and indirect, need to be estimated in monetary units. The compilation of a practical guideline for this estimation is recommended in order to derive a level of reliability.

Application of probabilistic methods in IMT design

In the research presented in Chapter 4, only covariance lengths for soil stiffness and dredging depth are considered, and both lengths are considered independent parameters. The latter could be the topic of discussion, if the top part of the soil influences the dredging process, a correlation between both could appear. However, if the soil consists of a multi-layer profile, this influence of the top layer on the total stiffness of the soil will reduce.

In tunnel design, even parts of the method can be used. As a recommendation for further research, more parameters should be included in the scope. In addition, the parameters used in this study are all based on a distribution with a fixed set of parameters. This could represent a single situation; however, to draw more robust conclusions, it is recommended to extend further research with, but not limited to:

- Soil:
  - Multiple layers of subsoil
  - Development of soil stiffness over the tunnel foundation area
  - Settlements
- IMT geometry:
  - Variation of IMT section over the longitudinal direction
  - Different segment lengths over the tunnel length
  - More than 2 keys in the segment joint
  - Interaction between 2 elements
- Other:
  - Transition areas of tunnel to cut and cover sections
  - Dredging scenarios or methods
  - Non uniform loading

Dependency between traffic loads and leakage failure

The presented research is based on a hypothetical model in which several variations can be considered. Specific recommendations concern:

- The research showed that the results are sensitive to the choice of the BWR; therefore, this choice should be handled with caution when designing an SFT. Although BWR was varied in the research, further research on BWR also for other types of SFT should be considered as it will be part of the stability challenges of an SFT
- Other limit states; the study only focussed on failure of the SFT due to leakage caused by bending. Even with the simplified model, limit states based on displacements, rotations, and shear forces of the SFT can also be considered.
- Shore connection; the simplified method can also present support reactions, which can be specifically of interest as at the transition area the support conditions change from buoyant structure to bedding supported.

- Multiple tubes and a 3 dimensional approach, the considered model is considered a straight connection in the vertical plane and without any out-of-plane curvature. The simplified model could be extended to 3 dimensions and could also consider a double or different tube layout in which torsional effect can be addressed.
- Span length; the current span length is kept constant and symmetric; different span lengths will influence the force distribution in the structure.
- Nonlinear analyses; the current analysis is based on a linear static analysis. Using non-linear analyses, redistribution of forces and stresses can be considered. A large disadvantage is that the superposition principle cannot be used and for the current considered limit state this redistribution effect is limited. However, for other limit states, this might be of essence and will better describe the actual response of the SFT.

Selection of Regular Vine structure by brute force using a high performance computer

With respect to the DMA model, only one geometry has been used with a uniform length of the tethers. It is recommended to test different geometries and different support conditions at the end of the structure, which is also addressed in the recommendations on the traffic study. When we focus on the statistical part and the process of finding the Regular Vine structure, the following recommendations can be made:

- Obviously in probabilistic analyses using Vine Copula, the quality of the probabilistic analysis is improved by increasing the number of samples in the dataset, so in case of data generation like using the DMA analyses, generate as many samples as reasonably possible.
- The current BF approach is limited to eight variables; recommendation on the BF approach is to extend the Chimera database [3] with RV sets with 9 or more variables, although there will always be a need for sets for more variables, and we must think of ways to store this large amount of data and make it publicly available.
- The BF approach on eight variables requires a lot of time even on a HPC compared to an algorithm-based approach, as the BF process is a parallel analysis, increasing resources, and the BF process will reduce time.
- In the current approach only one-parameter copulas are allowed, to improve the method, other copulas with more parameters can be allowed as well; this has a penalty time wise, as the fitting procedures will require more time.
- In order to reduce the amount of resources and/or reduce the amount of time needed, a better BF algorithm could be developed.
- Considering the selection of the best RV that describes the dependencies of the data, a new algorithm can be developed that would show a closer similarity to the BF approach.

- VC describe dependencies in the unit domain; if simulation and conditioning are performed and the solutions are transferred back to the original domain, the values can only be found within the original data ranges. The extreme value estimation beyond the original interval of the dataset should be explored and assessed.

Acknowledgements

Firstly, I would like to acknowledge the Submerged Floating Tunnel Technical Joint Research Team that is led by the Chinese engineering and construction company China Communications Construction Co., Ltd. (CCCC). I started the research in 2019, not really knowing what to expect, but open to anything. Today, a few years later, we literally survived a pandemic and the world looks quite different now with all the geopolitical stress going on. But personally, an important period of my life will end, which I would mark as very special. A time in which I was able to expand my knowledge, expand my social network, and expand my network of experts from all over the world.

This research was not possible without the support of my employer, Royal HaskoningDHV, who not only supported financially by creating a non-order related funding for the research but also gave all trust and flexibility to organise the research in a way that it would fit within the limitations of operational projects and my personal life. I give a great thank you to all the Royal HaskoningDHV colleagues in the advisory group **Infrastructuur Rotterdam**. Special thanks goes to **Hans de Wit**, words cannot describe the gratitude I owe you. You recommended the position at TU Delft for this study to me and convinced me to go for it; without you there was no thesis at all. We work together for a long period of time and each time you still amaze me with your skills, pragmatism, and coaching support within the challenging projects we continuously work on.

During the period, it was great to discuss not only the progress in the research with **Peter de Jonge** but also to reflect on the things happening in our lives. We will certainly continue our coffee catch-ups. In the SFT research team, Tunnel Engineering Consultants (TEC) participate, and projects on Immersed and Submerged Floating Tunnels are specifically carried out within TEC, as a joint venture of Royal HaskoningDHV and Witteveen en Bos. The inspiration, innovation and cooperation I experienced during the research programme increased the quality of the thesis, thanks to **Piet Barten**, **Ying Li**, and **Arjan Luttikholt** for their support and cooperation both in projects and within the research programme. Second, I am very grateful for the help of **Lisa Koopman-Meijer** and **Coen Eggermont** on the dynamic mooring analysis analyses.

Of course, this thesis would not have come about without the support of **Bas Jonkman**, I really enjoyed our discussions on several topics but specifically on the safety aspects of Tunnels. Although we had a lot of misunderstandings about variables and parameters but **Oswaldo Morales**, thank you for introducing me into the wonderful world of Vine Copulas. It has been a journey of which I think it will never reach its final destiny soon and I look forward to working on it together with you in the future. Even before I was employed by Royal HaskoningDHV, I already met **Dirk Jan Peters** as a specialist with many talents, it was my honour to have you as a copromotor in my committee. Thank you for your supervision and collegiality, and I sincerely hope our cooperation in challenging projects within the Royal HaskoningDHV continues.

In the beginning of the PhD traject, I felt like a kind of odd duck, with one leg in the business and one in the world of research, but the feeling of being a member of the team within the department of hydraulic engineering of the Faculty of Civil Engineering at Delft University of Technology was heart-warming. Thanks go to **Pengxu, Danny, Miguel, Rieke, and Dorette** for their support, the coffees and lunches in which we could exchange experiences and you act as a sounding board. **Gina**, I really enjoyed working on the traffic paper and it was really nice to work on the same subject but both in different directions. I am confident that you will be successful in your future career and wish you all the best in it.

As part of obtaining a Ph.D. degree, the Graduate School is truly of important and large influence within the Delft University. The part I enjoyed the most was to supervise and support students at the final thesis. It not only helped them (hopefully) but also gave me fruitful insights for my own work and research. Thanks to all of them for allowing me to supervise you.

Last but certainly not least, special thanks and appreciation go to my family at home. My parents who supported me not only during my thesis. It is sad that my mother has passed away and misses the end of this journey, but **dad**, you do great and we keep her in our hearts and memories. **Maaike, Marieke, and Marije**, you had to miss me on several occasions, but you make me proud of all the things you are doing and I love you with all I have. Thank you for your moral support and understanding. Finally, **Daniëlle**, thank you for all your love, support, patience, and care throughout the period; nothing was too much for you. I really look forward to our future, which I hope will be even brighter than our already bright past.

Nomenclature

$[K]$	Stiffness matrix
$[K_f]$	Filtered stiffness matrix
$[R_{BWR}]$	Matrix of results due to the BWR
$[R_e]$	Matrix of enveloped results
$[R_t]$	Matrix of results due to BWR and traffic loads
β	Reliability index
β_n	Reliability index with reference period n years
Δt_{dl}	Dredging tolerance
Δt_{pl}	Gravel placement tolerance
$\ln(\hat{L})$	Log-likelihood
μ	Mean value
ϕ	Angle of impact $[degrees]$
ϕ	Gaussian distribution function
Σ	Covariance matrix
σ	Standard deviation
σ_a	Average contact pressure
σ_b	Bedding response
σ_f	Stress in fibre
θ_z	Rotation
ε_x	Axial strain
$\vec{F}$	Force vector
$\vec{F}_f$	Filtered force vector
$\vec{F}_p$	Support forces vector

$\vec{F}_t$	Vector of a sub-train of axle loads
$\vec{u}$	Displacement vector
$\vec{u}_f$	Filtered displacement vector
A	Area
a	Lever arm
A_b	Contact area underneath the tunnel
A_b	Bedding-tunnel contact area
C	Bivariate copula
C_{θ_X}	Auto-correlation model of order 1 for the time series of interest
da_{xi}	Axial accelerations point i $[m/s^2]$
da_{yi}	Lateral accelerations point i $[m/s^2]$
da_{zi}	Vertical accelerations point i $[m/s^2]$
du_{xi}	Axial displacements point i $[m]$
du_{yi}	Lateral displacements point i $[m]$
du_{zi}	Vertical displacements point i $[m]$
E	Young's Modulus
F	Force
F_i	Tether force in tether i $[N]$
F_i	Force at segment i
F_k	Absolute force at shear key
F_t	Matrix of all sub-trains of axle loads
$F_X(x), G_Y(y)$	Marginal distributions
h	cross section thickness - Eurocode definition
H_s	Wave height $[m]$
h_f	Foundation thickness
$H_{XY})$	Joint distribution
i	Discrete time indices of the variable of interest (Not calendar time)
I_z	Second moment of area

I_z	Second moment of area
k	Number of parameters in AIC
k_b	Bedding stiffness
k_f	Foundation material stiffness
k_s	Soil stiffness
L_{cov}	Covariance length [m]
L_i	Influence depth of the tunnel
M	Regular vine matrix
M	Total bending moment.
M_{al}	Matrix representation of Regular Vine obtained using algorithm method
M_{bf}	Matrix representation of Regular Vine obtained using brute force method
M_{BWR}	Bending moment due to BWR load
M_{cap}	Bending moment capacity
$M_{max,min}$	Maximum or minimum bending moment from envelope
M_{pt}	Bending moment due to asymmetric post tensioning
$M_{tr,cap}$	Bending moment capacity related to traffic
M_{tr}	Bending moment due to traffic load
$N_{as,pt}$	Asymmetric post tensioning
$N_{ax,pt}$	Axial post tensioning
n_x	Number of points in x direction
n_y	Number of points in y direction
P_f	Probability
P_f	Probability
R_i	Inner radius of tubular section
R_o	Outer radius of section
R_u	Matrix of results for each unit load
S_{i-1}	Vehicle's speed at time $t-1$ [km/h]

T_p	Wave period [s]
t_s	Thickness of the tubular shape
$u_{x,y}$	Displacement
w_f	Section modulus for fibre location
X	Location
x_0	Local coordinate at start of the beam
x_f	Local coordinate at position of the force on the beam
x_l	Local coordinate at end of the beam
x_{fi}	Location of fibre in the cross section
x_f	Vertical location of fibre
x_i	Inter-vehicle distance at discrete time t [km]
x_n	x-coordinate of point n [m]
y_n	y-coordinate of point n [m]
M_z	Bending moment
N_x	Normal force
q_x	Axial distributed force
q_y	Lateral distributed force
V_y	Shear force
AIC	Aikake Infomation Criterium
ecdf	Empirical cumulative distribution function.

Bibliography

[1] E. C. for Standardization, *En 1990. eurocode: basis of structural design* (CEN, Brussels, 2002).

[2] RWS, *Richtlijn ontwerp kunstwerken v1.4* (Ministerie van Infrastructuur en Milieu, 2017).

[3] M. 't Hart, O. Morales Napoles, M. Rajabi, and G. Torres Alves, *Chimera: an atlas of regular vines on up to 8 nodes*, en, `https://data.4tu.nl/collections/c17b8790-dfd2-4394-854a-7d98fd254c15/7`, 2023.

[4] Y. Duan, "Application of suction caissons to submerged floating tunnel at sognefjord in norway caisson design, deflection analysis and physical modelling", Master's thesis (CHALMERS UNIVERSITY OF TECHNOLOGY, Gothenburg, Sweden, 2014).

[5] F. M. Mazzolani, R. Landolfo, B. Faggiano, M. Esposto, F. Perotti, and G. Barbella, "Structural analyses of the submerged floating tunnel prototype in qiandao lake (pr of china)", Advances in Structural Engineering **11**, 439–454 (2008).

[6] F. Mazzolani, B. Faggiano, and G. Martire, "Design aspects of the ab prototype in the qiandao lake", Procedia Engineering **4**, ISAB-2010, 21–33 (2010).

[7] J. Yu, D. Zhong, B. Ren, D. Tong, and K. Hong, "Probabilistic risk analysis of diversion tunnel construction simulation", Computer-Aided Civil and Infrastructure Engineering **32**, 748–771 (2017).

[8] C. Liu and D. Lu, "Aftershock probabilistic seismic hazard analysis based on enhanced bayesian network considering frequency information", Computer-Aided Civil and Infrastructure Engineering **39**, 1963–1987 (2024).

[9] Y. Pan, J. Qin, L. Zhang, W. Pan, and J.-J. Chen, "A probabilistic deep reinforcement learning approach for optimal monitoring of a building adjacent to deep excavation", Computer-Aided Civil and Infrastructure Engineering **39**, 656–678 (2024).

[10] H. Cheng, J. Chen, R. Chen, and G. Chen, "Comparison of modeling soil parameters using random variables and random fields in reliability analysis of tunnel face", International Journal of Geomechanics **19**, 04018184 (2019).

[11] W. Gong, C. Juang, J. Martin, H. Tang, Q. Wang, and H. Huang, "Probabilistic analysis of tunnel longitudinal performance based upon conditional random field simulation of soil properties", Tunnelling and Underground Space Technology **73**, 1–14 (2018).

[12] X. Yu, J. Cheng, C. Cao, E. Li, and J. Feng, "Probabilistic analysis of tunnel liner performance using random field theory", Advances in Civil Engineering **2019**, 1–18 (2019).

[13] R. Adler and J. Taylor, *Random fields and geometry*, Springer Monographs in Mathematics (Springer New York, 2009).

[14] D. T. Hristopulos, *Random fields for spatial data modeling, a primer for scientists and engineers* (Springer Dordrecht, 2020).

[15] Y. Liu, J. Li, S. Sun, and B. Yu, "Advances in gaussian random field generation: a review", Computational Geosciences **23**, 1011–1047 (2019).

[16] M. A. Hicks and Y. Li, "Influence of length effect on embankment slope reliability in 3d", International Journal for Numerical and Analytical Methods in Geomechanics **42**, 891–915 (2018).

[17] Y. Li, M. Hicks, and P. Vardon, "Cost-effective design of long spatially variable soil slopes using conditional simulation", in Geo-risk 2017 (June 2017), pp. 394–402.

[18] I. Papaioannou and D. Straub, "Computing the reliability of shallow foundations with spatially distributed measurements", in *Geotechnical safety and risk v* (IOS Press, 2015), pp. 958–963.

[19] A.-H. Soubra, D. Youssef Abdel Massih, and M. Kalfa, "Bearing capacity of foundations resting on a spatially random soil", GeoCongress 2008, 66–73 (2008).

[20] K. Kasama and K. Zen, "Effects of spatial variability of soil property on slope stability", Proceedings, First International Symposium on Uncertainty Modeling and Analysis and Management (ICVRAM 2011), 691–698 (2011).

[21] C. Bucher, "Applications of random field models in stochastic structural mechanics", in Advances in engineering structures, mechanics & construction, Vol. 140 (Jan. 2006), pp. 471–484.

[22] P. Bocchini, "Probabilistic approaches in civil engineering: generation of random fields and structural identification with genetic algorithms", PhD thesis (Università di Bologna, 2008).

[23] E. Vanmarcke, M. Shinozuka, S. Nakagiri, G. Schuëller, and M. Grigoriu, "Random fields and stochastic finite elements", Structural Safety **3**, 143–166 (1986).

[24] W. Shengzhong, C. Xiang, L. Qinxi, and C. Gengren, "Research on type selection of submerged floating tunnel of qiongzhou strait", Procedia Engineering **166**, 307–316 (2016).

[25] M. Mendoza-Lugo, D. Delgado-Hernández, and O. Morales-Nápoles, "Reliability analysis of reinforced concrete vehicle bridges columns using non-parametric bayesian networks", Engineering Structures **188**, 178–187 (2019).

[26] M. A. Mendoza-Lugo, O. Morales-Nápoles, and D. J. Delgado-Hernández, "A non-parametric bayesian network for multivariate probabilistic modelling of weigh-in-motion system data", Transportation Research Interdisciplinary Perspectives **13**, 100552 (2022).

[27] J. Jonkman, A. Robertson, S. Gueydon, P. Wuillaume, and A. Platt, "Comparison of second-order loads on a tension-leg platform for wind turbines", American English, in The proceedings of the twenty-fifth (2015) international ocean and polar engineering conference, Twenty-Fifth International Offshore and Polar Engineering Conference ; Conference date: 21-06-2015 Through 26-06-2015 (International Society of Offshore and Polar Engineers, 2015).

[28] I. Bayati, S. Gueydon, and M. Belloli, "Study of the effect of water depth on potential flow solution of the oc4 semisubmersible floating offshore wind turbine", Energy Procedia **80**, 12th Deep Sea Offshore Wind R&D Conference, EERA DeepWind'2015, 168–176 (2015).

[29] *Comparison of second-order loads on a semisubmersible floating wind turbine*, 33rd International Conference on Ocean, Offshore and Arctic Engineering (June 2014), V09AT09A024.

[30] *Coupling of Two Tools for the Simulation of Floating Wind Turbines*, Vol. Volume 8: Ocean Renewable Energy, International Conference on Offshore Mechanics and Arctic Engineering, International Conference on Ocean, Offshore and Arctic Engineering (June 2013), V008T09A073.

[31] *Investigating the effect of damping originating from mooring and risers on the vim response of a semi-submersible floater using coupled cfd-time-domain simulations*, Vol. Day 4 Thu, May 04, 2023, OTC Offshore Technology Conference, Offshore Technology Conference, Houston (May 2023), D041S046R003.

[32] MARIN, *Maritime research institute netherlands*, `https://www.marin.nl/en`.

[33] J. Dißmann, E. Brechmann, C. Czado, and D. Kurowicka, "Selecting and estimating regular vine copulae and application to financial returns", Computational Statistics & Data Analysis **59**, 52–69 (2013).

[34] D. H. P. C. C. (DHPC), *DelftBlue Supercomputer (Phase 1)*, `https://www.tudelft.nl/dhpc/ark:/44463/DelftBluePhase1`, 2022.

[35] O. Morales-Nápoles, M. Rajabi-Bahaabadi, G. Torres-Alves, and C. 't Hart, "Chimera: an atlas of regular vines on up to 8 nodes", English, Scientific Data **10**, `10.1038/s41597-023-02252-6` (2023).

[36] P. Zou, "Dynamic response of a submerged floating tunnel subject to hydraulic loading numerical modelling for engineering design", PhD thesis (TU Delft, 2022).

[37] G. Torres Alves, "Multivariate probability distributions for reliability analysis of a submerged floating tunnel", PhD thesis (TU Delft, 2024).

[38] G. Torres-Alves, C. 't Hart, O. Morales-Nápoles, and S. Jonkman, "Structural reliability analysis of a submerged floating tunnel under copula-based traffic load simulations", Engineering Structures **269**, 114752 (2022).

[39] Norconsult, *K3 / K4 Technical Report - Bjørnafjord submerged floating tunnel*, tech. rep. (Norconsult, 2016).

7

[40] N. S. Rasmussen, “Concrete immersed tunnels — forty years of experience”, Tunnelling and Underground Space Technology **12**, 33–46 (1997).

[41] J. de Wit and E. van Putten, “The immersed tunnel as fixed link – a successful alternative pushed by innovation”, Proceedings of the World Tunnel Congress (2014).

[42] W. Grantz, “Chapter 3 structural design of immersed tunnels”, Tunnelling and Underground Space Technology - TUNN UNDERGR SPACE TECHNOL **12**, 93–109 (1997).

[43] A. Glerum, “Options for tunneling: a personal story”, Tunnelling and Underground Space Technology **7**, 313–315 (1992).

[44] H. van Tongeren, “The foundation of immersed tunnels”, Proceedings of Delta Tunneling Symposium, 48–57 (1978).

[45] W. Li, Y. Fang, H. Mo, R. Gu, J. Chen, Y. Wang, and D. Feng, “Model test of immersed tube tunnel foundation treated by sand-flow method”, Tunnelling and Underground Space Technology **40**, 102–108 (2014).

[46] A. Glerum, “Developments in immersed tunnelling in holland”, Tunnelling and Underground Space Technology **10**, 455–462 (1995).

[47] L. Gravesen and N. S. Rasmussen, “A milestone in tunnelling: rotterdam’s maas tunnel celebrates its fiftieth anniversary”, Tunnelling and Underground Space Technology **8**, 413–424 (1993).

[48] A. Sklar, “Fonctions de répartition à n dimensions et leurs marges”, Publications de l’Institut de Statistique de l’Université de Paris **8**, 229–231 (1959).

[49] T. Vatter and T. Nagler, *Pyvinecopulib 0.6.1*, 2022.

[50] R. Nelsen, *An introduction to copulas* (Springer, Jan. 2006).

[51] H. Joe, *Multivariate models and multivariate dependence concepts* (Chapman and Hall/CRC, 1997).

[52] A. Hanea, O. Morales Napoles, and D. Ababei, “Non-parametric bayesian networks: improving theory and reviewing applications”, Reliability Engineering & System Safety **144**, 265–284 (2015).

[53] D. Paprotny, O. Morales-Nápoles, D. T. Worm, and E. Ragno, “Banshee–a matlab toolbox for non-parametric bayesian networks”, SoftwareX **12**, 100588 (2020).

[54] P. Koot, M. A. Mendoza-Lugo, D. Paprotny, O. Morales-Nápoles, E. Ragno, and D. T. Worm, “Pybanshee version (1.0): a python implementation of the matlab toolbox banshee for non-parametric bayesian networks with updated features”, SoftwareX **21**, 101279 (2023).

[55] D. Paprotny and O. Morales Napoles, “Estimating extreme river discharges in europe through a bayesian network”, Hydrology and Earth System Sciences **21**, 2615–2636 (2017).

[56] D. Paprotny, H. Kreibich, O. Morales Napoles, D. Wagenaar, A. Castellarin, F. Carisi, X. Bertin, B. Merz, and K. Schröter, "A probabilistic approach to estimating residential losses from different flood types", Natural Hazards **105**, 1–33 (2021).

[57] A. Couasnon, A. Sebastian, and O. Morales-Nápoles, "A copula-based bayesian network for modeling compound flood hazard from riverine and coastal interactions at the catchment scale: an application to the houston ship channel, texas", Water (Switzerland) **10**, `10.3390/w10091190` (2018).

[58] O. Morales-Nápoles and R. D. J. M. Steenbergen, "Large-scale hybrid bayesian network for traffic load modeling from weigh-in-motion system data", Journal of Bridge Engineering **20**, 04014059 (2015).

[59] O. Morales-Nápoles and R. D. Steenbergen, "Analysis of axle and vehicle load properties through bayesian networks based on weigh-in-motion data", Reliability Engineering & System Safety **125**, Special issue of selected articles from ESREL 2012, 153–164 (2014).

[60] H. Joe, *Dependence modeling with copulas*, Chapman & Hall/CRC Monographs on Statistics & Applied Probability (Taylor & Francis, 2014).

[61] K. Aas, C. Czado, A. Frigessi, and H. Bakken, "Pair-copula constructions of multiple dependence", Insurance: Mathematics and Economics **44**, 182–198 (2009).

[62] K. Aas and D. Berg, "Models for construction of multivariate dependence", European Journal of Finance **15**, 639–659 (2009).

[63] C. Czado, "Multivariate distributions and copulas", in *Analyzing dependent data with vine copulas: a practical guide with r* (Springer International Publishing, Cham, 2019), pp. 1–25.

[64] L. Chollete, A. Heinen, and A. VALDESOGO, "Modeling international financial returns with a multivariate regime switching copula", SSRN Electronic Journal **7**, `10.2139/ssrn.1102632` (2008).

[65] G. Pouliasis, G. A. Torres-Alves, and O. Morales-Napoles, "Stochastic modeling of hydroclimatic processes using vine copulas", Water **13**, `10.3390/w13162156` (2021).

[66] W. Jäger and O. Nápoles, "A vine-copula model for time series of significant wave heights and mean zero-crossing periods in the north sea", ASCE-ASME Journal of Risk and Uncertainty in Engineering Systems, Part A: Civil Engineering **3**, `10.1061/AJRUA6.0000917` (2017).

[67] O. Morales Napoles, "Counting vines", in *Dependence modeling* (World Scientific, Dec. 2010), pp. 189–218.

[68] O. Morales Napoles, "Bayesian belief nets and vines in aviation safety and other applications", PhD thesis (Delft Unitiversity of Technology, Jan. 2010).

[69] R. Cooke, H. Joe, and K. Aas, "Vines arise", English, in *Dependence modeling*, edited by D. Kurowicka and H. Joe (World scientific, Dec. 2010), pp. 37–72.

[70] H. Akaike, “Information theory and an extension of the maximum likelihood principle”, in *Selected papers of hirotugu akaike*, edited by E. Parzen, K. Tanabe, and G. Kitagawa (Springer New York, New York, NY, 1998), pp. 199–213.

[71] C. Czado, S. Jeske, and M. W. Hofmann, “Selection strategies for regular vine copulae”, in (Journal de la société française de statistique, 2013).

[72] D. Kurowicka, “Optimal truncation of vines”, in *Dependence modeling* (World Scientific, 2010), pp. 233–247.

[73] P. Abrahamsen, *A review of gaussian random fields and correlation functions*, Apr. 1997.

[74] E. Vanmarcke, *Random fields: analysis and synthesis*, G - Reference,Information and Interdisciplinary Subjects Series (World Scientific, 2010).

[75] S. Müller, L. Schüler, A. Zech, and F. Heße, “`GSTools` v1.3: a toolbox for geostatistical modelling in python”, Geoscientific Model Development **15**, 3161–3182 (2022).

[76] World Road Association (PIARC), *Road tunnels manual*, Online electronic encyclopedia, `https://tunnels.piarc.org/en`, World Road Association (PIARC) (Paris, France, Oct. 2019).

[77] T. Vrouwenvelder, “The jcss probabilistic model code”, Structural Safety **19**, 245–251 (1997).

[78] ACI318, *Aci 318-14 building code requirements for structural concrete and commentary (metric)* (American Concrete Institute, 2014).

7

[79] NORSOK, *NORSOK: N-001 Integrity of offshore structures*, tech. rep. (NORSOK, 2010).

[80] IMO, “Decision parameters including risk acceptance criteria”, Interational Maritime Organization - Maritime Safety Committee 72/16, 28 (2000).

[81] DNV-GL, *RULES FOR CLASSIFICATION Naval vessels Edition Part 4 Sub-surface ships*, tech. rep. December (DNV, 2015).

[82] T. e. a. Schweckendiek, “Target Reliabilities and Partial Factors for Flood Defenses in the Netherlands”, Mod. Geotech. Codes Pract. - Code Dev. Calibration, 311–328 (2012).

[83] R. e. a. Jongejan, “Reliability-based partial factors for flood defenses”, Reliab. Eng. Syst. Saf. **193**, 106589 (2020).

[84] M. Baravalle and J. Köhler, “Risk and Reliability Based Calibration of Design Codes for Submerged Floating Tunnels”, Procedia Eng. **166**, 247–254 (2016).

[85] M. Baravalle and J. Köhler, “A risk-based approach for calibration of design codes”, Struct. Saf. **78**, 63–75 (2019).

[86] ISO, *ISO2394:2015: - General Principles on Reliability for Structures* (ISO, Geneva, Switzerland, Mar. 2015).

[87] T. Schweckendiek, S. Jonkman, R. Steenbergen, and A. Roubos, “Risk-based target reliability indices for quay walls”, Structural Safety **75**, `10.1016/j.strusafe.2018.06.005` (2018).

[88] B. Arends, S. Jonkman, J. Vrijling, and P. van Gelder, “Evaluation of tunnel safety: towards an economic safety optimum”, Reliability Engineering & System Safety **90**, Selected papers from ESREL 2003, 217–228 (2005).

[89] T. Geyer, M. Morris, and R. Hacquart, “Channel tunnel safety case: development of the risk criteria”, in 1995 international conference on electric railways in a united europe (1995), pp. 164–167.

[90] H. Mashimo, “State of the road tunnel safety technology in japan”, Tunnelling and Underground Space Technology **17**, 145–152 (2002).

[91] C. Cornell, “A probability-based structural code”, A Probability-based structural code **66** (1969).

[92] M. Pandey, C. Viljoen, A. Way, K. Fischer, M. Sýkora, D. Diamantidis, R. D. Steenbergen, N. Lind, D. M. Frangopol, D. Y. Yang, J. V. Retief, J. André, J. Nathwani, and R. Lenner, “Life safety in the reliability-based design and assessment of structures”, Structural Safety **113**, The Joint Committee of Structural Safety: past, present and a perspective on the future, 102453 (2025).

[93] L. Liu, D. Y. Yang, and D. M. Frangopol, “Determining target reliability index of structures based on cost optimization and acceptance criteria for fatality risk”, ASCE-ASME Journal of Risk and Uncertainty in Engineering Systems, Part A: Civil Engineering **7**, 04021013 (2021).

[94] M. Weber, R. Caspeele, J. Schnell, C. Glock, and W. Botte, “The new fib bulletin 80 - partial factor methods for existing concrete structures [das neue fib bulletin 80 - teilsicherheitsbeiwerte für die nachrechnung bestehender massivbauwerke]”, Beton- und Stahlbetonbau, 10.1002/best.201700104 (2018).

[95] S. G. Reid, “Perception and communication of risk, and the importance of dependability”, Structural Safety **21**, 373–384 (1999).

[96] J. Menzies, “Hazards, risks and structural safety”, **73**, 357–363 (1995).

[97] C. M. P. ’t Hart, O. Morales-Nápoles, and B. Jonkman, “The influence of spatial variation on the design of foundations of immersed tunnels: advanced probabilistic analysis”, Tunnelling and Underground Space Technology **147**, 105624 (2024).

[98] P. Virtanen, R. Gommers, T. E. Oliphant, M. Haberland, T. Reddy, D. Cournapeau, E. Burovski, P. Peterson, W. Weckesser, J. Bright, S. J. van der Walt, M. Brett, J. Wilson, K. J. Millman, N. Mayorov, A. R. J. Nelson, E. Jones, R. Kern, E. Larson, C. J. Carey, İ. Polat, Y. Feng, E. W. Moore, J. VanderPlas, D. Laxalde, J. Perktold, R. Cimrman, I. Henriksen, E. A. Quintero, C. R. Harris, A. M. Archibald, A. H. Ribeiro, F. Pedregosa, P. van Mulbregt, and SciPy 1.0 Contributors, “SciPy 1.0: Fundamental Algorithms for Scientific Computing in Python”, Nature Methods **17**, 261–272 (2020).

[99] O. Morales-Nápoles, A. Hanea, and D. Worm, “Experimental results about the assessments of conditional rank correlations by experts: example with air pollution estimates”, in Safety, reliability and risk analysis: beyond the horizon - proceedings of the european safety and reliability conference, esrel 2013 (2014), pp. 1359–1366.

[100] P. Tveit, “Submerged floating tunnels (sfts) for norwegian fjords”, Procedia Engineering **4**, ISAB-2010, 135–143 (2010).

[101] W. C. Grantz P.E., “Conceptual study for a deep water, long span, submerged floating tunnel (sft) crossing”, Procedia Engineering **4**, ISAB-2010, 61–70 (2010).

[102] R. Lunniss and J. Baber, *Immersed tunnels* (Taylor & Francis, 2013).

[103] F. internationale du béton, *Guidelines for submerged floating tube bridges - fib bulletin no. 96* (CEB-Fib, 2020).

[104] C. Ingerslev, “Immersed and floating tunnels”, Procedia Engineering **4**, 51–59 (2010).

[105] H. Tabatabai, H. Titi, and J. Zhao, “Wim-based assessment of load effects on bridges due to various classes of heavy trucks”, Engineering Structures **140**, 189–198 (2017).

[106] E. Spissu, A. Pinjari, R. Pendyala, and C. Bhat, “A copula-based joint multinomial discrete-continuous model of vehicle type choice and miles of travel”, English (US), Transportation **36**, Copyright: Copyright 2009 Elsevier B.V., All rights reserved., 403–422 (2009).

[107] C. R. Bhat and N. Eluru, “A copula-based approach to accommodate residential self-selection effects in travel behavior modeling”, Transportation Research Part B: Methodological **43**, 749–765 (2009).

[108] Y. Zou and Y. Zhang, “A copula-based approach to accommodate the dependence among microscopic traffic variables”, Transportation Research Part C: Emerging Technologies **70**, 53–68 (2016).

[109] H. Joe, *Dependence Modeling with Copulas* (Chapman and Hall/CRC, New York, 2014), 480 pp.

[110] Schepsmeier, Stöber, Brechmann, Gräler, Nagler, and Erhardt, *VineCopula: statistical inference of vine copulas*, version 2.1.8, Sept. 18, 2018.

[111] R Core Team, *R: a language and environment for statistical computing*, R Foundation for Statistical Computing (Vienna, Austria, 2020).

[112] O. Morales-Nápoles and R. D. J. M. Steenbergen, “Large-scale hybrid bayesian network for traffic load modeling from weigh-in-motion system data”, Journal of Bridge Engineering **20**, 04014059 (2015).

[113] G. A. Torres-Alves and O. Morales-Nápoles, “Reliability analysis of flood defenses: the case of the nezahualcoyotl dike in the aztec city of tenochtitlan”, Reliability Engineering & System Safety **203**, 107057 (2020).

[114] E. C. EN1992 Part 3 for Standardization, *EN1992 Part 3: Liquid retaining and containing structures* (CEN, 2006).

7

[115] A. Vervuurt, J. Pruiksma, R. Steenbergen, W. Courage, S. Miraglia, and O. M. N. (TUD), *Statische belastingen herijking verkeersbelastingen voor brugconstructies op basis van wim analyses van april 2013 (iq-2014-33c)*, Report (TNO, 2015).

[116] A. Nestegård, S. Haugerud, J. Solemsli, K. Engebretsen, K. Wåsjø, and A. Myhr, *K3- k4 design basis report - bjornafjord submerged floating tunnel*, Technical Report (Norconsult, 2016).

[117] C. J. Date and H. Darwen, *A guide to the sql standard*, Vol. 3 (Addison-Wesley New York, 1987).

[118] M. A. Jette and T. Wickberg, "Architecture of the slurm workload manager", in Job scheduling strategies for parallel processing, edited by D. Klusáček, J. Corbalán, and G. P. Rodrigo (2023), pp. 3–23.

[119] E. Gabriel, G. E. Fagg, G. Bosilca, T. Angskun, J. J. Dongarra, J. M. Squyres, V. Sahay, P. Kambadur, B. Barrett, A. Lumsdaine, R. H. Castain, D. J. Daniel, R. L. Graham, and T. S. Woodall, "Open MPI: goals, concept, and design of a next generation MPI implementation", in Proceedings, 11th european pvm/mpi users' group meeting (Sept. 2004), pp. 97–104.

[120] K. Hasselmann, T. Barnett, E. Bouws, H. Carlson, D. Cartwright, K. Enke, J. Ewing, H. Gienapp, D. Hasselmann, P. Kruseman, A. Meerburg, P. Muller, D. Olbers, K. Richter, W. Sell, and H. Walden, "Measurements of wind-wave growth and swell decay during the joint north sea wave project (jonswap)", Deut. Hydrogr. Z. **8**, 1–95 (1973).

[121] Hersbach, H., Bell, B., Berrisford, P., Biavati, G., Horányi, A., Muñoz Sabater, J., Nicolas, J., Peubey, C., Radu, R., Rozum, I., Schepers, D., Simmons, A., Soci, C., Dee, D., Thépaut, J-N., *Era5 hourly data on single levels from 1940 to present*, `http://10.24381/cds.adbb2d47`, 2019.

[122] G. Torres-Alves and O. Morales-Nápoles, "A vine-copula model for simulation of extreme metocean loads and estimation of hydrodynamic forces for a submerged floating tunnel at the qiongzhou strait - under review", (2022).

[123] G. Torres-Alves, O. Morales-Nápoles, and S. Jonkman, "Simulation of hydrodynamic loads for a submerged floating tunnel using a copula-based model", in *Bridge maintenance, safety, management, life-cycle sustainability, and innovations. iabmas 2020.* (CRC Press, 2021), pp. 844–852.

[124] D. DeGroot and G. Baecher, "Estimating autocovariance of in-situ soil properties", Journal of Geotechnical Engineering **119**, `10.1061/(ASCE)0733-9410(1993)119:1(147)` (1993).

[125] M. Turner, "The direct stiffness method of structural analysis", in (1959).

[126] C. Felippa, "A historical outline of matrix structural analysis: a play in three acts", Computers & Structures **79**, 1313–1324 (2001).

[127] S. Timoshenko, *History of strength of materials: with a brief account of the history of theory of elasticity and theory of structures* (Courier Corporation, 1953).

A

Spatial variation in tunnel foundations - results

A.1. Densities for different segment lengths

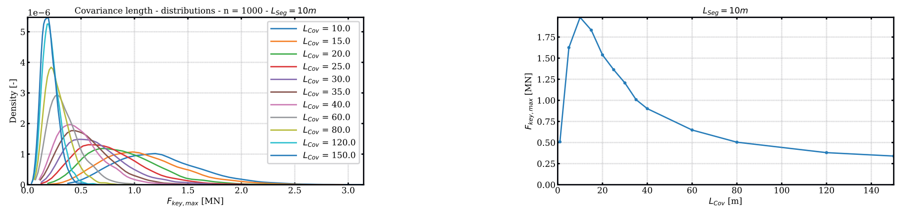

(a) Densities

(b) Force at 95 percentile

Figure A.1: Densities for segment length L_{seg} = 10m

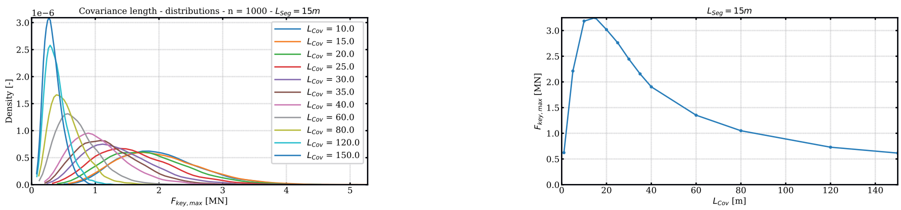

(a) Densities

(b) Force at 95 percentile

Figure A.2: Densities for segment length L_{seg} = 15m

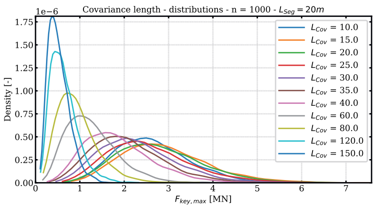

(a) Densities

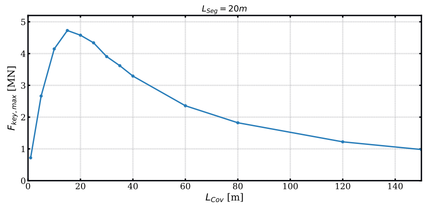

(b) Force at 95 percentile

Figure A.3: Densities for segment length L_{seg} = 20m

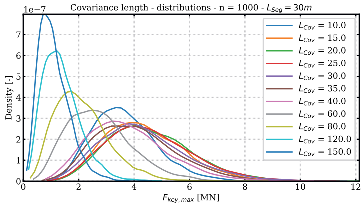

(a) Densities

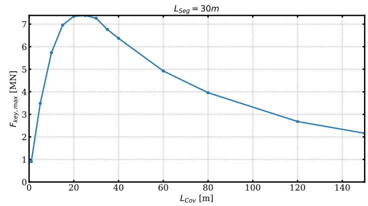

(b) Force at 95 percentile

Figure A.4: Densities for segment length L_{seg} = 30m

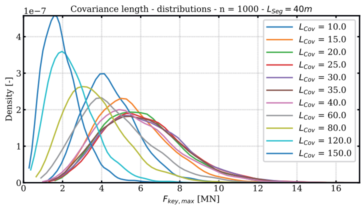

(a) Densities

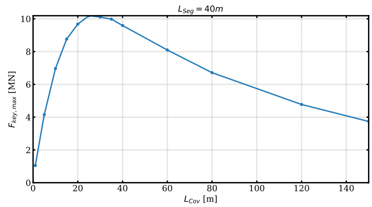

(b) Force at 95 percentile

Figure A.5: Densities for segment length L_{seg} = 40m

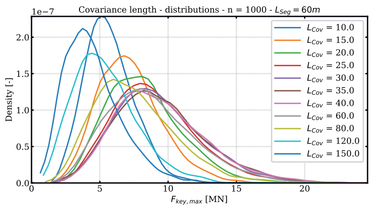

(a) Densities

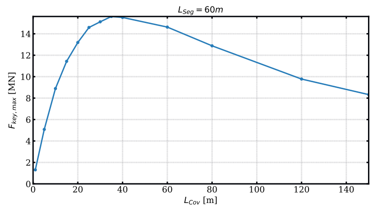

(b) Force at 95 percentile

Figure A.6: Densities for segment length L_{seg} = 60m

A

A.2. Non Parametric Bayesian Network

A.2.1. Part 1: Network setup

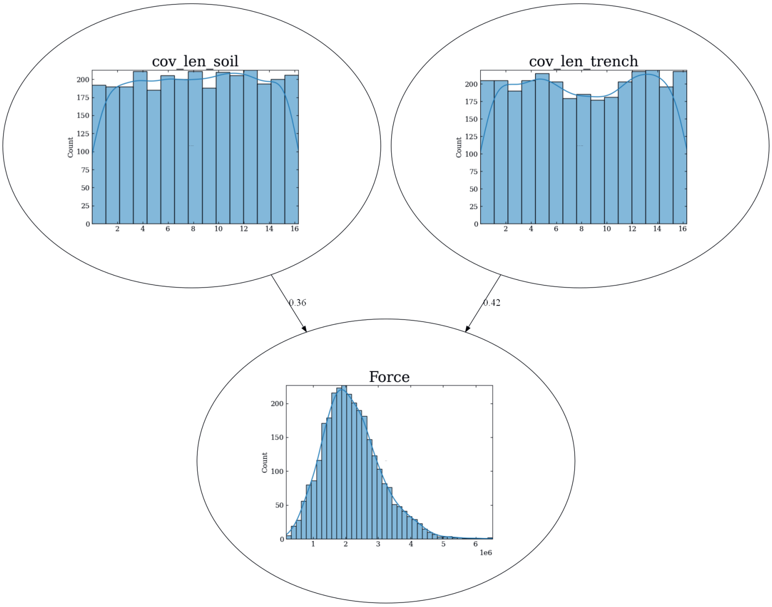

Figure A.7: Bayesian network - part 1

	$L_{cov,soil}$	$L_{cov,trench}$	F_{key}
$L_{cov,soil}$	1	0.006	0.355
$L_{cov,trench}$	0.006	1	0.426
F_{key}	0.355	0.426	1

Table A.1: Empirical rank correlation matrix for part 1

	$L_{cov,soil}$	$L_{cov,trench}$	F_{key}
$L_{cov,soil}$	1	0	0.355
$L_{cov,trench}$	0	1	0.424
F_{key}	0.355	0.424	1

Table A.2: Conditional normal rank correlation matrix for part 1

A

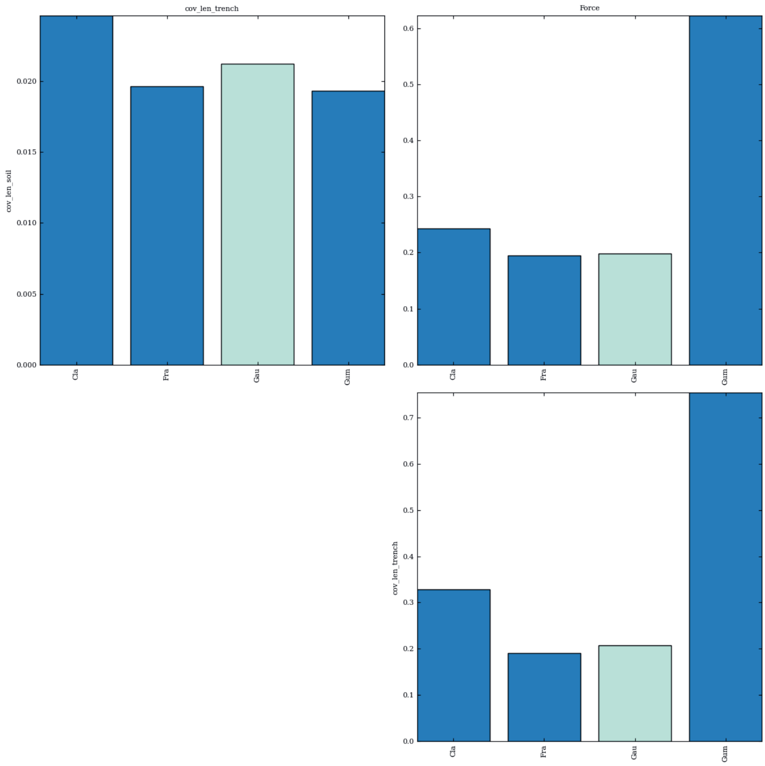

Figure A.8: Cramer von Mises statistics - part 1

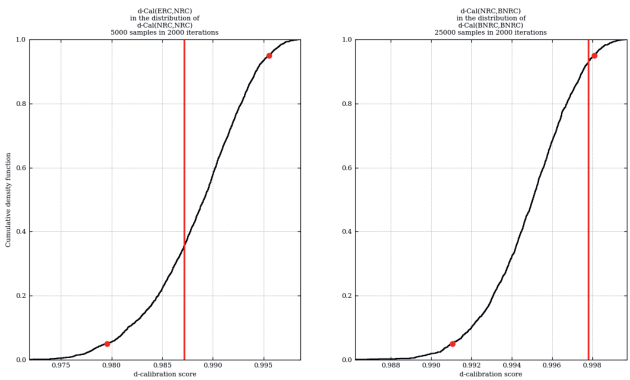

Figure A.9: Gaussian distance (d-score) - part 1

A.2.2. Part 1: Conditioning

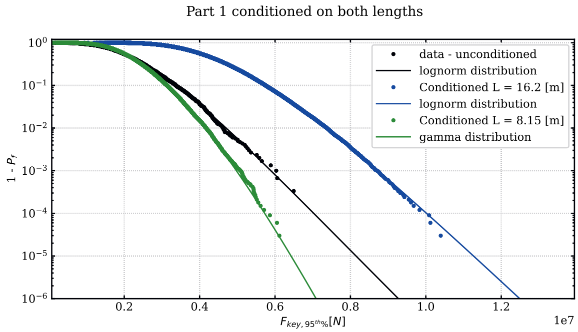

Figure A.10: Conditioned on 2 lengths

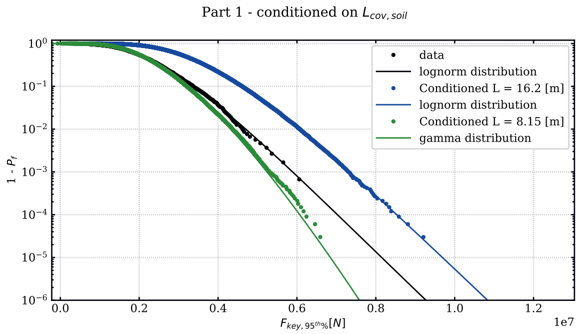

Figure A.11: Conditioned on $L_{cov,soil}$

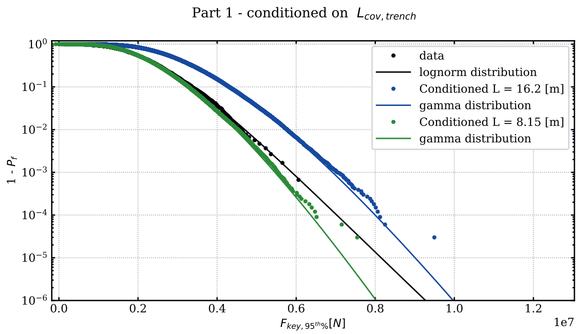

Figure A.12: Conditioned on $L_{cov,trench}$

A

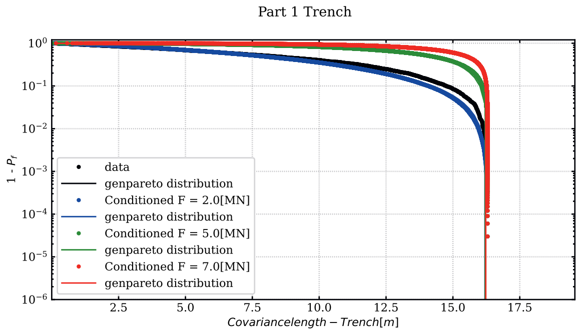

Figure A.13: Covariance length Trench, Conditioned on Force

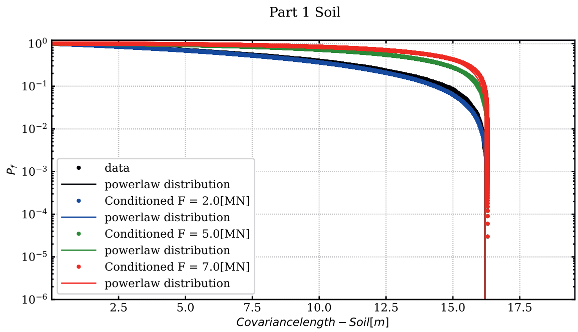

Figure A.14: Covariance length Soil, Conditioned on Force

A.2.3. Part 2: Network setup

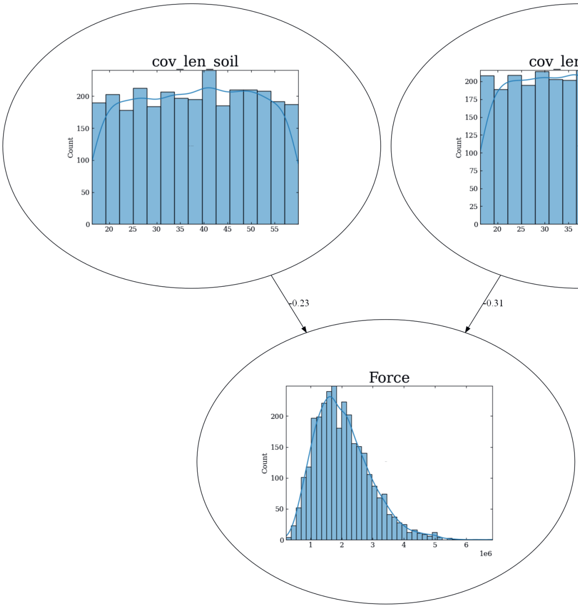

Figure A.15: Bayesian network - part 2

	$L_{cov,soil}$	$L_{cov,trench}$	F_{key}
$L_{cov,soil}$	1	-0.015	-0.230
$L_{cov,trench}$	-0.015	1	-0.303
F_{key}	-0.230	-0.303	1

Table A.3: Empirical rank correlation matrix for part 2

	$L_{cov,soil}$	$L_{cov,trench}$	F_{key}
$L_{cov,soil}$	1	0	-0.230
$L_{cov,trench}$	0	1	-0.307
F_{key}	-0.230	-0.307	1

Table A.4: Conditional normal rank correlation matrix for part 2

A

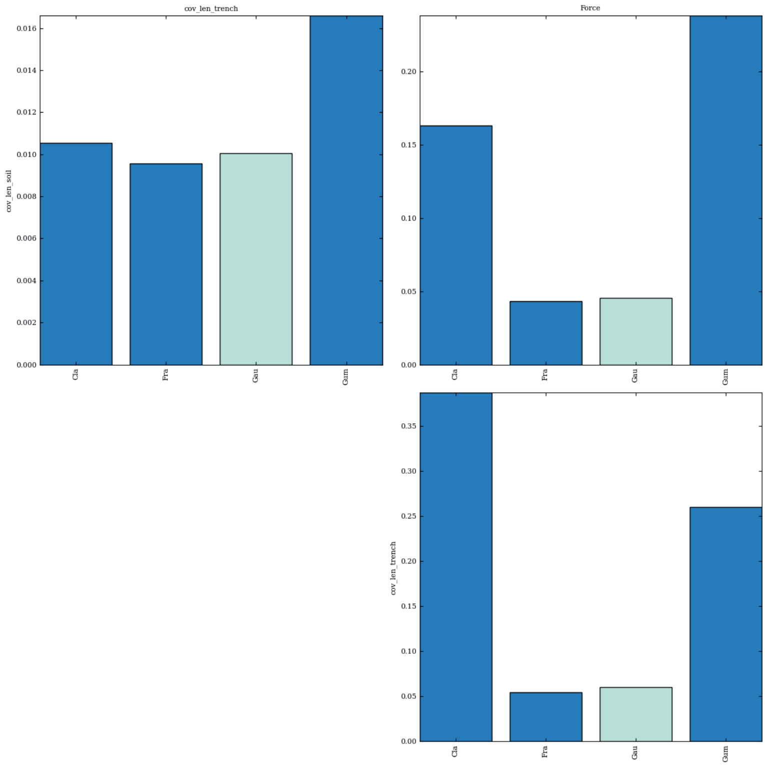

Figure A.16: Cramer von Mises statistics - part 2

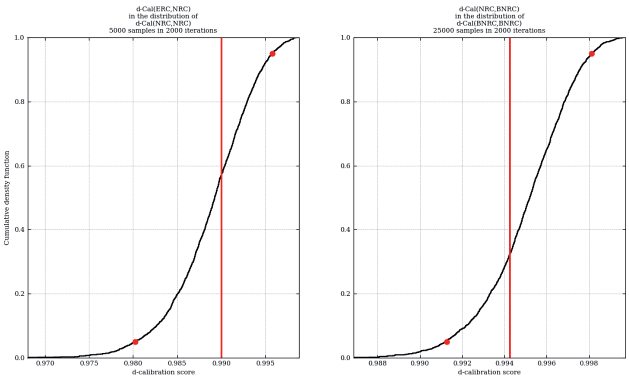

Figure A.17: Gaussian distance (d-score) - part 2

A.2.4. Part 2: Conditioning

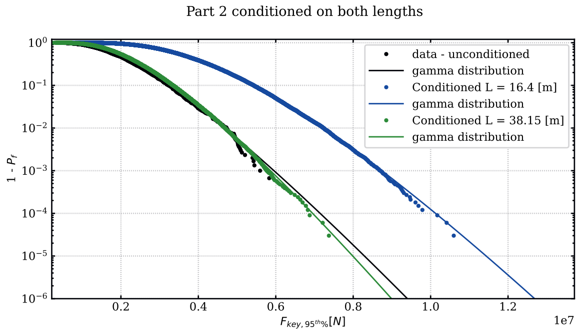

Figure A.18: Conditioned on 2 lengths

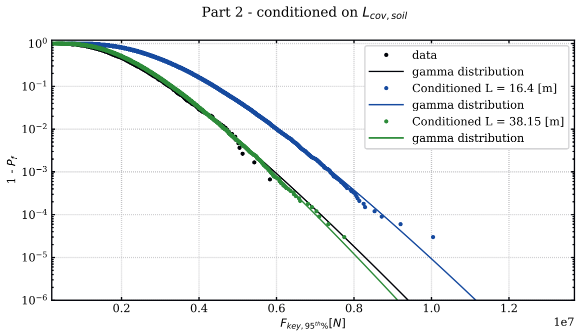

Figure A.19: Conditioned on $L_{cov,soil}$

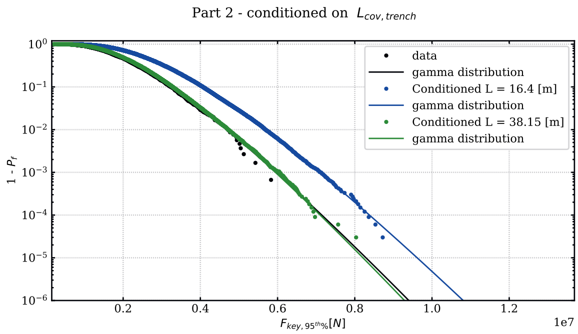

Figure A.20: Conditioned on $L_{cov,trench}$

A

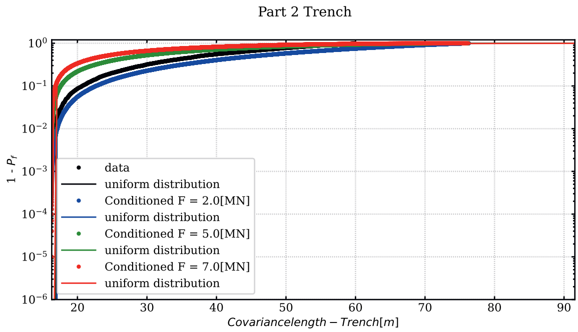

Figure A.21: Covariance length Trench, Conditioned on Force

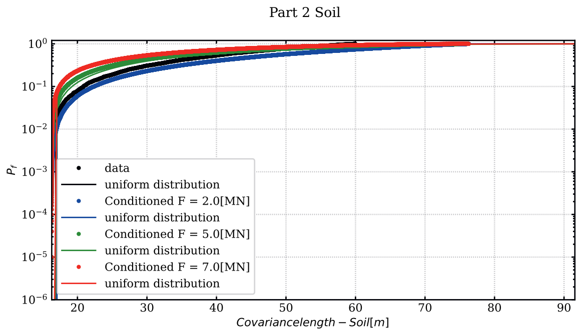

Figure A.22: Covariance length Soil, Conditioned on Force

A.3. Vine Copulas

A.3.1. Part 1: Data

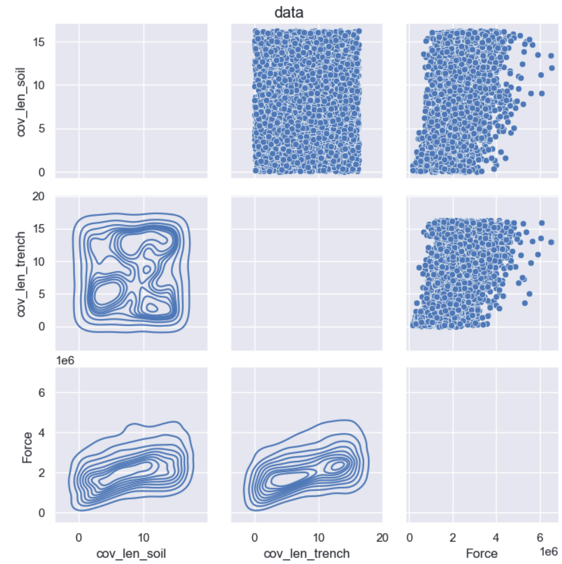

Figure A.23: Data overview

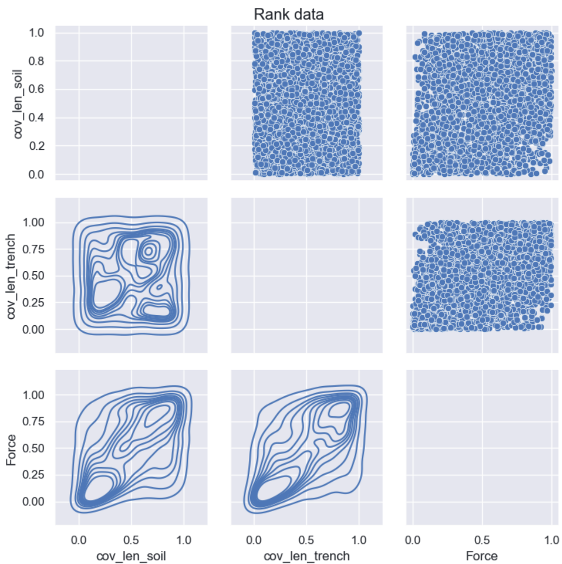

Figure A.24: Data overview - in [0,1]

A

Matrix based on 3-1-2 - Part 1

$$M = \begin{bmatrix} 1 & 1 & 1 \\ 2 & 2 & 0 \\ 3 & 0 & 0 \end{bmatrix}$$

Trees - Trace
$**Tree : 0$
$3, 1 <-> Gaussian, parameters = 0.371329$
$2, 1 <-> Joe, parameters = 1.00767$
$**Tree : 1$
$3, 2|1 <-> Gumbel180°, parameters = 1.46212$ AIC score: -1260.5

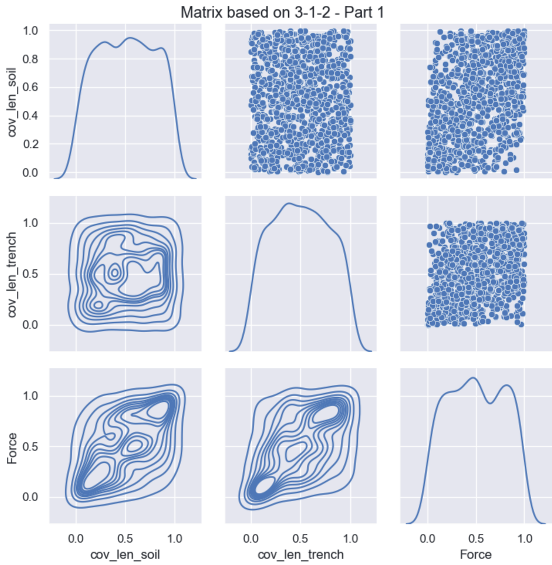

Figure A.25: sampling - matrix 3-1-2 - Part 1

Matrix based on 2-3-1 - Part 1

$$M = \begin{bmatrix} 3 & 3 & 3 \\ 1 & 1 & 0 \\ 2 & 0 & 0 \end{bmatrix}$$

Trees - Trace
$**Tree : 0$
$2, 3 <-> Gumbel180°, parameters = 1.38855$
$1, 3 <-> Gaussian, parameters = 0.371329$
$**Tree : 1$
$2, 1|3 <-> Frank, parameters = -1.4251$ AIC score: -1255.2

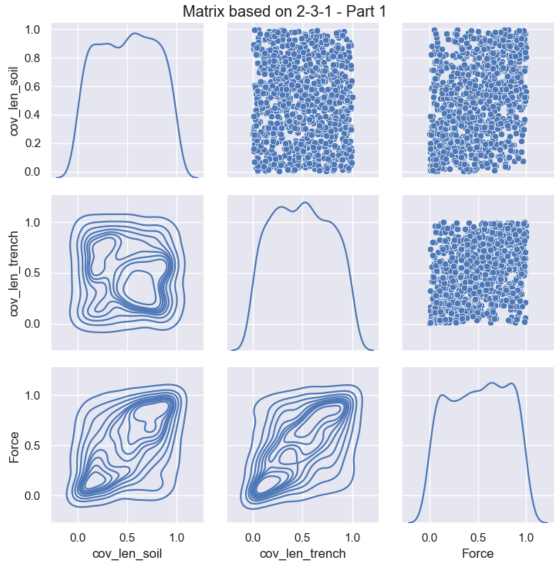

Figure A.26: sampling - matrix 2-3-1 - Part 1

Matrix based on 1-2-3 - Part 1

$$M = \begin{bmatrix} 2 & 2 & 2 \\ 3 & 3 & 0 \\ 1 & 0 & 0 \end{bmatrix}$$

Trees - Trace
$**Tree : 0$
$1,2 <-> Joe, parameters = 1.00767$
$3,2 <-> Gumbel180°, parameters = 1.38855$
$**Tree : 1$
$1,3|2 <-> Frank, parameters = 2.79775$ AIC score: -1254.9

A

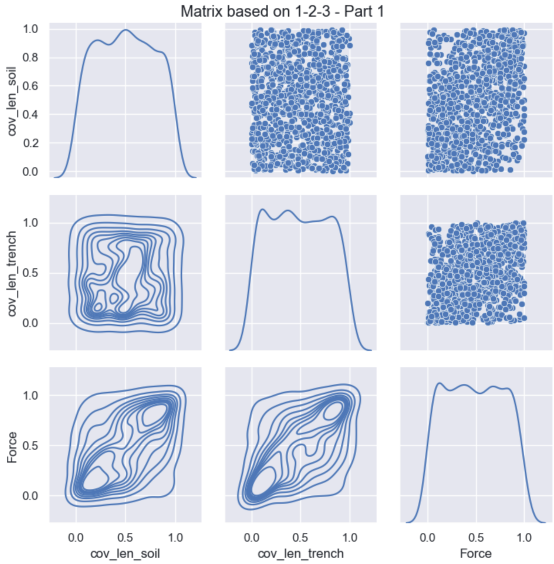

Figure A.27: sampling - matrix 1-2-3 - Part 1

A.3.2. Part 1: Conditioning - Vines

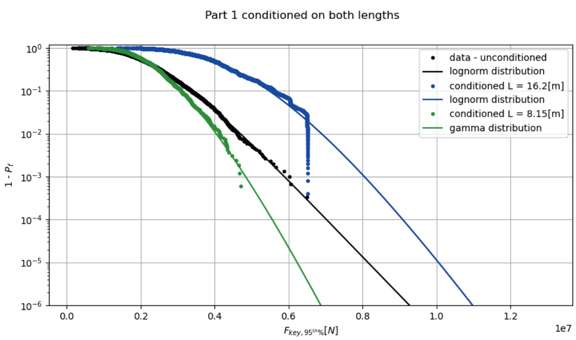

Figure A.28: Conditioned on 2 lengths

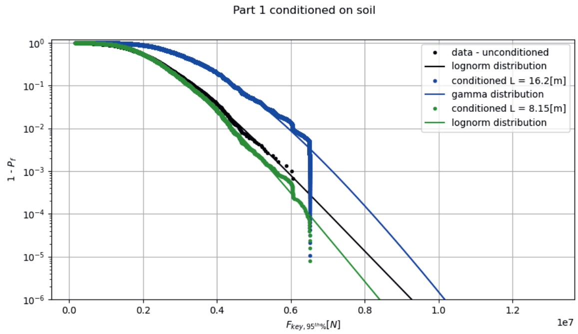

Figure A.29: Conditioned on $L_{cov,soil}$

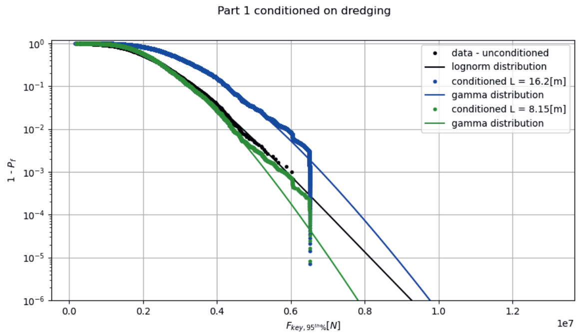

Figure A.30: Conditioned on $L_{cov,trench}$

A

A.3.3. Part 2: Data

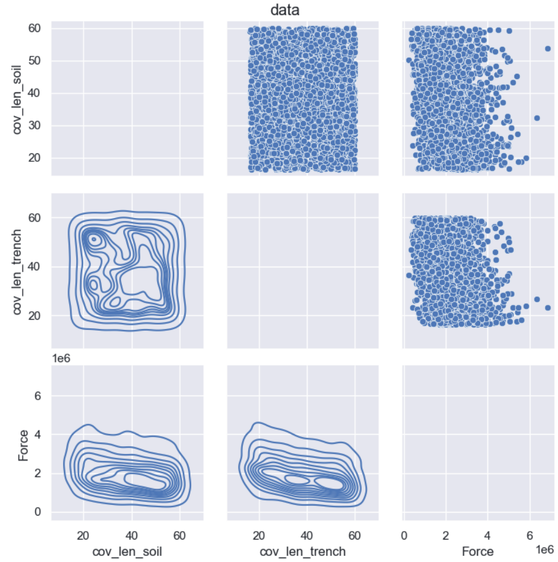

Figure A.31: Data overview

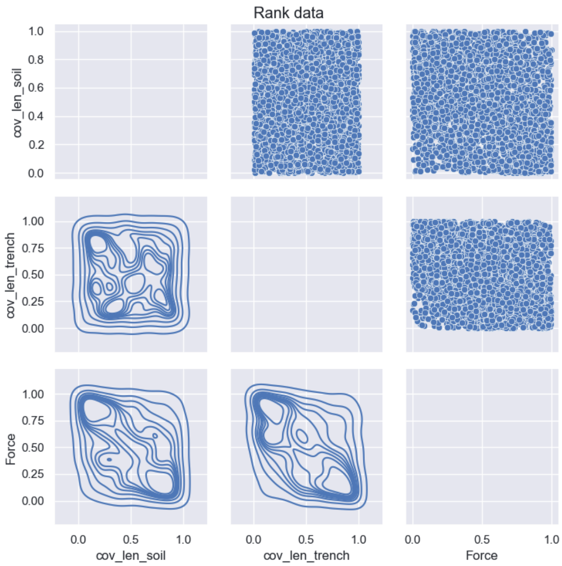

Figure A.32: Data overview - in [0,1]

A

Matrix based on 3-1-2 - Part 2

$$M = \begin{bmatrix} 1 & 1 & 1 \\ 2 & 2 & 0 \\ 3 & 0 & 0 \end{bmatrix}$$

Trees - Trace
$**Tree:0$
$3,1 <-> Frank, parameters = -1.48861$
$2,1 <-> Frank, parameters = -0.1289$
$**Tree:1$
$3,2|1 <-> Gaussian, parameters = -0.331021$ AIC score: -520.3

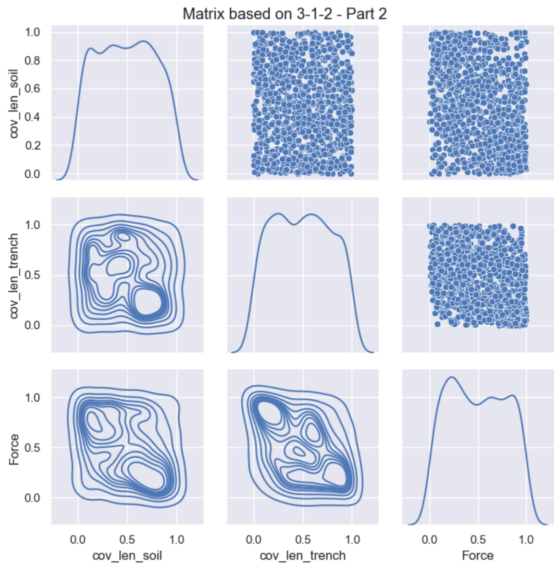

Figure A.33: sampling - matrix 3-1-2 - Part 2

Matrix based on 2-3-1 - Part 2

$$M = \begin{bmatrix} 3 & 3 & 3 \\ 1 & 1 & 0 \\ 2 & 0 & 0 \end{bmatrix}$$

Trees - Trace
$**Tree:0$
$2,3 <-> Frank, parameters = -1.99834$
$1,3 <-> Frank, parameters = -1.48861$
$**Tree:1$
$2,1|3 <-> Frank, parameters = -0.614899$ AIC score: -521.4

A

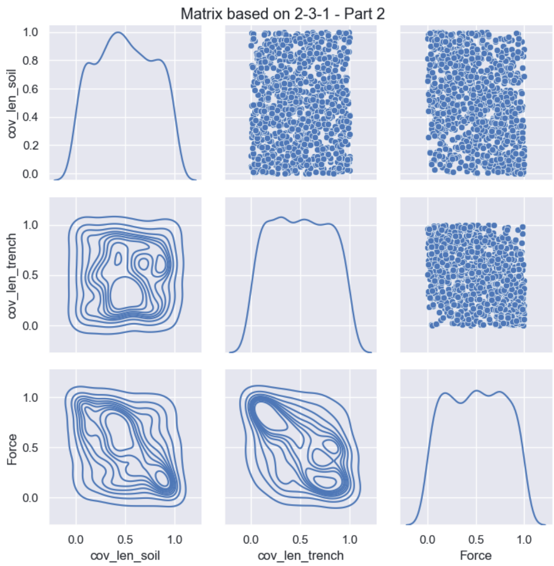

Figure A.34: sampling - matrix 2-3-1 - Part 2

Matrix based on 1-2-3 - Part 2

$$M = \begin{bmatrix} 2 & 2 & 2 \\ 3 & 3 & 0 \\ 1 & 0 & 0 \end{bmatrix}$$

Trees - Trace
$**Tree : 0$
$1, 2 <-> Frank, parameters = -0.1289$
$3, 2 <-> Frank, parameters = -1.99834$
$**Tree : 1$
$1, 3|2 <-> Gaussian, parameters = -0.260272$ AIC score: -519.9

A

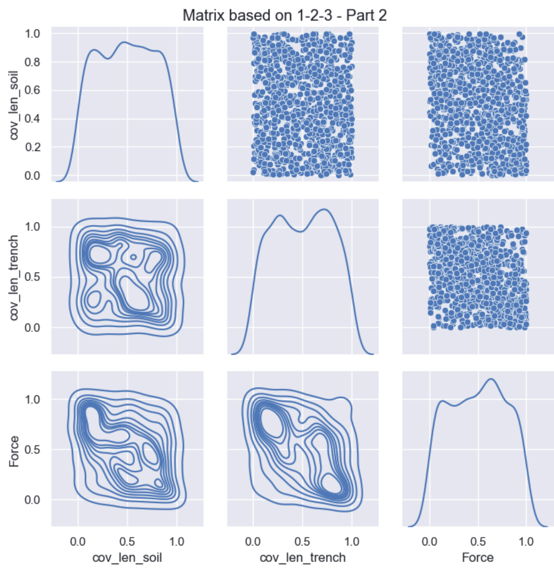

Figure A.35: sampling - matrix 1-2-3 - Part 2

A.3.4. Part 2: Conditioning - Vines

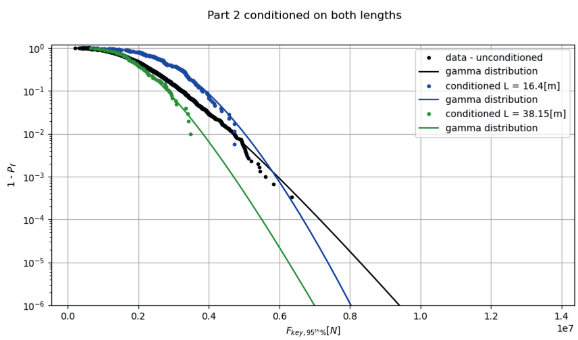

Figure A.36: Conditioned on 2 lengths

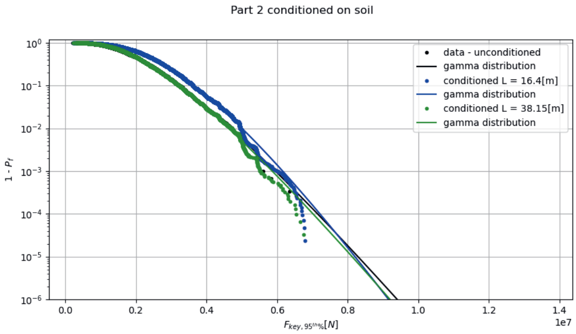

Figure A.37: Conditioned on $L_{cov,soil}$

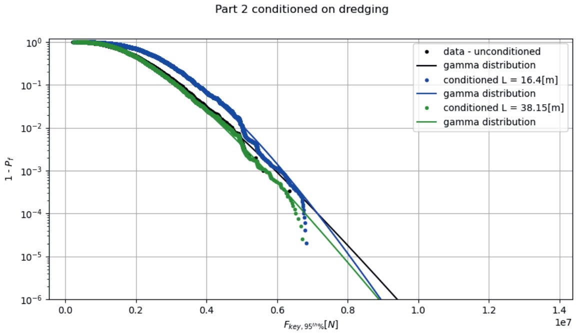

Figure A.38: Conditioned on $L_{cov,trench}$

B

Traffic - results

B.1. Vehicle categories

Item	Class	Code											
1	B2	B11	B2										
2	B3	B111	B12	B3									
3	O3	O3											
4	O4	O4											
5	O5	O5											
6	O6	O6											
7	O8	O8											
8	O9	O9											
9	O10	O=											
10	O11	O>											
11	R5	R11111	R1112	R1211	R122								
12	R6	R111111	R11112	R11121	R1113	R11211	R1122	R12111					
		R1212	R123	R1311	R132								
13	R7	R1111111	R111112	R111121	R11113	R111211	R11122	R112111					
		R124	R13111	R133	R2221	R223	R11311	R1123					
		R1132	R115	R121111	R12112	R1213	R12211	R1222					
		R11212	R11221										
14	R8	R11111111	R1111112	R1111121	R111113	R111122	R1112111	R111212	R111221	R11123	R1121111	R112112	R112121
		R11213	R112211	R11222	R1124	R113111	R11312	R11321	R1133	R1211111	R121112	R121121	R12113
		R121211	R12122	R1214	R122111	R12212	R12221	R1223	R12311	R1232	R125	R131111	R1313
		R13211	R1322	R134	R2123	R2213	R2222	R224					
15	R9	R1112121	R1112211	R11124	R1121121	R112113	R1122111	R112221	R11223	R1125	R1134	R12111111	R1211112
		R1211121	R121113	R1212111	R121212	R121221	R12123	R1221111	R122112	R122121	R12213	R1224	R123111
		R12321	R1233	R126	R1314	R132111	R13221	R1323	R1332	R1341	R135	R1413	R144
		R2214	R2223	R225	R234	R3312	R54						
16	T3	T11O1											
17	T4	T111O1	T11O11	T11O2	T12O1	T21O1	T2O2						
18	T5	T111O11	T111O2	T11O111	T11O12	T11O21	T11O3						
		T12O11	T12O2	T21O11	T21O2	T2O21	T2O3	T3O2					
19	T6	T111O111	T111O12	T111O21	T111O3	T11O1111	T11O112	T11O121	T11O13	T11O211	T11O22	T11O31	T11O4
		T12O111	T12O12	T12O21	T12O3	T21O111	T21O12	T21O21	T21O3	T2O22	T2O4	T3O3	
20	T7	T111O112	T111O121	T111O13	T111O22	T111O31	T111O4	T12O1111	T12O112	T12O121	T12O13	T12O211	T12O22
		T12O31	T12O4	T21O211	T21O22	T21O4	T3O4						
21	V2	V11											
22	V3	V111	V11A1	V12	V21	V3							
23	V4	V1111	V112	V11A11	V11A2	V121	V13	V211	V22	V4			
24	V5	V111A11	V111A2	V11A111	V11A12	V12A11	V12A2	V21A11	V21A2				
25	V6	V1111A11	V1111A2	V111A111	V111A12	V112A11	V112A2	V121A11	V12A111	V12A12	V12A21	V12A3	V13A11
		V13A2	V211A11	V211A2	V21A12	V22A11	V22A2						
26	V7	V1111A111	V1111A12	V1111A3	V112A111	V112A12	V112A21	V112A3	V121A111	V121A12	V121A3	V13A111	V13A12
		V13A21	V13A3	V211A12	V211A3	V22A111	V22A12	V22A21	V22A3	V4A12			

Table B.1: Vehicle categories of WIM observations.

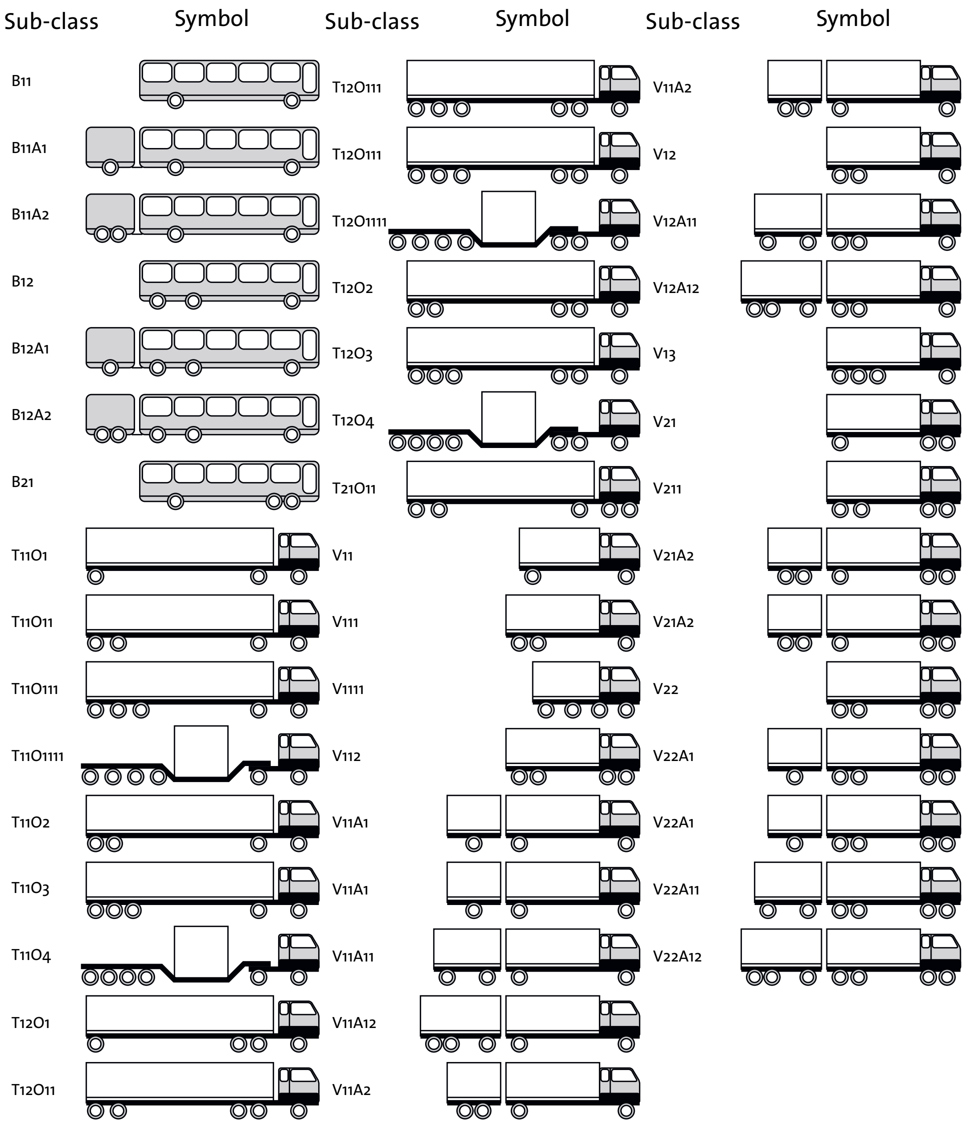

Figure B.1: WIM Vehicle indexing. [115]

B

B

B.2. Daily proportion of vehicles' categories

Vehicle Category	C_L2	F_L2_A	F_L2_B	C_L3	F_L3_A	F_L3_B
B2	0.61	5.56	1.65	0.69	0.58	0.39
B3	1.83	0.00	3.31	0.61	0.17	0.33
O3	3.05	1.85	2.13	0.69	0.42	1.11
O4	15.24	3.70	4.96	4.59	1.83	2.66
O5	0.61	1.85	0.71	0.61	0.58	0.20
O8	0.00	0.00	0.00	0.17	0.25	0.09
O9	0.00	0.00	0.00	0.00	0.08	0.00
OT10	0.00	0.00	0.00	0.00	0.00	0.02
OT11	0.00	0.00	0.00	0.00	0.00	0.00
R5	0.00	0.00	0.00	0.00	0.00	0.07
R6	0.00	0.00	0.00	0.17	0.83	0.11
R7	0.00	0.00	0.24	0.26	0.42	0.30
R8	0.00	0.00	0.00	0.26	0.17	0.41
R9	0.00	0.00	0.00	0.09	0.08	0.07
T3	1.83	3.70	2.60	5.37	4.33	4.22
T4	10.98	16.67	14.89	15.34	19.83	18.35
T5	26.83	33.33	37.12	29.29	38.25	36.04
T6	2.44	7.41	2.60	6.07	6.25	6.81
T7	0.61	0.00	0.00	0.26	0.33	0.33
V2	14.63	9.26	15.37	14.99	9.92	12.80
V3	3.66	1.85	1.65	4.51	1.92	4.16
V4	14.02	5.56	5.91	8.23	6.67	6.03
V5	1.83	5.56	4.73	5.37	5.33	3.53
V6	1.22	3.70	1.89	1.65	1.67	1.61
V7	0.61	0.00	0.24	0.61	0.08	0.37

Table B.1: Daily proportion of vehicles' categories. 10th April 2013.

B

B.3. Monthly proportion of vehicles' categories

Vehicle Category	Proportion [%]
B2	1.014
B3	0.779
O3	1.295
O4	3.116
O5	0.400
O8	0.128
O9	0.026
OT10	0.012
OT11	0.006
R5	0.047
R6	0.216
R7	0.264
R8	0.317
R9	0.054
T3	3.851
T4	17.795
T5	35.481
T6	5.871
T7	0.277
V2	12.801
V3	3.582
V4	6.902
V5	4.005
V6	1.445
V7	0.297

Table B.2: Monthly proportion of vehicles' categories. April 2013.

B.4. Copula Results-April 2013

Day	C_L2	C_L3	F_L2_A	F_L3_A	F_L2_B	F_L3_B
4	Joe	Frank	Joe	BB8	Joe	BB8
5	Gaussian	Gaussian	Clayton	Frank	Joe	Joe
6	t	Frank	Joe	t	Joe	Joe
7	Frank	Frank	Joe	Frank	Joe	BB7
8	Joe	Clayton	Clayton	Clayton	Gaussian	Gumbel
10	Gumbel	Frank	Joe	BB8	Joe	BB7
11	Gaussian	Frank	Joe	BB8	Joe	Joe
12	Gaussian	Joe	Joe	t	Joe	Joe
13	Clayton	Frank	t	BB8	Joe	Joe
14	t	Frank	Joe	Gaussian	Joe	Joe
15	t	Frank	Gaussian	Clayton	Joe	Joe
17	Gaussian	Gaussian	Joe	BB8	Gumbel	BB8
18	Gumbel	Frank	Joe	Frank	Joe	BB8
19	Frank	Frank	t	Clayton	Joe	Joe
20	Gaussian	Frank	Joe	t	Joe	Joe
21	BB7	Frank	BB7	Frank	Joe	BB8
22	t	Clayton	Clayton	Gaussian	Joe	Joe
24	Gaussian	Gaussian	t	BB8	Joe	Joe
25	Gaussian	Clayton	Joe	BB8	Joe	BB8
26	Joe	t	Gaussian	BB8	Joe	BB8
27	t	Frank	Gumbel	BB8	Joe	BB8
28	Joe	Frank	Joe	BB8	Joe	BB8
29	Gaussian	Clayton	Gaussian	Frank	Joe	BB7

Table B.1: Copula fit for inter-vehicle distances per traffic type. April 2013.

Day	C_L2		C_L3		F_L2_A		F_L3_A		F_L2_B		F_L3_B	
	Obs.	Sim.	Obs.	Sim.	Obs.	Sim.	Obs.	Sim.	Obs.	Sim.	Obs.	Sim.
4	0.213	0.091	-0.039	-0.088	0.477	0.584	0.218	0.300	0.149	0.177	0.088	0.113
5	0.084	0.259	-0.010	-0.017	0.535	0.563	0.177	0.170	0.109	0.129	0.097	0.140
6	0.068	-0.014	-0.103	-0.088	0.153	0.312	0.157	0.156	0.140	0.208	0.089	0.186
7	-0.045	0.004	-0.121	-0.160	0.508	0.163	0.265	0.240	0.152	0.186	0.136	0.173
8	0.099	0.231	0.033	-0.022	0.500	0.350	0.116	0.172	0.210	0.060	0.179	0.177
10	0.114	0.048	-0.050	-0.038	0.154	0.857	0.281	0.256	0.131	0.188	0.117	0.171
11	-0.003	-0.037	-0.023	0.007	0.106	0.367	0.245	0.242	0.162	0.218	0.102	0.112
12	-0.021	-0.142	0.004	-0.031	0.486	0.097	0.222	0.177	0.054	0.069	0.090	0.150
13	0.036	0.040	-0.029	-0.046	0.202	0.398	0.245	0.313	0.112	0.294	0.104	0.110
14	0.124	0.303	-0.035	0.023	0.414	0.419	0.190	0.227	0.147	0.226	0.118	0.147
15	-0.333	-0.103	0.065	0.003	0.300	0.400	0.115	0.176	0.154	0.078	0.119	0.165
17	0.133	0.170	-0.019	-0.043	0.365	0.351	0.289	0.290	0.156	0.132	0.099	0.138
18	0.154	0.100	-0.054	-0.068	0.388	-0.159	0.177	0.129	0.086	0.165	0.085	0.114
19	0.259	0.184	-0.086	-0.116	0.060	0.414	0.216	0.222	0.211	0.323	0.086	0.096
20	-0.001	-0.008	-0.009	0.017	0.566	0.712	0.165	0.100	0.121	0.152	0.101	0.136
21	0.148	0.262	-0.093	-0.088	0.307	0.384	0.231	0.256	0.204	0.270	0.086	0.122
22	-0.355	-0.346	0.036	0.079	0.164	0.291	0.059	0.112	0.197	0.067	0.112	0.152
24	0.103	0.107	0.001	-0.045	0.102	-0.278	0.168	0.176	0.106	0.146	0.067	0.123
25	0.115	0.125	0.007	0.059	0.389	0.218	0.139	0.068	0.217	0.296	0.122	0.155
26	0.088	0.007	-0.044	-0.067	0.470	0.517	0.256	0.277	0.161	0.228	0.091	0.150
27	-0.049	-0.147	-0.006	0.013	0.535	0.348	0.284	0.288	0.105	0.220	0.113	0.148
28	0.002	-0.108	-0.055	-0.025	0.558	0.593	0.222	0.240	0.066	0.120	0.092	0.155
29	-0.257	-0.388	0.023	0.047	0.543	0.257	0.053	0.100	0.274	0.325	0.158	0.125

Table B.2: Spearman's correlation coefficient for observations and simulations for inter-vehicle distance. April 2013.

B.5. Structural model

B.5.1. Direct Stiffness Method

In this paper, the structural system of the SFT is characterised by beams supported by pontoons. The methodology for the structural model is based on the Direct Stiffness Method (DSM) and the Differential Equation Method (DEM).

The origin of these models started around 1930 with the Matrix Structural Analysis (MSA). In later decades, "human computers" are replaced by "programmable digital computers". Then, MSA translates into FEM with continuum mathematical models instead of discrete models. Later in history, this was named the DSM formulation. In 1959, [125] proposed the DSM as an implementation of the Finite Element Method (not named at that moment). The evolution of computer power allowed engineers to use larger matrices and solving methods, but DSM's theory is still fundamental for today's engineering. A detailed description of the evolution of these methods can be found in [126].

The SFT model is defined in a 2-dimensional Cartesian coordinate system with the X-axis corresponding to the longitudinal direction of the SFT. A beam element connects two points (nodes), and the deformation of the nodes describes the internal forces based on the axial and bending stiffness of the beam element. In the 2 dimensional domain, the number of degrees of freedom in a node is 3 and on a beam element is 6. The relation between the force vector ($\vec{F}_b$) and the displacement vector ($\vec{u}_b$) each of length 6 can be described by a matrix (6×6) K_b as in Equation B.1. A graphical representation of K_b is shown in Fig. B.1. The elements of the 6×6 stiffness matrix are based on the relations according to Euler-Bernoulli beam theory [127], see also B.5.2. For this case, units for $\vec{u}_b$ are metres and radians, and for $\vec{F}_b$ the units are Newton and Newton-metre. The stiffness matrix K_b contains direct relationships of forces with displacements and moments with rotations on the diagonal terms, but it also contains cross terms (the influence of forces on rotations and vice versa). The units of each cross-term in K_b depend on the relation it describes.

$$\vec{F}_b = [K_b]\vec{u}_b \tag{B.1}$$

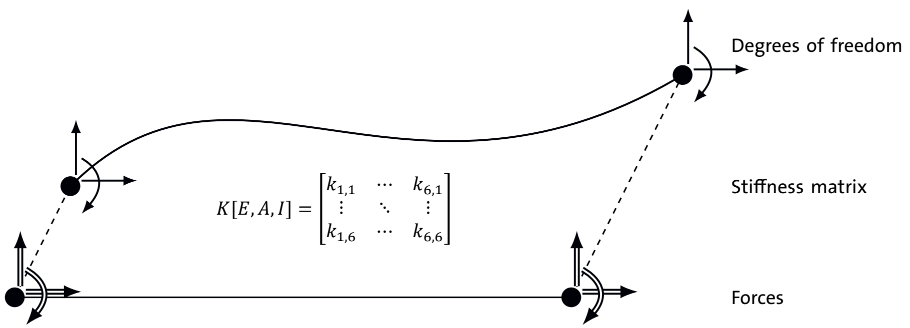

Figure B.1: Local stiffness relation

The system stiffness matrix K_s can be compiled by connecting the nodes on the beam stiffness matrix $[K_b]$. Thus, the stiffness relations between the beams' nodes are combined in the system stiffness matrix K_s and describe the system relationship between the system degrees of freedom u_s and the system forces F_s. The relation between forces and degrees of freedom is described by Equation B.2 and is shown graphically in Fig. B.2 (where z defines the out-of-plane axis, to define the rotations θ in the 2-dimensional plane). The system stiffness matrix K_s has the size of the number of nodes 3 times (for each degree of freedom) in both dimensions. The global force and displacement vectors have dimensions equal to the length of the number of nodes multiplied by 3 (for each degree of freedom at each node).

$$\vec{F_s} = K_s \vec{u_s} \tag{B.2}$$

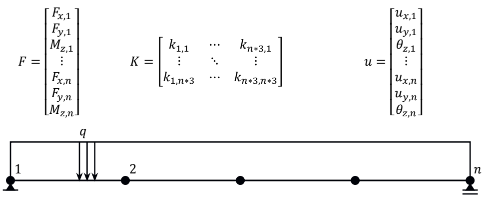

Figure B.2: Global stiffness relation

Both the force and displacement vectors are discrete and describe the external loads on the nodes and the displacements and rotations of the nodes. The distributed forces (q in Figure B.2) in the beams are internal forces and need to be translated into global nodal forces, because the DSM only describes the relationship between the forces in the nodes and the degrees of freedom of the nodes. Global displacements can theoretically be found by multiplying the global force vector by the inverse of the system stiffness matrix (Equation B.3). To successfully perform this, the vectors and matrix need to be filtered (swept) for supports, where displacements or rotations are assumed to be 0. The rows and columns related to these globally supported degrees of freedom are swept from the stiffness matrix of the system K_s and both vectors $\vec{u_f}$ and $\vec{F_s}$, resulting in the filtered vectors $\vec{u_f}$ and $\vec{F_f}$ and the stiffness matrix K_f.

$$\vec{u_f} = [K_f]^{-1} \vec{F_f} \tag{B.3}$$

Deriving the inverse of large matrices can be quite intensive in terms of computational effort. The use of more advanced numerical routines decreases the calculation time. Despite advanced numeric routines, the reduction of beam-elements and the number of total degrees of freedom of the system, will reduce the matrix size. Therefore, the performance penalty for larger systems is reduced.

To find the support reactions, the global stiffness matrix K_s is multiplied by the full displacement vector $\vec{u_s}$ which is compiled by adding zeros to $\vec{u_f}$ due to supports (that were previously swept) and then the internal force vector $\vec{F_s}$ is subtracted (Equation B.4). When the displacements and rotations at the nodes are known, the internal forces in the beams can be derived using the DEM (to be discussed in the next subsection).

$$\vec{F}_p = [K_s]\vec{u}_s - \vec{F}_s \tag{B.4}$$

B

B.5.2. Differential Equation Method

The DEM is also known as the Euler-Bernoulli method. This method is based on the relationship between the applied distributed load q and the deflection u as presented in Equation B.5 and B.6. Here E is the stiffness of the element, I is the second moment of area, and A the sectional area. For more details, see [127] and references therein.

In the DEM, the cross-sectional forces and degrees of freedom are assumed to be continuous along the beam element and are considered constant in the SFT model. The basis of DEM is presented by the differential equations in Equation B.5 and Equation B.6. In the differential equation x is defined as the axial coordinate. By solving Equation B.5 for the lateral direction y the shear force V_y, the bending moment M_z and the rotations θ_z as well as the lateral displacements u_y can be found as a relation to x. By solving the differential Equation B.6 for axial direction, the normal force N_x, the axial strain ε_x and the axial displacements u_x as a function of x can be determined.

$$EI\frac{\mathrm{d}^4u_y}{\mathrm{d}x^4} = q_y \tag{B.5}$$

$$EA\frac{\mathrm{d}^2u_x}{\mathrm{d}x^2} = q_x \tag{B.6}$$

$$\frac{\mathrm{d}q_y(x)}{\mathrm{d}x} = V_y(x) \tag{B.7}$$

$$\frac{\mathrm{d}V_y(x)}{\mathrm{d}x} = M_z(x) \tag{B.8}$$

$$\frac{\mathrm{d}M_z(x)}{\mathrm{d}x} = -EI\theta_z(x) \tag{B.9}$$

$$\frac{\mathrm{d}\theta_z(x)}{\mathrm{d}x} = u_y(x) \tag{B.10}$$

$$\frac{\mathrm{d}q_x(x)}{\mathrm{d}x} = N_x(x) \tag{B.11}$$

$$N_x(x) = -EA\varepsilon_x(x) \tag{B.12}$$

$$\frac{\mathrm{d}u_x(x)}{\mathrm{d}x} = \varepsilon_x(x) \tag{B.13}$$

The derived displacements and rotations from the DSM ($u_{x,\mathrm{DSM}}$,$u_{y,\mathrm{DSM}}$, θ_{DSM}) are input to the DEM. These results are located at both ends of the beam (x_0 and x_l, in Equation B.14 to B.16), the forces, bending moments, displacements, and rotations along the beam can be determined.

$$u_y[x_0] = u_{y,\text{DSM},1} \quad \text{and} \quad u_y[x_l] = u_{y,\text{DSM},2} \tag{B.14}$$

$$\theta[x_0] = \theta_{\text{DSM},1} \quad \text{and} \quad \theta[x_l] = \theta_{\text{DSM},2} \tag{B.15}$$

$$u_x[x_0] = u_{x,\text{DSM},1} \quad \text{and} \quad u_x[x_l] = u_{x,\text{DSM},2} \tag{B.16}$$

B

B.5.3. Discrete loads

For discrete loads, the beams could be split into smaller beams with connecting nodes and degrees of freedom. Force loads can then be applied on the node and the DSM can be used successfully. However, when there are a large number of discrete loads, the system becomes more complex with an increasing number of beams and nodes. In such a case, a performance penalty is paid. In this paper, an alternative is presented. The nodes are applied only where the beams are physically connected or supported. For example, at the (symmetric) ends of the SFT and at the connections with the tethers. At the connecting nodes, the full coupling of degrees of freedom is assumed. To account for the discrete force load on the beam, the internal force vector is set so that the force is redistributed to x_0 and x_l. In the global analysis, the forces are taken into account at the beam element's nodes. Equivalent to the distributed load, a force load acting on the beam but not at the node needs to be transferred to the global force vector to use the DSM. The displacements and rotations are derived from this method and are input to the DEM.

In the DEM the force load is a discrete load, which causes non-continuous results along the beam. To account for the load, the equations for the beam are divided at the location of the force x_f into two separate systems of equations, i) from x_0 to the location of the force load x_f (marked as 1 in Fig. B.3) and ii) from x_f to x_l (marked as 2 in Fig. B.3). For both systems, the assumption of continuity suffices and can be connected to each other by the transitional conditions at x_f and an extra variable to these conditions, load $F_{y,ext}$ as defined in Equation B.17 to Equation B.22.

$$u_{y,2}[x_f] - u_{y,1}[x_f] = 0 \tag{B.17}$$

$$\theta_{z,2}[x_f] - \theta_{z,1}[x_f] = 0 \tag{B.18}$$

$$V_{y,2}[x_f] - V_{y,1}[x_f] = F_{y,ext} \tag{B.19}$$

$$M_{z,2}[x_f] - M_{z,1}[x_f] = 0 \tag{B.20}$$

$$u_{x,2}[x_f] - u_{x,1}[x_f] = 0 \tag{B.21}$$

$$N_{x,2}[x_f] - N_{x,1}[x_f] = F_{x,ext} \tag{B.22}$$

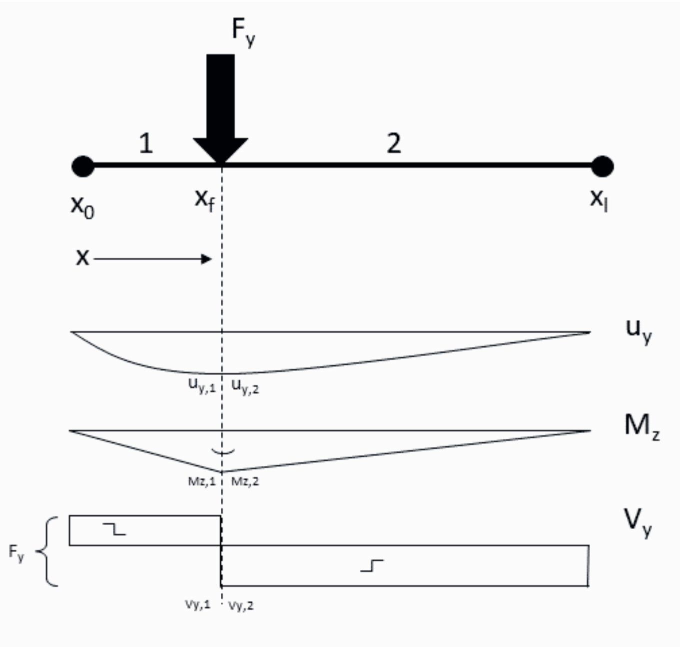

Figure B.3: Discrete loading - split differential equation method at loading location

C

Dynamic Mooring analysis - results

C.1. Dataset run 6

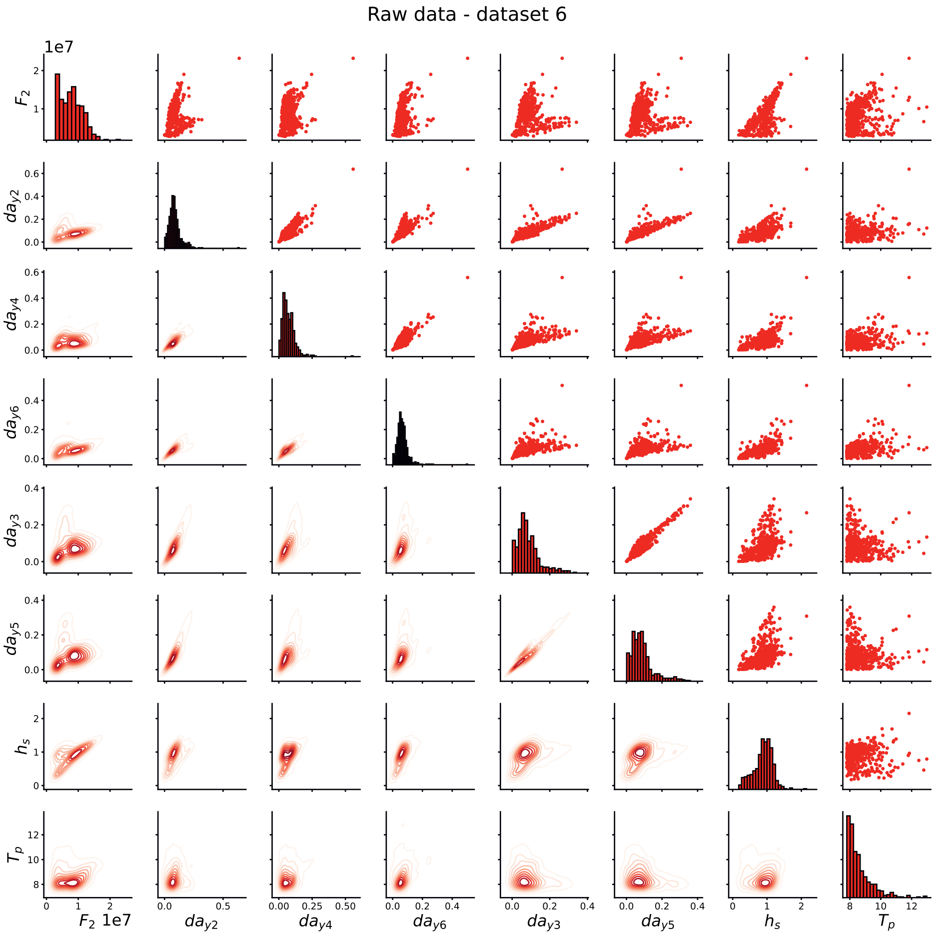

Figure C.1: Pairplot of raw data - dataset 6 - maximum values

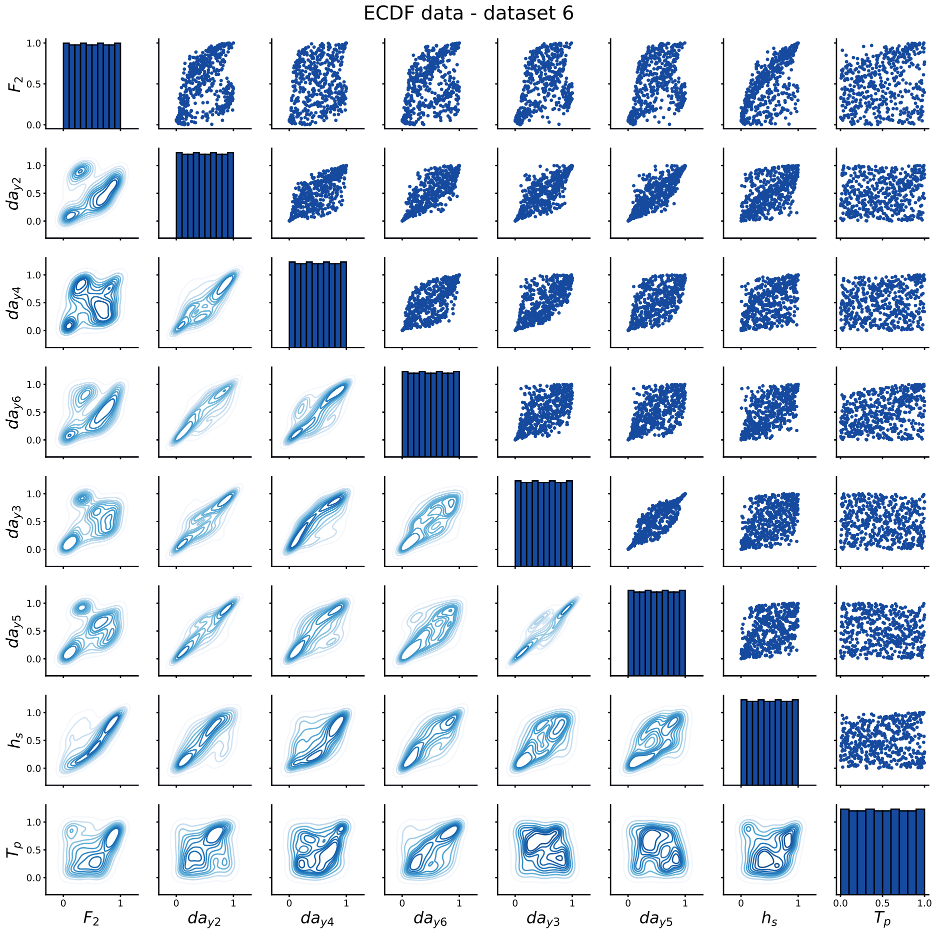

Figure C.2: Pairplot of [0,1] data - dataset 6 - maximum values

C

C.2. Copulas run 6 max

C.2.1. Bruteforce copulas run 6 - max

** Tree: 0

7,1: Gumbel, parameters = 1.97873

8,5: Frank, parameters = -0.624052

6,1: Joe 180°, parameters = 1.793

1,5: Joe 180°, parameters = 1.77868

4,5: Clayton, parameters = 1.73407

2,5: Gumbel 180°, parameters = 2.63637

5,3: Gumbel 180°, parameters = 2.13151

** Tree: 1

7,5 | 1: Gumbel 180°, parameters = 1.53788

8,1 | 5: Gaussian, parameters = 0.269532

6,5 | 1: Clayton 180°, parameters = 4.04453

1,2 | 5: Joe, parameters = 1.16717

4,2 | 5: Gumbel, parameters = 1.85992

2,3 | 5: Joe, parameters = 1.6687

** Tree: 2

7,8 | 5,1: Joe 90°, parameters = 1.26675

8,6 | 1,5: Clayton 270°, parameters = 0.134474

6,2 | 5,1: Clayton, parameters = 0.942429

1,4 | 2,5: Gumbel 180°, parameters = 1.06652

4,3 | 2,5: Gaussian, parameters = 0.328418

** Tree: 3

7,6 | 8,5,1: Frank, parameters = 0.290663

8,2 | 6,1,5: Gumbel, parameters = 1.22375

6,4 | 2,5,1: Joe 270°, parameters = 1.59279

1,3 | 4,2,5: Frank, parameters = -0.900501

** Tree: 4

7,2 | 6,8,5,1: Gumbel 180°, parameters = 1.48827

8,4 | 2,6,1,5: Frank, parameters = 2.08272

6,3 | 4,2,5,1: Clayton, parameters = 0.0568479

** Tree: 5

7,4 | 2,6,8,5,1: Gumbel 180°, parameters = 1.50522

8,3 | 4,2,6,1,5: Frank, parameters = 0.857961

** Tree: 6

7,3 | 4,2,6,8,5,1: Frank, parameters = 1.16051

C.2.2. Algorithm copulas run 6 - max:

** Tree: 0

3,2: Gaussian, parameters = 0.795419

5,6: Gumbel 180°, parameters = 3.83403

1,7: Gumbel, parameters = 1.97873

6,2: Gumbel 180°, parameters = 2.99466

7,4: Gumbel 180°, parameters = 1.87266

2,4: Gumbel 180°, parameters = 2.75072

4,8: Frank, parameters = 2.12004

** Tree: 1

3,4 | 2: Gaussian, parameters = 0.366655

5,2 | 6: Clayton, parameters = 0.315595

1,4 | 7: Frank, parameters = -0.694517

6,4 | 2: Frank, parameters = -2.37023

7,2 | 4: Clayton, parameters = 0.221927

2,8 | 4: Clayton 90°, parameters = 0.289757

** Tree: 2

3,6 | 4,2: Frank, parameters = 1.19606

5,4 | 2,6: Clayton, parameters = 0.316158

1,2 | 4,7: Frank, parameters = -0.330219

6,8 | 4,2: Frank, parameters = -1.81063

7,8 | 2,4: Clayton 270°, parameters = 0.228907

** Tree: 3

3,5 | 6,4,2: Gumbel 180°, parameters = 1.24157

5,8 | 4,2,6: Gaussian, parameters = -0.157498

1,8 | 2,4,7: Joe, parameters = 1.44932

6,7 | 8,4,2: Frank, parameters = -0.173433

** Tree: 4

3,8 | 5,6,4,2: Gaussian, parameters = 0.098223

5,7 | 8,4,2,6: Clayton 270°, parameters = 0.0733898

1,6 | 8,2,4,7: Frank, parameters = 1.62048

** Tree: 5

3,7 | 8,5,6,4,2: Clayton 180°, parameters = 0.139457

5,1 | 7,8,4,2,6: Frank, parameters = 0.164759

** Tree: 6

3,1 | 7,8,5,6,4,2: Joe 90°, parameters = 1.36178

C.2.3. Regular Vines run 6 - max:

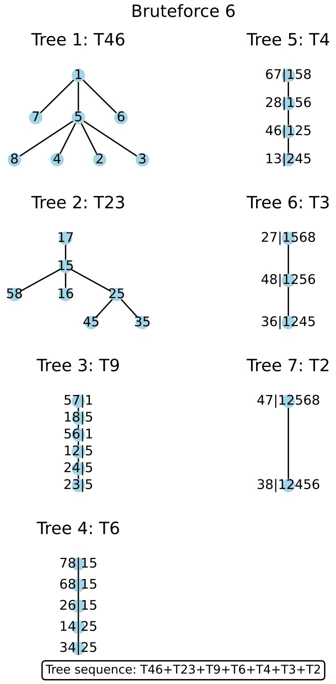

Figure C.3: Regular for run 6 - maximum values - Bruteforce

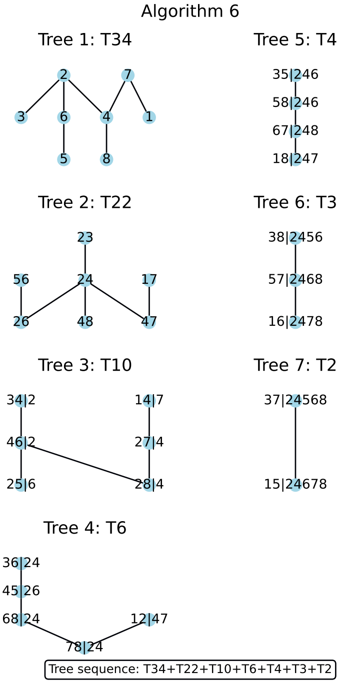

Figure C.4: Regular for run 6 - maximum values - Algorithm

C

C.3. percentile estimation

C.3.1. Second variable - maximum values

Table C.1: Conditioning on 2^{nd} variable - percentile estimation

Analysis		1	2	3	4	5	6	7
Variable		F_4	F_4	F_4	F_4	da_{y4}	da_{y4}	da_{z4}
1.0e-01	BF	1.584e+07	1.574e+07	1.555e+07	1.660e+07	2.461e-01	2.462e-01	3.667e-01
	AL	1.574e+07	1.528e+07	1.556e+07	1.647e+07	2.110e-01	2.382e-01	3.679e-01
	Δ	0.65%	3.03%	0.06%	0.79%	16.64%	3.37%	0.31%
5.0e-02	BF	1.728e+07	1.716e+07	1.713e+07	1.746e+07	2.541e-01	2.584e-01	3.687e-01
	AL	1.708e+07	1.632e+07	1.705e+07	1.736e+07	2.525e-01	2.540e-01	3.699e-01
	Δ	1.17%	5.14%	0.48%	0.58%	0.63%	1.75%	0.33%
1.0e-02	BF	1.947e+07	1.947e+07	1.947e+07	1.947e+07	4.603e-01	4.830e-01	3.738e-01
	AL	1.946e+07	1.868e+07	1.946e+07	1.947e+07	3.824e-01	4.321e-01	3.742e-01
	Δ	0.01%	4.22%	0.01%	0.00%	20.37%	11.78%	0.11%
5.0e-03	BF	1.947e+07	1.947e+07	1.947e+07	1.947e+07	5.107e-01	5.237e-01	3.745e-01
	AL	1.947e+07	1.946e+07	1.947e+07	1.947e+07	4.705e-01	4.970e-01	3.746e-01
	Δ	0.00%	0.01%	0.00%	0.00%	8.53%	5.36%	0.01%

C.3.2. Third variable - maximum values

Table C.2: Conditioning on 3^{rd} variable - percentile estimation

Analysis		1	2	3	4	5	6	7
Variable		du_{y2}	du_{z3}	da_{y2}	da_{z3}	du_{y2}	da_{y6}	da_{z6}
1.0e-01	BF	5.928e-01	1.334e-01	2.199e-01	3.585e-01	6.893e-01	2.427e-01	3.687e-01
	AL	5.883e-01	1.332e-01	2.150e-01	3.574e-01	6.356e-01	2.374e-01	3.687e-01
	Δ	0.76%	0.20%	2.29%	0.31%	8.45%	2.21%	0.01%
5.0e-02	BF	6.909e-01	1.415e-01	2.471e-01	3.713e-01	9.213e-01	2.618e-01	3.702e-01
	AL	6.885e-01	1.398e-01	2.373e-01	3.709e-01	8.076e-01	2.576e-01	3.703e-01
	Δ	0.35%	1.23%	4.16%	0.08%	14.08%	1.64%	0.02%
1.0e-02	BF	1.450e+00	1.686e-01	3.885e-01	3.805e-01	1.812e+00	4.326e-01	3.749e-01
	AL	1.334e+00	1.655e-01	3.132e-01	3.801e-01	1.589e+00	4.182e-01	3.753e-01
	Δ	8.72%	1.84%	24.06%	0.11%	14.01%	3.45%	0.11%
5.0e-03	BF	1.802e+00	1.899e-01	5.110e-01	3.833e-01	1.988e+00	4.698e-01	3.767e-01
	AL	1.730e+00	1.757e-01	4.424e-01	3.831e-01	1.875e+00	4.605e-01	3.769e-01
	Δ	4.13%	8.07%	15.50%	0.06%	6.04%	2.02%	0.05%

Curriculum Vitæ

Cornelis Marcel Pieter 't Hart

06-09-1974	Born in Maassluis, The Netherlands.

Education

1986–1991	HAVO Westland-Zuid, Vlaardingen The Netherlands
1981–1993	VWO Westland-Zuid, Vlaardingen The Netherlands
1993–1999	Master of Science in Civil Engineering Delft University of Technology, Computational mechanics, Delft

Thesis:	Camus Benchmark A seismic analysis of a reinforced concrete structure
Professor:	Prof.dr.ir. H.C. de Borst

Experience

1998–1999	Graduate Intern TNO bouw en ondergrond, Rijswijk The Netherlands
1999–2003	Researcher and consultant numerical analytics TNO bouw en ondergrond, Rijswijk/Delft The Netherlands
2003–2007	Consultant, sales and support engineer DIANAFEA, Delft The Netherlands
2011–current	Senior structural engineer Tunnel Engineering Consultants, Amersfoort The Netherlands
2022–current	Animateur Workgroup 11: Immersed and Floating tunnels ITA-AITES, Châtelaine Switserland
2007–current	Leading Professional Structural Engineering - Infrastructure Royal Haskoning/Royal HaskoningDHV, Rotterdam The Netherlands

List of Publications

- 2024 - Spatial variation in estimation of shear key forces in segmented immersed tunnels, HERON Vol. 69 (2024) No. 1
- 2024 - Dynamic mooring analysis of a submerged floating tunnel – World congress on floating structures - Hong Kong December 2024
- 2024 - Computational aspects of the structural reliability assessment of submerged floating tunnels using vine copulas – Dependence models, Vines, and their Applications - Munich July 2024
- 2024 - Submerged floating tunnel: State of art and future perspective – Tunnel Construction China - Shenzhen April 2024
- 2024 - The influence of spatial variation on the design of foundations of immersed tunnels: advanced probabilistic analysis – Tunnelling and Underground Space Technology
- 2023 - An Owner's Guide to Submerged Floating Tunnels – ITA Worgroup 11 publicaton at WTC 2024 in Athens
- 2022 - Structural reliability analysis of a submerged floating tunnel under copula-based traffic load simulations - Engineering Structures
- 2022 - Assessment of the Limfjordtunnel using nonlinear FEA (accepted paper WTC Copenhagen 2022)
- 2022 - Target reliability for submerged floating tunnels
- 2020 - Limfjordtunnel - Geavanceerde rekenmodellen vergroten inzicht in draagvermogen, Civiele Techniek, November 2019
- 2019 - Update (1.1) to ANDURIL — A MATLAB toolbox for ANalysis and Decisions with UnceRtaInty: Learning from expert judgments: ANDURYL – SoftwareX – Sciencedirect
- 2018 - Accidental loads on Immersed tunnels; ITA congres april 2018 Dubai
- 2017 - Bijzondere belastingen op tunnels; Cement September 2017
- 2017 - Shear Capacity Crossing Borders; FIB congress
- 2013 - Quick scan on Shear in existing slab type viaducts; IABSE 2013
- 2012 - UHSB in LNG-opslagtanks; CEMENT September 2012
- 2010 - Een kade met een tweede leven; CEMENT October 2010
- 2005 - A Velocity-Based Approach to Visco-Elastic Flow of Rock, Mathematical Geology, 37(2), pages 141-162

- 2004 - 3D Finite Element modelling of buried pipelines 13 on the interaction of beam action of pipelines and cross sectional behaviour in The Power of Technology, Proceedings of the 5th International ASME Pipelines Conference, Calgary, Canada, October 4-8, 2004
- 2004 - ”Finite element modelling of buried steel pipelines in settlement areas” in Pipeline Technology, Proceedings of the 4th International Conference on Pipeline Technology, Edited by Rudi Denys, Oostende, Belgium, May 9-12, 2004.
- 2004 - ”Elasto-plastic design and assessment of pipelines: 3D Finite element Modelling” in Pipeline Engineering and Construction, Proceedings of the ASCE Pipelines 2004 International Conference, Edited by John J. Galleher and Michael T. Stift, San Diego, California, August 1-4, 2004.
- 2003 - Numerical homogenisation of the rigidity tensor in Hooke’s law using the node-based finite element method, In Mathematical Geology, 34(3)
- 2003 - “Review of the tensile strain method for predicting building damage due to ground movement”, ITA congress 2003 Amsterdam


Element
Joint
Shearkey
Enforced Displacement
Joints
Segment
Tunnel
Load on tunnel
Bedding response
Bedding